Proceedings of the 22nd Nordic Process Control Workshop

August 21-23, 2019

Technical University of Denmark, Kgs. Lyngby, Denmark

Editors: Gürkan Sin, John Bagterp Jørgensen, Jakob Kjøbsted Huusom

Technical University of Denmark

DTU Chemical Engineering

DK-2800 Kgs. Lyngby

Denmark

ISBN-13: 978-87-93054-88-2

Printed in Denmark,

Technical University of Denmark, Lyngby, 2019

Contents

22nd Nordic Process Control Workshop (NPCW)

Welcome to the 22nd Nordic Process Control Workshop (NPCW22) and Technical University of Denmark. The NPCW22 is held this year at the Technical University of Denmark (DTU) and jointly organized by DTU Compute and PROSYS research center at DTU Chemical Engineering.

The Nordic Process Control Workshop has been and continues to be an informal gathering that brings together academics and researchers from Nordic universities as well as professionals from industry. The workshop offers an excellent opportunity to present recent developments, exchange ideas, to network and engage with both academic and industrial communities in the field of process-simulation, process-control and process-optimization applied across multiple sectors and domains. The workshops are organized once every one and half year and the venue alternates between Denmark, Finland, Norway and Sweden.

The workshop is organized by the Nordic Working Group on Process Control currently consisting of the following members: Gürkan Sin, DTU, Denmark (2009; 2015) (Chair), Wolfgang Birk, Luleå University of technology (2018) (Co-chair), Kurt Erik Häggblom, Åbo Akademi, Finland (1998; 2004; 2010; 2016) (Past chair), Elling W. Jacobsen, KTH, Sweden (1994; 2000; 2006; 2012, 2018), Sigurd Skogestad, NTNU, Norway (1994; 2000; 2012, 2018), Jeno Kovacs, Foster Wheeler Co., Finland (2010; 2016), John Bagterp Jørgensen, DTU, Denmark (2009; 2015), Jan Peter Axelsson, Vascaia, Sweden (1997; 2003; 2009; 2015), Annika Leonard, Vattenfall, Sweden (2004; 2010; 2016), Alf Isaksson, ABB, Sweden (2004; 2010; 2016), Bernt Lie, Telemark Univ. College, Norway (2007; 2013), Hans Aalto, Neste Jacobs, Finland (2007; 2013), Bjørn Glemmestad, Yara, Norway (2007; 2013), Tore Hägglund, Sweden (2009; 2015), Torsten Wik, CTH, Sweden (2013), Krister Forsman, Perstorp, Sweden (2013), Christer Utzen, GEA Process Engineering A/S, Denmark (2015), Iiro Harjunkoski, ABB Germany/Aalto Univ., Finland (2016)
Morten Hovd, NTNU, Norway (2018), Johannes Jäschke, NTNU, Norway (2018), Jakob Kjøbstedt Huusom, DTU, Denmark (2018).

An important event of the workshop is the Nordic Process Control Award given by the Nordic Working Group on Process Control. The Award is given to outstanding process control professionals, who have made "lasting and significant contributions to the field of process control". **Nordic Process Control Award will be given to Prof. Nina Thornhill at NPCW22** in recognition of her lasting and significant contributions to the field of process control and automation. We congratulate Prof. Thornhill and look forward to her award lecture entitled "*Discovery through process data analytics*".

On behalf of the local organizing committee, we wish to thank many of our PhD and postdoctoral students for their help during the organization among others we wish to acknowledge the contribution of especially Merve Öner, Nikolaus Vollmer, Emil Krabbe Nielsen, Ergys Pahija and Soonho Hwangbo. Moreover, we also would like to thank Mrs. Anja Ninett Jensen for her excellent secretarial support during the organization of the event.

Finally, we hope you will enjoy the workshop which promises to provide a platform for rich scientific and social activities together with critical discussions, networking and inspiring ideas for further collaboration across the board in the field of process control.

Lyngby, August 2019

Gürkan Sin,
DTU Chemical Engineering

Jakob Kjøbsted Huusom,
DTU Chemical Engineering

John Bagterp Jørgensen
DTU Compute

List of Contributions

Self-optimizing control of a continuous pharmaceutical manufacturing plant; D. P. Piñeiro, A. Nikolakopoulou, J. Jäschke, T. Gundersen, R. D. Braatz

Model -based monitoring of pH gradients in a pilot-scale lactic acid bacteria fermentation; R. Spann, K. V. Gernaey, G. Sin

Nonlinear model predictive control of wastewater treatment for smart, cost efficient aeration; P. A. Stentoft, A.K. Vangsgaard, T. M.-Nielsen

Energy savings using MPC on a TES unit for heat exchange in industrial clusters; M. Thombre, J. Jäschke

Discovery through process data analytics; N. Thornhill

Linear-quadratic differential game control: two ways to ensure solvability; V. Turetsky

Transformed manipulated variables for decoupling and perfect disturbance rejection; C. Zotica, Sigurd Skogestad

Simplified model of CHO-cultivation in bioprocess library for Modelica - some experience; J. P. Axelsson

Physics-aware machine learning in multiphase flow estimation; T. Bikmukhametov, J. Jäschke

Free-floating sensor devices as a tool for characterizing mixing performance in stirred vessels; J. Bisgaard, J. K. Huusom, J. K., T. Rasmussen, K. V. Gernaey

Simulation and control of a secondary crushing circuit; H. Ibarra, A. Johansson, T. Euzébio, V. S. Moreira, K. T. Atta

Relay feedback excitation for identification of Fuel Cell performance parameters; I. J. Halvorsen, F. Zenith

Digital Twin platform for pharmaceutical process using deep-learning and reinforcement learning algorithm, S. Hwangbo, G. Sin

A Python toolbox for model predictive control; M. K. Nielsen, D. Boiroux, S. Hørsholt, J. K. Huusom, J. B. Jørgensen

On the allowable uncertainty in control configuration selection; R. Lucchese, W. Birk

Optimization of parametric uncertain designs using a novel stochastic optimization methodology; A. F. Magnússon, R. Al, and G. Sin

Online model maintenance–combining Output Modifier Adaptation with simultaneous model structure identification and parameter estimation; J. Matias and J. Jäschke

Computing the relative gain array for uncertain multivariable processes; B. Moaveni, R. Tahzibi, W. Birk

Uncertainty-based causal analysis of process systems for causal inference; E. K. Nielsen. G. Sin, X. Zhang, A. Gofuku, O. Ravn

Sequential Monte Carlo to model lactic acid bacteria fermentation; E. Pahija, R. Spann, G. Sin

Comparative analysis of plantwide control methodologies based on established benchmark models; M.L. Pedersen, F.D. Bähner, X. Zhang, J.K. Huusom

Mechanistic modelling of heat and mass transfer coupled with poremechanics during the baking process; F. Rabeler, A. H. Feyissa

Modelling of a cyclic distillation process; J. B. Rasmussen, S. S. Mansouri, J. Abildskov, J. K. Huusom

Gray-box identification using polynomial Narmax models; A. M. dos Santos, A. R. Secchi, M. B. de Souza Jr., S. Skogestad and D. Krishnamoorthy

Heat load prediction for district heating using a latent variable approach; J. Simonsson, K. Atta, D. Zachariah, W. Birk

Systematic tuning of PI controllers in non-steady-state return sludge flow of wastewater treatment systems; A.K. Vangsgaard, S. B. Jepsen, J. K. Huusom, T. M.-Nielsen

Health-aware control - current status and future outlook; A. Verheyleweghen
Sustainable value chain design for biorefineries; N. I. Vollmer, K. V. Gernaey, S. I. Mussatto, G. Sin

Identification of Low-Order Processes Using Ramp Input

Pasi Airikka, Mikko Numminen

Tampere University of Applied Sciences, Kuntokatu 3, 33520 Tampere, Finland (Tel: +358 40 587 2730; e-mail: pasi.airikka@tuni.fi, mikko.numminen@tuni.fi).

Abstract: Step signals are dominant transient inputs used for exciting processes for process identification. Several simple graphical methods are available for estimating process model parameters that capture the essence of the process dynamics. However, a process can also be excited by a ramp input. The resulted ramp response can be equally used for estimating the process model parameters. This paper introduces a simple graphical process model identification procedure for some typical low-order single-input single-output transfer function models. The proposed method requires no data storage or computational tools for data analysis but instead allows a fast and straightforward way to access the process dynamics.

Keywords: Identification, process, ramp input, transfer function.

1. INTRODUCTION

Process model identification is a cornerstone of control engineering. Control design and tuning require a process model that enables analysis both the identified project and the closed-loop system after closing the feedback loop. In most cases, for single-input single-output systems, the process model is of low-order capturing the essential process dynamics for an upper-limited frequency range that is adequate for control design (Åström & Hägglund, 1995).

To excite the process to be identified, there are transient inputs such as impulse, step and ramp function that are applicable. There are many reasons for selecting an input among many candidates (Antoulas & Anderson, 1999). Equally, control engineering literature recognises several methods for estimating a process model for transient responses, in particular for step responses such as those presented by Åström and Hägglund (1995) Vilanova and Visioli (2012). The known methods, however, typically neglect ramp inputs by favouring step or impulse inputs. Impulse inputs are primarily recommended for integrating systems and step inputs are both non-integrating and integrating systems (Visioli & Zhong, 2011).

Ramp inputs are equally applicable for process identification (Ahmed, 2010). The resulted ramp response allows to identify key model parameters equally to impulse and step responses. For identification, using a ramp input is not nearby as common as using a step input. However, there are cases when they are applicable. An automation system or a controller may have a push button for setting the manual control value. By pushing the button for a limited time period or several times in a row, it generates a linearly changed input signal, that is, a ramp input, for a process. The resulted response is a ramp response.

In some cases, an automation system may filter a step-wise input signal in manual mode through an integrator resulting in a ramp input. Similarly, it may be safer to excite a process by a sequence of small consecutive steps instead of one bigger step. Once again, the resulted input is a ramp input which eventually generates a ramp response.

Moving computationally between impulse, step and responses is rather solid. By integrating an impulse response with respect to time, a step response is generated. By integrating it twice, a ramp response is generated. Similarly, through derivation of a ramp response with respect to time, a step response is obtained. And by repeating that, an impulse response is available. Obviously, any ramp response could be returned back to a step response allowing to use any of those numerous identification methods available in literature.

However, in this paper, it is shown that a ramp response can be used as such for process identification. This saves time and effort as there is no need for any computation. And even further, it is shown that identifying process model dynamics is even simpler with ramp responses than that of step responses as the interpretation of the ramp response is more straightforward. The purpose of the presented identification method is to provide with a simple and a graphical way to identify a process model without any further computation or data analysis.

There are sources presenting bits and pieces of applying ramp excitation. But the topic is rather scattered among control engineering literature and typically rather limited space is given to ramp responses resulting in a lack of formal identification guidelines. Furthermore, literature typically deals with a first-order delay-free model ignoring both dead time and other low-order model types. However, the book written by Seborg et. al (2011) dedicates a whole page for introducing an identification method for a FOPDT (First-

Order Plus Dead Time) process model. Owing to their contribution, this paper expands the very same method for some other simple, low-order process models. So far, the authors have not come across with other sources treating a ramp identification for linear, time-invariant systems and that initiated writing this paper. Yet, the authors believe that the topic has been treated in detail along the past and therefore they would be grateful for receiving information of such a source.

This paper provides with a ramp response -based identification procedure for four different low-order, linear, time-invariant process model types with no restrictions on the model parameters. The paper contains both explicit equations but, more importantly, the proposed identification procedures with illustration.

2. RAMP INPUT

A ramp input signal with a rate of change of $r \neq 0$ determined by a user or a computer is given as

$$u_{ramp}(t) = r \cdot t, t \geq 0 \qquad (1)$$

Its Laplace-transformed signal is a double-integrator

$$u_{ramp}(s) = r / s^2 \qquad (2)$$

For a unit ramp response $r = 1$ but the only requirement for its value range is basically $r \neq 0$. Figure 1 shows ramp input signals for different ramp rates.

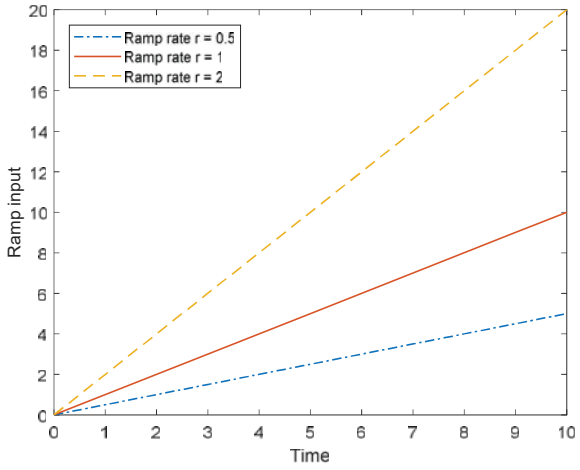

Fig. 1. Ramp input signals with different ramp rates (r = 0.5, 1, 2).

The ramp input signal can be generated from an impulse or a step input using an integrator. Figure 2 illustrates generation of a ramp input signal using a rate of change with a step input and an integrator. Any input, and similarly any response, could be translated to any other form by either derivating or integrating with respect to time. As this would require computational tool and data storage for real identification data, this relationship between signals is not used in the proposed method by any means.

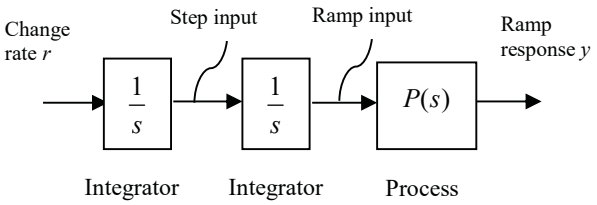

Fig. 2. Ramp input signal generation.

In practice, the ramp input is terminated at a certain point and either kept at constant or driven back to the starting level. However, in this study, only the linearly changing ramp input signal is of significance and the proposed identification method does not make use of the information after termination of the ramp input experiment.

3. RAMP RESPONSES TO SELECTED MODEL TYPES

3.1 First-Order Plus Dead Time model

The most common process model used in both literature and practice for presenting the relation between process input and output is a First-Order Plus Dead Time (FOPDT) model. It contains three model parameters to be identified and it can be presented as a transfer function as below

$$P(s) = \frac{k}{Ts+1} e^{-Ds} \qquad (3)$$

The process model parameters are static gain k, time constant T and dead time D. The assumption is that the parameters satisfy the following requirements $k \neq 0, T \geq 0$ and $D \geq 0$.

The ramp response $y(s)$ of (3) is now given as

$$y(s) = P(s)\, u_{ramp}(s) = \frac{k \cdot r}{s^2(Ts+1)} e^{-Ds} \qquad (4)$$

The Laplace-domain response can be transformed to a time-domain representation using an inverse Laplace transform resulting in an ordinary differential equation

$$T \frac{d}{dt} y(t) + y(t) = k \cdot r \cdot (t - D) \qquad (5)$$

The solution of (5) is

$$y(t) = k \cdot r \cdot (t - D) + k \cdot r \cdot T \cdot (e^{-(t-D)/T} - 1) \qquad (6)$$

For processes with a dead time, the time interval $0 \leq t < D$ is not of significance as the ramp response is zero during the interval. The ramp input being started at $t = 0$ as given by (3), the take-off time instant $t = D$ where the ramp response leaves zero is, however, of most significance for identification.

In literature, the solution (6) is often given only to a process model without dead time ($D = 0$) leading to a solution

$$y(t) = k \cdot r \cdot t + k \cdot r \cdot (Te^{-t/T} - 1) \qquad (7)$$

which is obviously less applicable for identification as it restricts the method only to processes with no dead time.

Ramp responses for three static process gain values of 0.5, 1 and 2 are plotted in figure 3 with time constant $T = 10$ and dead time $D = 5$. The static error remains unchanged if the static process gain is 1 but increases for static gain smaller than 1 and even crosses with a ramp input signal eventually for static gain bigger than 1. This observation serves as a classification basis for separating processes with static gain smaller or larger than one. However, it will be shown later, that the static gain can be estimated more precisely using just the same ramp response.

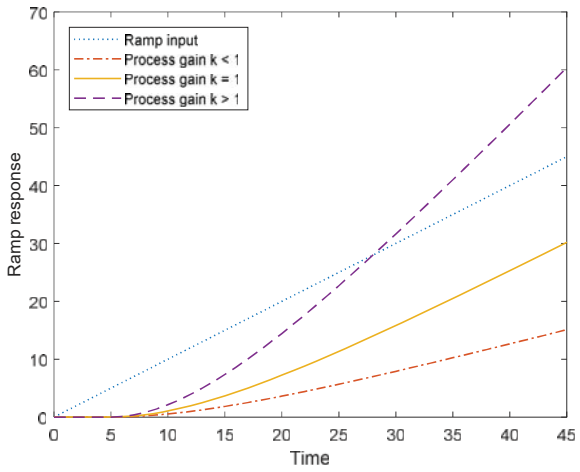

Fig. 3. Ramp responses to a FOPDT model for different process gain ($k = 0.5, 1, 2$) with $D = 5$ and $T = 10$.

The ramp response (6) has an interesting property of approaching to a straight line $y_s(t) = a \cdot t + b$ for large t

$$\begin{aligned} y(t) &\approx y_s(t) = k \cdot r \cdot (t - D - T), \quad t >> T + D \\ &= k \cdot r \cdot t - k \cdot r \cdot (D + T) \end{aligned} \qquad (8)$$

The straight line $y_s(t)$ has a slope of $a = k \cdot r$ and a constant $b = -k \cdot r \cdot (D + T)$ with a zero $y_s(t_s) = 0$ at $t_s = D + T$.

There is an error signal between input (1) and output (8) as given in (9). The error increases with time for $k \neq 1$. For unit gain processes, the error remains stationary.

$$e(t) = r \cdot (1 - k)t + r \cdot k \cdot (D + T) \qquad (9)$$

For processes with $k > 1$, the ramp response crosses with the ramp input at $t = \dfrac{k(D+T)}{k-1}$. Figure 4 shows ramp input (1) and response for a FOPDT model (7) with a fitted straight line (8) for the response. Figure 5 shows how the FOPDT model parameters can be graphically estimated through reducing the ramp response to a straight line as given in (8). The process gain k is calculated as a slope of the ramp response as soon as the ramp response shows a constant rate of change. The dead time D is determined as a time interval between starting the ramp input and a take-off moment for the ramp response. The fitted line to the ramp response with a crossing point to zero-level (zero of the straight line) yields $D + T$ allowing separation as soon as the dead time has been estimated.

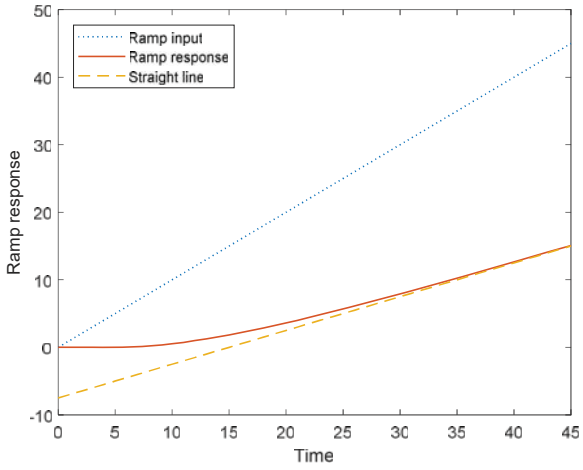

Fig. 4. Ramp responses to a FOPDT model with a fitted straight line for large *t*.

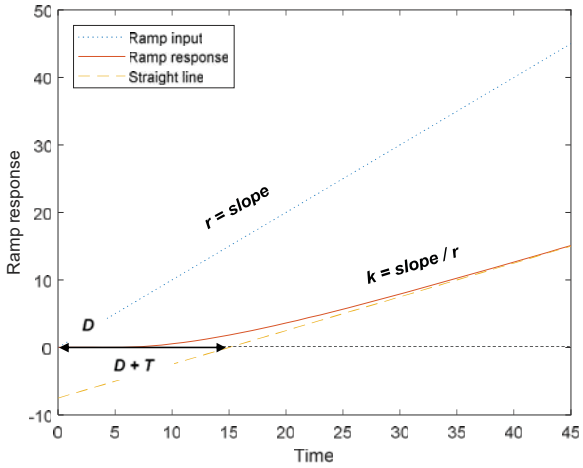

Fig. 5. Identifying FOPDT model parameters using a ramp response.

Figure 6 illustrates what typically is given for readers regarding ramp responses. The figure illustrates a ramp response and correctly introduces how time constant T could be identified using both the ramp input and the ramp response signals. The proposed, rather appealing method, is however, applicable only to FOPDT process with a unit process gain and with a unit ramp input with no dead time. These assumptions make the usage of the proposed method rather restricted.

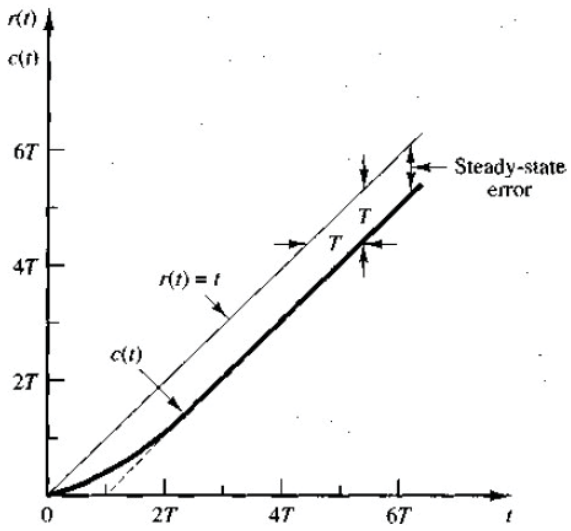

Fig. 6. Typical visualisation of ramp response showing how time constant can be determined.

3.2 Second order Plus Dead Time model

The identifiable process may have two time constants. For simplicity, the time constants are assumed to be equal resulting in a Second-Order Plus Dead Time (SOPDT) model

$$P(s) = \frac{k}{(Ts+1)^2} e^{-Ds} \qquad (10)$$

The model involves three parameters: static gain, time constant and dead time. The value ranges of the parameters are the same as in the case of the model (1). Now, the ramp response is

$$y(s) = P(s)\, u_{ramp}(s) = \frac{k \cdot r}{s^2 (Ts+1)^2} e^{-Ds} \qquad (11)$$

And, the time-domain ramp response with a take-off condition of $y(D) = 0$ is given as

$$y(t) = k \cdot r \cdot (t - D - 2T) + k \cdot r \cdot e^{-(t-D)/T}(t - D + 2T) \qquad (12)$$

Figure 7 shows the ramp responses for a SOPDT model with three different process gains. Resembling with the ramp response of the FOPDT model (6), the ramp response of SOPDT also approaches a straight line $y_s(t) = a \cdot t + b$ for large t

$$\begin{aligned} y(t) \approx y_s(t) &= k \cdot r \cdot (t - D - 2T), \quad t >> T + D \\ &= k \cdot r \cdot t - k \cdot r \cdot (D + 2T) \end{aligned} \qquad (13)$$

Now, the straight line has a slope of $a = k \cdot r$ and a constant $b = -k \cdot r \cdot (D + 2T)$ resulting in a zero $y_s(t_s) = 0$ at $t_s = D + 2T$. Figure 8 shows ramp input (1) and response for a FOPDT model (12) with a fitted straight line (13) for the response.

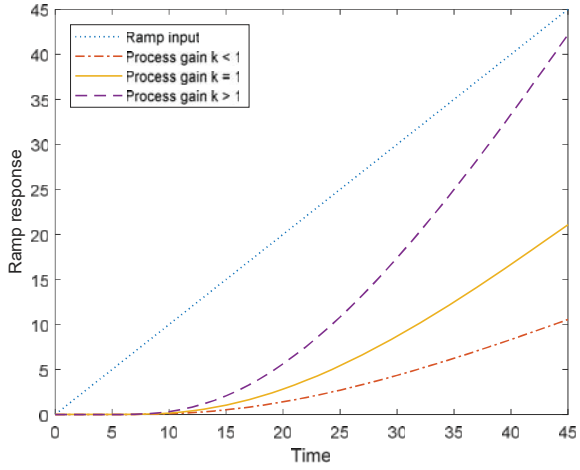

Fig. 7. Ramp responses to a SOPDT model for different process gain ($k = 0.5, 1, 2$) with $D = 5$ and $T = 10$.

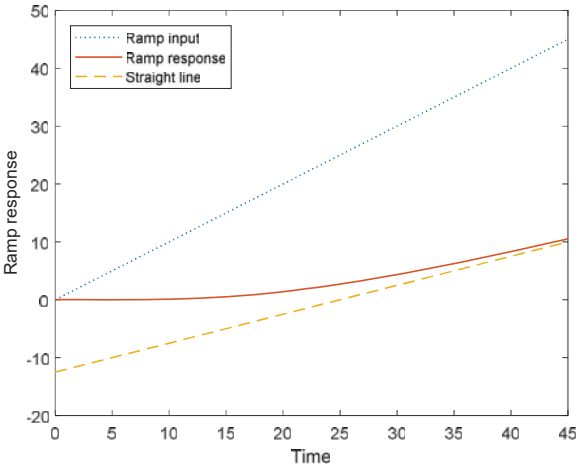

Fig. 8. Ramp responses to a SOPDT model with a fitted straight line for large *t*.

Following the principle and visualisation given in figure 5, the SOPDT model parameters can be calculated almost similarly by replacing the $D + T$ in figure 5 by $D + 2T$ and solving the time constant accordingly.

3.3 Integrator plus Dead Time model

The Integrator Plus Dead Time model (IPDT) only involves two model parameters: integrator gain and dead time.

$$P(s) = \frac{k}{s} e^{-Ds} \qquad (14)$$

Its ramp response can be given as

$$y(s) = P(s)\, u_{ramp}(s) = \frac{k \cdot r}{s^3} e^{-Ds} \qquad (15)$$

which results in a time-domain expression with an initial condition of $y(D) = 0$

$$y(t) = \frac{1}{2} k \cdot r \cdot (t - D)^2 \qquad (16)$$

The ramp response is of the second order with respect to time and it has a zero $y(t_s) = 0$ at $t_s = D$.

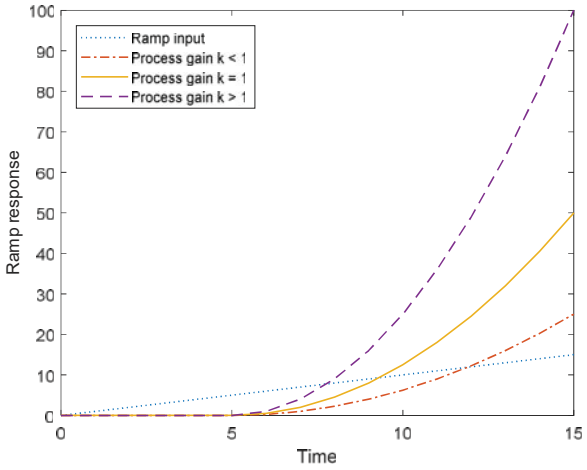

Fig. 9. Ramp responses to an IPDT model for different process gain (k = 0.5, 1, 2) with $D = 5$.

Now, the identification procedure visualised in figure 5, significantly simplifies as only process gain and dead time are to be calculated using the ramp response.

3.4 Integrator plus First-Order Plus Dead Time model

An IPDT model can be extended to cover a time constant resulting in an Integrating First-Order Plus Dead Time (IFOPDT) model. The model has three parameters: integrator gain, time constant and dead time.

$$P(s) = \frac{k}{s(Ts + 1)} e^{-Ds} \qquad (17)$$

Similar to other model types, the ramp response can be formulated in terms of the model parameters being

$$y(t) = Te^{-(t-D)/T} + \frac{1}{2} k \cdot r \cdot (t - D)^2 - k \cdot r \cdot T \cdot (t - D) - T \qquad (18)$$

Now, the ramp response approaches to a second-order polynomial with respect to time

$$y(t) \approx \frac{1}{2} k \cdot r \cdot (t - D)^2 - k \cdot r \cdot T \cdot (t - D) - T \qquad (19)$$

The resulted equation (19) is of the second degree with respect to time. By drawing a tangent for the ramp response in (18) for large t, equals to derivation of (19) with respect to time

$$\frac{d}{dt} y(t) \approx k \cdot r \cdot (t - D) - k \cdot r \cdot T \qquad (20)$$

The resulted equation (20) could be used for fitting estimating the zero-level crossing point and computing the parameters exactly as visualised in figure. However, the proposed method contains uncertainty as it requires approximating the response of the second degree for large time value.

4. IDENTIFICATION PROCEDURE

4.1 Identification of low-order process models

In previous chapter, four different low-order process model types (FOPTD, SOPTD, IPDT, IFOPDT) were presented with their explicit ramp responses and approximations for large values of time. The approximations for large values of time can be effectively used for identifying model parameters of every model type introduced.

For real identification, it is not of use to expect the ramp response to carry on infinitely after applying a ramp input. Instead, it is adequate to follow the ramp response up to a point where the ramp clearly increases linearly. At this point, the ramp response experiment can be interrupted by e.g. freezing the ramp input or returning back to the starting level (zero-level).

As illustrated in figure 5, a straight line can be drawn along with the linearly changing ramp response. The slope of the straight line is then to be calculated and used for determining process gain k

$$k \approx \frac{slope\{y(t)\}}{r} = \frac{\Delta y / \Delta t_y}{r} \qquad (21)$$

If for any reason the ramp rate of the ramp input signal is unknown, as $r = slope\{r(t)\}$, the process gain can be equally computed by determining the slope of the ramp

$$k \approx \frac{slope\{y(t)\}}{slope\{r(t)\}} = \frac{\Delta y / \Delta t_y}{\Delta r / \Delta t_r} \qquad (22)$$

An estimate for the dead time is obtained by determining the take-off time instant where the ramp response starts to deviate from the level it had at the time of the starting the ramp experiment. Measurement noise or any other unmodeled high-order dynamics or process disturbances might corrupt interpretation of the take-off point but otherwise, it is the most straightforward parameters to be estimated graphically.

Estimation of a time constant for the model types excluding an IPDT model requires determination of the crossing point with the drawn straight line along the ramp response and the starting level of the ramp response. The estimated crossing point t_s, that is, a zero or a root of the straight line, is essential for estimating the time constant. It is a function of the time-based model parameters, e.g. for a FOPDT model it is $t_s = T + D$ and for SOPDT model it is $t_s = T + 2D$. After solving the dead time as explained before, it is then straightforward to solve the time constant using the estimated

crossing point t_s. Table 1 lists simple equations for computing the time constant for all the given model types with the other model parameters, also.

Table 1. Process model parameters for typical process model types (t_s is a zero of the fitted straight line along the ramp response)

Model type	Dead time D	Process gain k	Time constant T
FOPDT	*Take-off time instant*	$k = \frac{\Delta y / \Delta t}{r}$ or $k = \Delta y / \Delta r$	$T = t_s - D$
SOPDT			$T = (t_s - D)/2$
NOPDT			$T = (t_s - D)/N$
IPDT			-
IFOPDT			$T = t_s - D$

Although it has not been proven here, it could be shown, that for a Nth-Order Plus Dead Time (NOPDT) model with multiple equal time constants, the ramp response for large values of t can be formulated as

$$\begin{aligned} y(t) \approx y_s(t) &= k \cdot r \cdot (t - D - N \cdot T), \quad t >> T + D \\ &= k \cdot r \cdot t - k \cdot r \cdot (D + N \cdot T) \end{aligned} \tag{22}$$

Now, the fitted straight line has a slope of $a = k \cdot r$ and a constant $b = -k \cdot r \cdot (D + N \cdot T)$ resulting in a zero $y_s(t_s) = 0$ at $t_s = D + N \cdot T$ allowing to compute the time constant as given in Table 1.

4.2 Identification procedure step by step

The identification method introduced in the previous sub-section can be given as a step-by-step recipe starting with ramp response experiment preparations.

Preparing step

Set a process to be identified in an open loop by setting a feedback controller (if it exists) in manual. Make sure that the process is in steady state and that all the disturbances affecting the process output are as steady as possible. Record an initial level of the process output.

Step 1

Start a ramp response experiment by injecting a ramp input to the process and set clock to zero. Record a ramp rate r (slope of the ramp input).

Step 2

Allow the ramp response (of the process output) to take off its initial recorded level. At the earliest, stop the experiment as soon as linear progression can be seen. Otherwise, continue with the experiment as long as it is safe.

Step 3

After stopping the experiment, record the slope of the ramp response $\Delta y / \Delta t$ and its take-off time instant D from the initial level. Then, fit a straight line graphically to the last points of the ramp response and determine the crossing point t_s of the fitted line with the initial starting level of the response.

Step 4

Using the calculated variables r, $\Delta y / \Delta t$, t_s and D calculate the model parameters of the selected model type as given in table 1.

5. PRACTICAL HINTS

As with any other identification procedure, a strong assumption of having the process in steady state before conducting a ramp response experiment is made. The steady state level of the process output is crucial for determining the crossing point of the fitted straight line to the ramp response.

Although being rather obvious, also a strong assumption of having no process disturbances corrupting the ramp response is made. There may be both measurable and non-measurable variables affecting the process while the test and, therefore, one should secure that they remain as unchanged as possible throughout the experiment.

The ramp response experiment needs to be continued up to a time instant when the response has been changing linearly for some time. To secure a successful experiment, it is clearly beneficial to allow the ramp response change as much as possible. There is no thumb rule given for a perfect timing of interruption as it would obviously require a priori knowledge of the process dynamics. Therefore, the recommendation is to allow the ramp experiment to continue as far as possible without compromising safety or production.

In terms of identification, it is not of any significance what happens after interrupting the ramp response experiment. The ramp may be frozen to a constant level or it can be driven or set back to its starting level. This has no impact and, therefore, relevance to the given identification procedure. However, it is advised to consider the ramp experiment beforehand by considering also necessary actions after ceasing the experiment.

Ramp input signal can also be decreasing, that is negative by sign. Equally, the process can have a negative process gain. The negative values result in a different orientation of the ramp response but they have no effect what so ever on the identification procedure as long as the negative sign is considered in computation.

The ramp response rate is a user-specific or a computer-determined parameter. It also has no deteriorating impact on the identification procedure but it has to be known for securing successful identification results.

6. CONCLUSIONS

Process model identification based on ramp response is by no means a new topic in control literature. Ramp input excitation is an option to other simple transients such as impulse and step signals. Therefore, it should equally have space when teaching transient-based identification methods.

This paper introduced a graphical method to identify model parameters for some typical low-order transfer function models. The method has been earlier introduced in control literature but, to the knowledge of the authors, has not been wider covered. Hence, this paper expanded the simple graphical method to some other low-order model types than that of the first-order plus dead time model.

The authors are now considering taking the method in use for bachelor-level control engineering studies as an expansion to the conventional teaching of process model identification.

REFERENCES

Ahmed, S. (2010). Process Identification using Nonideal Step Inputs. *Proc. of the 9th International Symposium on Dynamics and Control of Process Systems (DYCOPS)*, p. 353-358.

Antoulas A.C. and Anderson, B.D.O. (1999). On the choice of inputs in identification for robust control. *Automatica,* 35, p. 1009-1031.

Seborg, D.E., Edgar, T.F, Mellichamp, D.A, Doyle III, F.J (2011). *Process dynamics and control.* p. 62-63. John Wiley & Sons, Asia.

Vilanova, R. and Visioli, A. (2012). *PID control in the third millennium.* Springer-Verlag, New York.

Visioli, A. and Zhong, Q-C. (2011). *Control of the integral processes with dead time*. Springer-Verlag, London.

Åström, K.J. and Hägglund, T. (1995). *PID controllers: theory, design and tuning.* page numbers. Instrument Society of America, United States of America.

The Symbiosis within the Control Hierarchy: On Application for Enterprise Wide Decision Making

Marcel Stenevang[1], Emma S. Grønkjær[1], Laila Bering Larsen[2], Deenesh K. Babi[1*]
[1]IM1 BIO – Insulin & Manufacturing 1 Bioprocess Improvement-Optimization
[2]Fermentation and Recovery - Insulin & Manufacturing 1
Novo Nordisk A/S, Hallas Allé DK-4400 Kalundborg, Denmark
**Corresponding author: dekb@novonordisk.com*

The control hierarchy consists of, at the lower bound, regulatory control (time scale typically seconds) and, at the upper bound, production planning – scheduling (time scale typically weeks to months). For the design of new and retrofit of existing flowsheets, the quantification of the impact of design decisions/changes is of importance in order to feasibly analyze, evaluate and generate the best investment portfolio for the multiscale, that is, from flowsheet to unit operations. To do so, production planning-scheduling (PPS) can be used to model the flowsheet of the process and facility. Here, the process limitations and bottlenecks related to unit operations are identified for a deeper dive, for example, application of regulatory control (RC). The models are of low fidelity (mass balance models) however, solution complexity of the flowsheet model requires the solution of a high number of equations subject to constraints (superstructure optimization). Such problems can be formulated as a mixed integer non-linear programming (MI[N]LP) problem because of the decision making (for example, equipment selection) using integer variables and the models for the unit operations can be non-linear [1]. This problem can either be solved using optimization or discrete event algorithms or a combination of both [2].
For an automated flowsheet, the mass balance profiles of the RC and PPS model, in principle, should correspond because the latter models the so-called recipe of the process and the former executes the recipe. As an analogy, the PPS is the brain sending signals to the fingers, the RC to perform a task. Therefore, for an unautomated flowsheet the PPS model can assist in identifying manual interventions and the need for RC when benchmarked against data from a data historian. As an example, consider the filling levels estimated from the PPS and those measured in an existing flowsheet.
The objective of this presentation is to present the approach used in Novo Nordisk for enterprise wide decision making for improvement-optimization. The method will be presented, and its application expounded through an example of an existing flowsheet. First, PPS is used for providing information for decision making and portfolio investment through the evaluation of current capacity, and the identification of process limitations/bottlenecks. Second, a RC problem is defined and solved based on the PPS output in order to automate a sub-process within the flowsheet.

References

1. Iiro Harjunkoski, Christos T. Maravelias, Peter Bongers, Pedro M. Castro, Sebastian Engell, Ignacio E. Grossmann, John Hooker, Carlos Méndez, Guido Sand, John Wassick, Scope for industrial applications of production scheduling models and solution methods, Computers & Chemical Engineering, Volume 62, 2014, Pages 161-193
2. Lifei Cheng, Marco A. Duran, Logistics for world-wide crude oil transportation using discrete event simulation and optimal control, Computers & Chemical Engineering, Volume 28, Issues 6–7, 2004, Pages 897-911

Simulating Batch Process Plants in MATLAB Simulink / StateFlow ⋆

F.D. Bähner * **O.A. Prado-Rubio** ** **J.K. Huusom** *

* *Process and Systems Engineering Center (PROSYS), Department of Chemical and Biochemical Engineering, Technical University of Denmark, 2800 Lyngby, Denmark (e-mail: fdav@kt.dtu.dk).*
** *Departamento de Ingeniería Química, Universidad Nacional de Colombia, Campus La Nubia Manizales, Caldas, Colombia*

Abstract: Optimisation of batch-operated process plants is an inherently complex task. Therefore, modelling constitutes an auspicious tool in batch process systems engineering. Discrete-event simulators are increasingly popular also in industry. To this end, a number of specialised vendors (e.g. ExtendSim^{TM}, INOSIM^{TM}, SchedulePro^{TM}) offer customised solutions. Continuous simulators are shun both for the risk of numerical error from time-based rather than event-based discretization as well as unnecessary computation steps. However, this work indicates that MATLAB Simulink^{TM}'s variable-step solvers, in combination with the MATLAB StateFlow^{TM} framework for state machine models, allow building and solving hybrid systems accurately and performant. This implementation offers advantages such as

- Vast flexibility in modelling scope due to Simulink's extensive libraries and the facile inclusion of native MATLAB functions
- Fast routing of data to/from root workspace enables advanced function calls
- Powerful tools available for post-hoc visualisation and analysis of simulated data-sets
- The potential to simulate continuous states during periods of semi-continuous operation
- Familiarity of many engineering graduates with MATLAB and Simulink

The cost is on the one hand a higher computational burden, but this is not necessarily a problem given today's computing resources. However, implementation and debugging of complex systems in the current frame is tedious. This is specifically due to the restrictions in object-oriented modelling that arise when solving StateFlow models within continuous flowsheets. Yet, this framework allows the efficient generation of data sets containing both continuous and discrete states and thus enables simulation-based process optimisation for this class of processes. Secondly, these data sets may have potential as benchmarks for advanced data analytics including machine learning and artificial intelligence in the context of batch process plants.

⋆ The authors would like to acknowledge the Technical University of Denmark (DTU) and BIOPRO2. The project received financial support from Innovation Fund Denmark through the BIOPRO2 strategic research center (Grant number 4105-00020B).

Finding sparse control structures using gramian based interaction measures (Extended abstract)

Fredrik Bengtsson * **Torsten Wik** *

* *Department of Electrical Engineering, Chalmers University of Technology, SE 412 96 Göteborg, Sweden, (email:fredben@chalmers.se, torsten.wik@chalmers.se)*

Abstract: A common control structure is a sparse control scheme, in which a decentralized controller is expanded to include feed-forward or MIMO blocks. In this paper, use of the gramian based interaction measures to determine a sparse control structure with feed-forward is examined. The method suggested today is examined, and a modification is proposed. It is demonstrated that this modification provides a considerable improvement. Furthermore, newly proposed modifications to scaling the gramian based measures are expanded to also cover sparse control structure. We show that the method that yields the best result is when two different scaling methods are combined , using one to design a decentralized controller and another to find elements for feedforward.

Keywords: Feedforward, Sparse Control, Control configuration selection, Gramian based interaction measures, input-output pairing.

INTRODUCTION

A common issue in industrial process control systems is that interaction between different parts of the plant gives rise to a multiple input multiple output (MIMO) system, where the same input may affect multiple outputs, or conversely, the same output is affected by multiple inputs. One method to control a MIMO system is to divide it into subsystems of one input and one output and implement SISO controllers for each of the subsystems. This control strategy is called decentralized control and remains widely used in industry (Khaki-Sedigh and Moaveni [2009]). It has several advantages compared to implementing a MIMO controller for the entire system, as it allows the use of relatively easy to design low dimensional controllers. Moreover, it is less vulnerable to sensor and actuator failures than more complex control schemes that try to control the entire system with one overarching control scheme.

However, sometimes interactions between the different inputs on the output results in a decentralized control scheme yielding a poor result. One solution to this is to expand the decentralized control structure to include decoupling feedforward to remove the most problematic interactions. This yields what is called a sparse controller structure. However, this requires determining which interactions that are appropriate to remove with feedforward, and which ones where implementing feedforward may create interactions that result in a poorer control outcome.

One group of measures which can be used to device a sparse controller structure are the gramian based measures. This group includes the Σ_2 method (Birk and Medvedev [2003]), the participation matrix (PM) (Conley and Salgado [2000]) and the Hankel interaction index array (HIIA) (Wittenmark and Salgado [2002]). These methods use the controllability and observability gramians to create an interaction matrix which gives a gauge of how much each input affects each output. The interaction matricies (IMs) can then be used to device both decentralized and sparse control structure.

While a rule of thumb on how to select a sparse control structure from the gramian based measures has been presented in Conley and Salgado [2000], no deeper analysis on the subject has been presented. Here we will further examine how to best derive a sparse controller structure when using the HIIA and propose a new method for determining which signals are appropriate for feedforward.

A new method of scaling the gramian based measures have been proposed, and it has been demonstrated that it yields improved results (Bengtsson et al. [2019]). We will here further examine the scaling of the IMs and see how it can best be adapted when designing sparse control structures.

1. THE GRAMIAN BASED MEASURES

1.1 Gramian based measures

The gramian based measures (PM, HIIA and Σ_2) can be calculated from a system's transfer function matrix (TFM) (Birk and Medvedev [2003], Conley and Salgado [2000], Wittenmark and Salgado [2002]). Given a TFM

$$G(s) = \begin{bmatrix} g_{11}(s) & g_{12}(s) & \cdots & g_{1n}(s) \\ g_{21}(s) & g_{22}(s) & & \\ \vdots & & \ddots & \\ g_{n1}(s) & & & g_{nn}(s) \end{bmatrix}$$

each measure generates an interaction matrix (IM). For the HIIA and Σ_2 it is generated by

$$[\Gamma]_{ij} = \frac{||g_{ij}(s)||}{\sum_{kl} ||g_{kl}(s)||}$$

using the Hankel norm and 2-norm for the HIIA and Σ_2 respectively. The PM is derived in a similar fashion, but it uses the squared Hilbert-Schmidt norm, i.e. the IM is generated by:

$$[\Gamma]_{ij} = \frac{||g_{ij}(s)||^2_{HS}}{\sum_{kl} ||g_{kl}(s)||^2_{HS}}.$$

Once an IM is generated, a decentralized pairing is generated by choosing the pairing that yields the largest sum of elements from the IM. For efficient implementation in finding which pairing yields the largest sum of elements one can for example use the Hungarian algorithm as in Fatehi [2011].

1.2 Sparse control

Once a decentralized control structure has been found it can be expanded to include feedforward blocks. To understand how this works, we begin by examining a 3 by 3 system, i.e.

$$\begin{bmatrix} y_1 \\ y_2 \\ y_3 \end{bmatrix} = \begin{bmatrix} G_{11}(s) & G_{12}(s) & G_{13}(s) \\ G_{21}(s) & G_{22}(s) & G_{23}(s) \\ G_{31}(s) & G_{32}(s) & G_{33}(s) \end{bmatrix} \begin{bmatrix} u_1 \\ u_2 \\ u_3 \end{bmatrix}.$$

Let us assume that the inputs and outputs have been ordered such that our decentralized controller design decided on a diagonal pairing where y_i is controlled by u_i for $\forall i$. Now, u_1 will also affect y_2 and y_3 by $G_{21}(s)$ and $G_{31}(s)$, respectively. If u_1 affects y_3 to such an extent that it poses a problem, this can ideally be resolved by using the feedforward

$$u_3 = u_3^* - \frac{G_{31}(s)}{G_{33}(s)} u_1, \tag{1}$$

where u_3^* is the control signal from the decentralized controller and we assume $\frac{G_{31}(s)}{G_{33}(s)}$ is stable and proper. If we implement this feed-forward loop we will have removed the direct effect of u_1 on y_3. However, there are other consequences of this implementation since the change of u_3 will also affect y_1 and y_2. If these interactions are significant the feed-forward loop might do more harm than good. Having this in mind, we examine how the IM can be used to determine when feed-forward might be appropriate. Consider an interaction matrix

$$\Gamma = \begin{bmatrix} \gamma_{11} & \cdots & \gamma_{1N} \\ \vdots & \ddots & \vdots \\ \gamma_{N1} & \cdots & \gamma_{NN} \end{bmatrix}.$$

First we choose the elements for the decentralized pairing as described previously and assume, without loss of generality, that the pairing elements are on the diagonal. After this, we look in the interaction matrix for large elements not yet selected for pairing. The current method for determining feedforward is simply to use the largest elements not selected for pairing. However, doing this means that other potential interactions are not taken into account. For example, assume that γ_{N1} is a large value and thus u_1 is a potential candidate for feed-forward. However, as described in the example, this will impact u_N, which will not only impact y_N, but also the other outputs. A gauge of the size of this impact is $\sum_{i=1}^{N-1} \gamma_{iN}$. If these values are very large then the IM indicates that adding the described feed-forward on u_1 is unwise. To determine the use of feed-forward in the general case we therefore create a new matrix IM^*, whose elements are defined by

$$\gamma_{ij}^* = \gamma_{ij} - \rho \sum_{\substack{k=1 \\ k \neq i}}^{N} \gamma_{ki},$$

where ρ is a tuning parameter. With this new IM, the largest elements where $i \neq j$ are chosen for feed-forward until the sum of elements chosen (both for control and feedforward) is larger than 0.7, a rule of thumb for gramian based measures (Salgado and Conley [2004]). However, as feed-forward increases controller complexity it is only implemented if it seems likely that it will have a positive impact. This is determined by checking if $\gamma_{ij}^* > 0$ in which case feed-forward is considered appropriate, and otherwise it is not implemented. Further precautions also have to be taken to avoid implementing an unstable or non-proper feed-forward block. Note that if $\rho = 0$ the largest elements of the IM are chosen without taking into account other interactions.

1.3 Scaling of the IMs

An issue with these three methods is that the interaction matrix will be affected by the scaling of the inputs and outputs such that different scalings may yield different results. Generally, this is resolved by scaling the input and outputs from 0 to 1, setting zero to the lowest value they are likely to reach and 1 to the highest value Salgado and Conley [2004]. However, this scaling is at times insufficient , and we will present a few ways in which the IMs could be rescaled for improved results which were discussed in Bengtsson et al. [2019].

Row or Column scaling Each column in the IM corresponds to the interactions from one input, while each row corresponds to the interactions affecting one output. If one column contains significantly less interaction than the other columns (as may be the case if one input is relatively poorly suited for control), little importance will be given to the decision of which output should be controlled by this input. This may lead to a poor input-output pairing as will be demonstrated with an example in Section 3. One way to resolve this would be to normalize the columns, that is to divide the elements in each column of the IM by the corresponding column sum. This will ensure that when conducting the pairing algorithm, equal importance is given to each input. In the new IM the scaled elements would become:

$$[\Gamma_c]_{ij} = \frac{[\Gamma]_{ij}}{\sum_{k=1}^{N} [\Gamma]_{kj}},$$

where Γ_c is an interaction matrix with normalized columns. If we instead wish to ensure that equal importance is given

to each output, we can instead normalize the rows, which gives a interaction measure defined by

$$[\Gamma_r]_{ij} = \frac{[\Gamma]_{ij}}{\sum_{k=1}^{N}[\Gamma]_{ik}}.$$

Choosing between row and column scaling It may be difficult to determine if it is preferable to scale by rows or columns. Therefore we have proposed an approach to scaling that tries to determine which is the most appropriate for a given IM. In this approach the column sums and row sums were first calculated. If the smallest sum is a row sum, then the rows are scaled, and otherwise the columns are scaled. This approach will be refered to as Row/column scaling.

Sinkhorn-Knopp algorithm By scaling the columns or rows we can guarantee that equal importance is given to either each input or each output when determining pairing. If we, however, wish to have both the columns and rows scaled we can use the Sinkhorn-Knopp algorithm. This algorithm combines row and column scaling by alternating between normalizing the rows and normalizing the columns. In cases where the matrix can be made to have positive elements on the diagonal (as is always the case with gramian based measures) this algorithm is guaranteed to converge to a matrix that will have both rows and columns normalized Sinkhorn and Knopp [1967].

Scaling the IMs with the Sinkhorn-Knopp algorithm has the additional benefit of removing the impact of input and output scaling on the IMs. Using the Sinkhorn-Knopp algorithm to scale the system will yield the same IM, regardless of what the original scaling of the system was.

Hybrid scaling schemes The Sinkhorn-Knopp scaling algorithm is not entirely well suited for design of sparse systems systems . The reason for this is that using Sinkhorn-Knopp scaling may remove information from the IM useful for when designing a sparse controller, take for example a 3by3 system:

$$\begin{bmatrix} y_1 \\ y_2 \\ y_3 \end{bmatrix} = \begin{bmatrix} G_{11}(s) & G_{12}(s) & G_{13}(s) \\ 0 & G_{22}(s) & G_{23}(s) \\ 0 & G_{32}(s) & G_{33}(s) \end{bmatrix} \begin{bmatrix} u_1 \\ u_2 \\ u_3 \end{bmatrix}.$$

If we use one of the gramian based measures to find a IM it will result in the following:

$$\Gamma = \begin{bmatrix} \gamma_{11} & \gamma_{12} & \gamma_{13} \\ 0 & \gamma_{22} & \gamma_{23} \\ 0 & \gamma_{32} & \gamma_{33} \end{bmatrix}.$$

Scaling this with the Sinkhorn-Knopp algorithm will ensure that both the rows and columns are normalized resulting in the following IM:

$$\Gamma_{SK} = \begin{bmatrix} \gamma_{11} & 0 & 0 \\ 0 & \gamma_{22}^* & \gamma_{23}^* \\ 0 & \gamma_{32}^* & \gamma_{33}^* \end{bmatrix}.$$

As can be seen the elements γ_{12} and γ_{13} in the interaction measure become zero. This means that if the Sinkhorn-Knopp scaled IM is used to find elements for feedforward it will disregard the possibility of adding feedforward to u_1. However, this is not desirable as γ_{12} or γ_{13} may indicate that feedforward on u_1 is appropriate. To resolve this we propose a hybrid system, where Sinkhorn-Knopp scaling is used to design a decentralized controller, and one of the other scaling methods is then used to determine which elements are appropriate for feedforward.

1.4 Testing the scaling methods for sparse control

To properly evaluate the feedforward methods we use the MIMO model generator described in Bengtsson and Wik [2017] to generate 200 linear MIMO-systems. We then generate sparse control configurations using the HIIA, with values of ρ ranging from 0 to 5. For each control configuration lambda tuned controllers are implemented, along with decoupling feedforward. The TFM was then tested for both reference step as well as disturbances. For disturbances we tested a step disturbance on u for only one of the outputs, for example:

$$\begin{aligned} y_1 &= G_{11}(s)(u_1 + d_1) + G_{12}(s)u_2 + ... + G_{1N}(s)u_N \\ y_2 &= G_{21}(s)u_1 + G_{22}(s)u_2 + ... + G_{2N}(s)u_N \\ &\vdots \end{aligned}$$

where the disturbance henceforth referred to as an individual disturbance is only on the transfer function from u_1 to y_1 in this case. This disturbance was tested on each transfer function in the TFM. Once the tests were conducted we evaluated how well the different scaling methods worked for reference steps and for disturbances. We defined a cost being the squared deviation from the reference for 2000 time units after the reference step or the input disturbance. Having calculated this cost for each IM, each IM is given a score defined as

$$S = \frac{c_{min}}{c}$$

where S is the score of the IM, c is it's cost, and c_{min} is the lowest cost of all IMs for the system. The score was set to zero if the control scheme yielded unstable results. This measure was chosen to normalize the scores for each system between 0 and 1, to ensure that the results on different systems are comparable. This was done with each method given a score depending on how much it deviated from the set point compared to the other methods.

The average score for each method for each ρ is shown in Figure 1. Note that $\rho = -1$ is used to denote the system without any feedforward.

As can be seen in Figure 1 the hybrid scheme with Sinkhorn-Knopp scaling to design a decentralized controllers, and then column scaling to find feedforward elements yields the best result, at least for reference following. For individual disturbances, most of the hybrid methods seem to yield comparable results, with no method of scaling clearly preferable when finding elements for feedforward.

Fig. 1. Scores for different ρ and for difference reference steps and disturbances

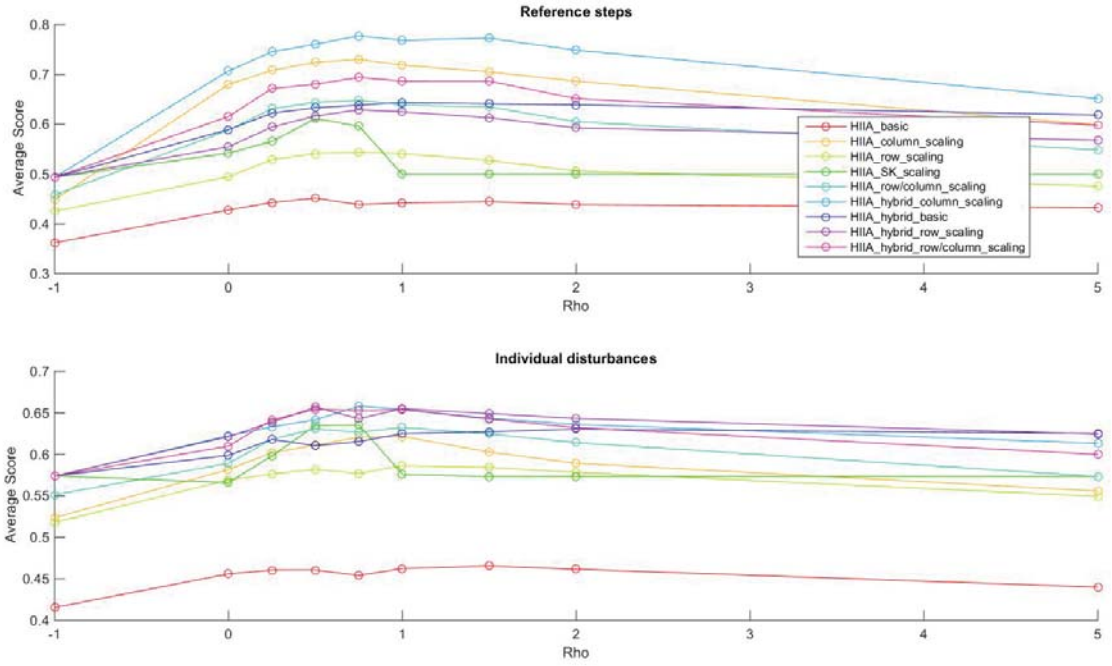

2. CONCLUSION

We have examined implementing feedforward using the HIIA interaction measure, and found that the best results were found when using Sinkhorn-Knopp scaling to find the decentralized control scheme, and then use column scaling to find elements for feedforward.

Furthermore, we also found that in general values of ρ ranging from $0.5 - 1$ seemed to yield the best results when implementing feedforward. It is noteworthy that $\rho = 0$ yielded comparably poor result, demonstrating the need to take into account the entire interaction matrix when choosing elements for feedforward, not only choosing the element representing the largest interaction.

REFERENCES

Bengtsson, F. and Wik, T. (2017). A multiple input, multiple output model generator. Technical report, Department of Signals and Systems, Chalmers University of Technology. URL `https://research.chalmers.se/publication/253490`.

Bengtsson, F., Wik, T., and Svensson, E. (2019). Resolving issues of scaling for gramian based input-output pairing methods. *Submitted for publication in Chemical Engineering Research and Design*.

Birk, W. and Medvedev, A. (2003). A note on gramian-based interaction measures. In *Proceedings of European Control Conference (ECC)*, 2625–2630.

Conley, A. and Salgado, M.E. (2000). Gramian based interaction measure. In *Proceedings of the 39th IEEE Conference on Decision and Control*, volume 5, 5020–5022. Citeseer.

Fatehi, A. (2011). Automatic pairing of large scale mimo plants using normalised rga. *International Journal of Modelling, Identification and Control*, 14(1-2), 37–45.

Khaki-Sedigh, A. and Moaveni, B. (2009). *Control configuration selection for multivariable plants*, volume 391. Springer.

Salgado, M.E. and Conley, A. (2004). MIMO interaction measure and controller structure selection. *International Journal of Control*, 77(4), 367–383.

Sinkhorn, R. and Knopp, P. (1967). Concerning nonnegative matrices and doubly stochastic matrices. *Pacific Journal of Mathematics*, 21(2), 343–348.

Wittenmark, B. and Salgado, M.E. (2002). Hankel-norm based interaction measure for input-output pairing. In *Proceedings of the 2002 IFAC World Congress*, volume 139.

Nonlinear Model Predictive Control-Based Algorithms for the Artificial Pancreas

Dimitri Boiroux [*], **Maria Sejersen Jensen** [*],
Ajenthen Ranjan [**], **Kirsten Nørgaard** [**],
John Bagterp Jørgensen [*]

[*] *Department of Applied Mathematics and Computer Science, Technical University of Denmark, DK-2800 Kgs. Lyngby, Denmark.*
[**] *Steno Diabetes Center Copenhagen, DK-2820 Gentofte, Denmark.*

Abstract: People with type 1 diabetes (T1D) can benefit from an automated system to administer the optimal dosage of diabetes-related drugs (insulin, and in some cases glucagon), also referred to as the artificial pancreas (AP). We present a prototype of AP developed at the Technical University of Denmark (DTU). The optimal drug dosage is based on continuous measurements of interstitial glucose concentration (and possibly other signals), previous drug administrations and a control algorithm using nonlinear model predictive control (NMPC). We build a nonlinear T1D model including the effects of insulin, glucagon, meal absorption and physical activity on the blood glucose concentration. We identify the T1D model using maximum likelihood estimation (MLE). Our algorithm for MLE is based on a continuous-discrete Kalman filter (CDEKF) for filtering and prediction, and the same filter is used in our NMPC algorithm. We use a local sequential quadratic programming algorithm to solve the optimal control problem. We present the outcomes of numerical simulations using virtual patients, and we show the implementation of our platform on an Android platform for clinical studies. We also discuss future possible improvements of our system.

Keywords: Closed-loop control, Nonlinear model predictive control, diabetes technology

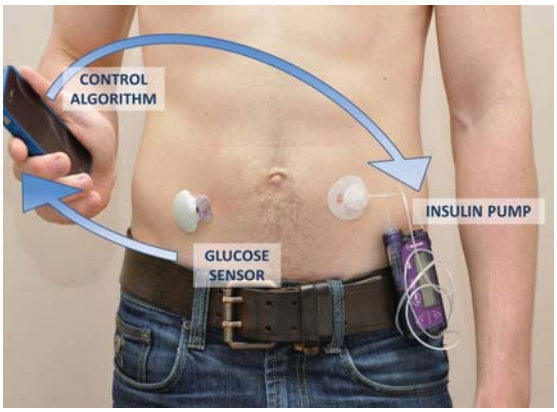

(a) Illustration of an AP system. A continuous glucose monitor provides frequent measurements of the interstitial glucose concentration. A control algorithm computes the optimal insulin (and possibly glucagon) dose and sends it to a pump.

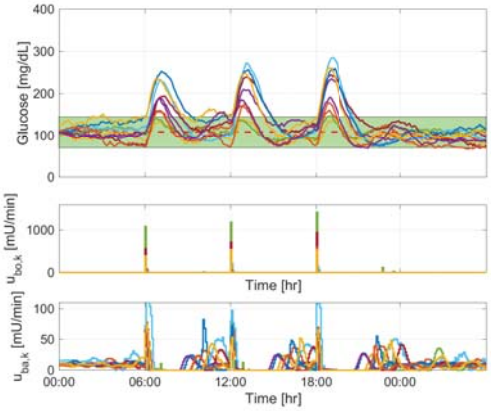

(b) Blood glucose concentration profiles (top), bolus insulin administration profile (middle) and basal insulin administration profile (bottom) for the 10 virtual patients.

(c) Illustration of the AP prototype used in clinical studies. The glucose sensor is a Dexcom G6. Two Dana RS pumps are used to administer insulin and glucagon. The smartphone (Samsung Galaxy A5) is used to monitor the blood glucose concentration and previous injections of insulin/glucagon, to announce meals and to announce physical activity.

Fig. 1. The AP system.

Proceedings of the 22nd Nordic Process Control Workshop
August 2019, Kgs. Lyngby, Denmark

A note on communicating vessels dynamics and controllability

Claes Breitholtz *

* *Chalmers University of Technology, Division of Systems and Control (e-mail: claesbr@chalmers.se).*

Abstract: Some hydrodynamical properties, static as well as dynamic, of communicating liquid vessels are considered in this article. It is shown how the back-stepping approach can be applied to control an arbitrary number of communicating vessels, hence indirectly showing local controllability of such a nonlinear system. Also, linearized models are investigated and compared to mathematically similar electrical networks. The analysis is extended to include a study on an infinite number of linearized communicating vessels, for which the passivity property is established.

Keywords: Communicating vessels, nonlinear model, steady states, back-stepping nonlinear control, linear model, electrical analogy, passivity property.

1. INTRODUCTION

There are a very large number of obvious applications of communicating vessels. They are to be found in nature such as biological systems (for example inside of human bodies), or geological formations (where water is fed into one cavity and further on into the next and so on). Also man-made systems, for example technologies for chemical plants as well as medical engineering make use of the communicating vessels principle. Two examples of the latter are the papers [1], [2]. Yet another example is the distribution of water over an agricultural plant.

A practical definition of the communicating vessels principle might be that the stored fluid in one vessel interacts mutually with the stored fluid of its closest neighbors. Communicating vessels constitutes a special case of tank systems. Such are investigated in the literature very early. As an example of general tank system investigation, could be mensioned the report [3]. Here the dynamics of substance propagation in hydrodynamical steady state is emphasized, implying the analysis of a time-invariant linear system, using impulse responses and transfer functions.

The use of tank systems as a way of demonstrating particular approaches to control is frequently seen. This is to a large extent due to that a suitable experimental setup most often is not too hard or expensive to realize in a laboratory environment. One (out of many) recent example is the article [4]. Here a three-tank system is used to demonstrate a modelling approach using neural networks to approximate coefficients in a state dependent ARX-model. This model is then used in MPC-control.

A recent paper [5] deals with the model analysis of two coupled communicating vessels for an ideal fluid. Here an autonomous system (without external flow), assuming ignorable dissipation, is studied. The system oscillatory properties is analyzed using a perturbation method and demonstrated in phase plane.

This work emphasizes some hydrodynamical aspects on communicating vessels. One such aspect is which steady states that are possible, assuming one external source of liquid flow to the system. Another aspect is how perturbations in a neighborhood of steady state relates to this steady state. The control of a sequence of communicating vessels is considered, using the back-stepping approach on the nonlinear system model. See [6].

Attention to the corresponding linearized systems is made as well. Particularly the mathematical analogy between linearized tank-systems and electrical RC-networks, as described by [7], is applied to communicating vessels. For example, the external liquid flow entering a tank system corresponds to an ideal current source entering a network of resistors and capacitors and the stored liquid volumes correspond to voltages. Finally, one example is given on the dynamics of a countably infinite number of vessels, for which the passivity property is shown.

2. PRELIMINARY ASSUMPTIONS

The model system is depicted in figure 1. The treatment is here restricted to one external input flow. There is no particular difficulty in adding more external inputs. However, some detailed results are then due to which vessels having an external input and which have not. The same thing can be said of exactly how a pipe connecting two vessels is positioned. Here it is assumed that all connections are positioned at the vessel bottom, vertically if the fluid is departing the system or horizontally if transported to a neighboring vessel. All vessels are assumed cylindrical in the sense that their volumes are given by the product of vessel cross sectional area and surface level related to vessel bottom. Channel volumes are assumed to be ignorable compared to vessel volumes. Consequently, communicating channel dynamics is ignored in the following. Furthermore, stored as well as flowing fluid is assumed to be in the incompressible liquid phase.

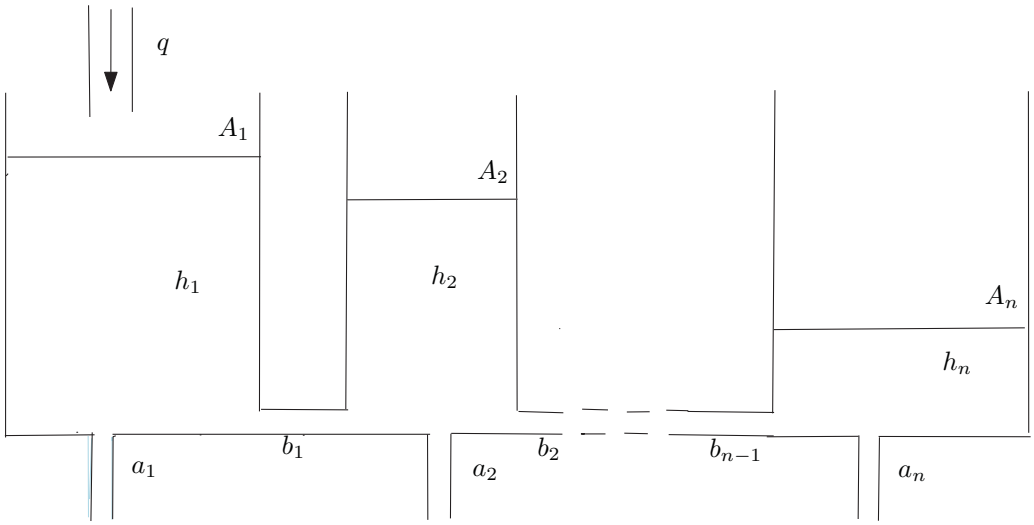

Fig. 1. The communicating vessels system

The external liquid flow $[m^3/s]$ is denoted by q and the dynamical liquid levels by $h_1, h_2, ..., h_n$, respectively. Vessel cross sectional areas are denoted by $A_1, A_2, ...A_n$. Vessel bottom outlet areas are denoted by $a_1, a_2, ...a_n$ and communicating channel areas by $b_1, b_2, ...b_{n-1}$. g denotes the acceleration of gravity, here assumed a constant.

3. SYSTEM MODEL AND STEADY STATES

Based on the Bernoulli law, see [6], and provided the above system assumptions hold, the following ordinary differential equation model describes the system sufficiently well:

$$\begin{aligned}
\frac{d}{dt}(A_1h_1(t)) &= q(t) - a_1\sqrt{2gh_1(t)} - \\
&\quad b_1\sqrt{2g(h_1(t)-h_2(t))} \\
\frac{d}{dt}(A_2h_2(t)) &= b_1\sqrt{2g(h_1(t)-h_2(t))} - \\
&\quad a_2\sqrt{2gh_2(t)} - b_2\sqrt{2g(h_2(t)-h_3(t))} \\
&\vdots \\
\frac{d}{dt}(A_{n-1}h_{n-1}(t)) &= b_{n-2}\sqrt{2g(h_{n-2}(t)-h_{n-1}(t))} - \\
&\quad a_{n-1}\sqrt{2gh_{n-1}(t)} - b_{n-1}\sqrt{2g(h_{n-1}(t)-h_n(t))} \\
\frac{d}{dt}(A_nh_n(t)) &= b_{n-1}\sqrt{2g(h_{n-1}(t)-h_n(t))} - \\
&\quad a_n\sqrt{2gh_n(t)}
\end{aligned} \tag{1}$$

To secure a well defined model, obviously it must hold that $h_k(t) \geq h_{k+1}(t)$ for all integer k and real t. This is intuitively correct assuming that the external inlet flow enters from one side (here the left) and the internal channel flow is driven by a positive level difference between one vessel and its right neighbor. The possible steady states $h_{1,0}, ..., h_{n,0}$ corresponding to a constant external input q_0 are given by the following system of equations. The extra index 0, denoting steady state, is temporarily dropped for the sake of simplicity.

$$\begin{aligned}
q/\sqrt{2g} &= a_1\sqrt{h_1} + b_1\sqrt{h_1-h_2} \\
0 &= b_1\sqrt{h_1-h_2} - a_2\sqrt{h_2} - b_2\sqrt{h_2-h_3} \\
&\vdots \\
0 &= b_{n-2}\sqrt{h_{n-2}-h_{n-1}} - a_{n-1}\sqrt{h_{n-1}} \\
&\quad - b_{n-1}\sqrt{h_{n-1}-h_n} \\
0 &= b_{n-1}\sqrt{h_{n-1}-h_n} - a_n\sqrt{h_n}
\end{aligned} \tag{2}$$

Using the last equation, h_{n-1} can be expressed as function of h_n:

$$h_{n-1} = [1 + (\frac{a_n}{b_{n-1}})^2]h_n = (\psi_{n-1})^2 h_n \tag{3}$$

$$\psi_{n-1} = \sqrt{1 + (\frac{a_n}{b_{n-1}})^2} \tag{4}$$

The next step is to express h_{n-2} as function of h_n:

$b_{n-2}\sqrt{h_{n-2}-h_{n-1}} = a_{n-1}\sqrt{h_{n-1}} + b_{n-1}\sqrt{h_{n-1}-h_n} = a_{n-1}\psi_{n-1}\sqrt{h_n} + a_n\sqrt{h_n}$

$h_{n-2} = [(\psi_{n-1})^2 + (\frac{a_{n-1}\psi_{n-1}+a_n}{b_{n-2}})^2]h_n = (\psi_{n-2})^2 h_n$

In the last step we can express

$$h_{n-k} = (\psi_{n-k})^2 h_n \tag{5}$$

$$\psi_{n-k} = \sqrt{(\psi_{n-k+1})^2 + (b_{n-k})^{-2}(\sum_{i=n}^{n-k+1} a_i\psi_i)^2} \tag{6}$$

$$\psi_n = 1 \tag{7}$$

Using equations 5,6 and 7, all vessel levels can be expressed as function of h_n and piping cross sectional areas. h_n, finally, can then be directly related to the external input flow using the upper line of equation (2):

$$h_n = \frac{q^2}{2g[a_1\psi_1 + b_1\sqrt{\psi_1^2 - \psi_2^2}]} \tag{8}$$

It is then concluded that the steady state liquid levels decrease, to guarantee a one-direction steady state liquid flow. Obviously, the sequence of coefficients ψ_k is monotonically decreasing, having a lower bound $\psi_n = 1$.

The steady state output flow from vessel k (leaving the system) is obviously $q_k = a_k\sqrt{2gh_k}$. Assume that equal steady state output flows are requested in, for the sake of simplicity, a system of two vessels. Then, $a_1^2h_1 = a_2^2h_2$ must hold, resulting in the geometrically interpretable condition: $(\frac{a_1}{a_2})^2 + (\frac{a_1}{b_1})^2 = 1$.

Lets, still without introducing dynamics, consider small perturbations in neighborhoods of the steady states. Starting by linerizing equation 2, we get

$$\begin{aligned}
\Delta q &= a_1\sqrt{\frac{g}{2h_1}}\Delta h_1 + b_1\sqrt{\frac{g}{2(h_1-h_2)}}(\Delta h_1 - \Delta h_2)\\
0 &= b_1\sqrt{\frac{g}{2(h_1-h_2)}}(\Delta h_1 - \Delta h_2) - a_2\sqrt{\frac{g}{2h_2}}\Delta h_2 -\\
&\quad b_2\sqrt{\frac{g}{2(h_2-h_3)}}(\Delta h_2 - \Delta h_3)\\
&\vdots\\
0 &= b_{n-2}\sqrt{\frac{g}{2(h_{n-2}-h_{n-1})}}(\Delta h_{n-2} - \Delta h_{n-1}) -\\
&\quad a_{n-1}\sqrt{\frac{g}{2h_{n-1}}}\Delta h_{n-1} - b_{n-1}\sqrt{\frac{g}{2(h_{n-1}-h_n)}}(\Delta h_{n-1} - \Delta h_n)\\
0 &= b_{n-1}\sqrt{\frac{g}{2(h_{n-1}-h_n)}}(\Delta h_{n-1} - \Delta h_n) - a_n\sqrt{\frac{g}{2h_n}}\Delta h_n
\end{aligned} \tag{9}$$

Let us introduce the flow conductances (inverses of flow resistances), ϑ_k and $\eta_{k,k+1}$, where

$$\vartheta_k = a_k\sqrt{\frac{g}{2h_k}} \tag{10}$$

$$\eta_k = b_k\sqrt{\frac{g}{2(h_k - h_{k+1})}} \tag{11}$$

Using equations 10 and 11, the linearized model 9 can be rewritten as

$$\begin{aligned}
\Delta q - (\vartheta_1 + \eta_1)\Delta h_1 + \eta_1\Delta h_2 &= 0\\
\eta_1\Delta h_1 - (\vartheta_2 + \eta_1 + \eta_2)\Delta h_2 + \eta_2\Delta h_3 &= 0\\
&\vdots\\
\eta_{n-2}\Delta h_{n-2} - (\vartheta_{n-1} + \eta_{n-2} + \eta_{n-1})\Delta h_{n-1} +&\\
\eta_{n-1}\Delta h_n &= 0\\
\eta_{n-1}\Delta h_{n-1} - (\vartheta_n + \eta_{n-1})\Delta h_n &= 0
\end{aligned} \tag{12}$$

Suppose it is desirable that all ϑ_k and all η_k were independent of k. If so, equation (13) would be modified into

$$\begin{aligned}
\Delta q - (\vartheta + \eta)\Delta h_1 + \eta\Delta h_2 &= 0\\
\eta\Delta h_1 - (\vartheta + 2\eta)\Delta h_2 + \eta\Delta h_3 &= 0\\
&\vdots\\
\eta\Delta h_{n-2} - (\vartheta + 2\eta)\Delta h_{n-1} + \eta\Delta h_n &= 0\\
\eta\Delta h_{n-1} - (\vartheta + \eta)\Delta h_n &= 0
\end{aligned} \tag{13}$$

This is indeed possible. The implication from equations (5) and (11) would be that

$$\frac{a_{n-k+1}}{a_{n-k}} = \frac{\psi_{n-k+1}}{\psi_{n-k}}, k = 1, 2, ..., n-1 \tag{14}$$

which is an under determined system of equations. If, for example n=2, we would obtain: $(\frac{a_1}{a_2})^2 - (\frac{a_2}{b_1})^2 = 1$.

From this simple example, we can also conclude that equal flow conductances *and* equal stationary flows implies a contradiction: $(\frac{a_1}{a_2})^2 = 1 + (\frac{a_2}{b_1})^2 = 1 - (\frac{a_1}{b_1})^2$.

Suppose that, again for n=2, equal flow conductances ϑ_1, ϑ_2 are required and the possible ranges of stationary outlet flows q_1, q_2 are to be determined. Assume that $0 < \theta < 1$ and that $q_1 = \theta q, q_2 = (1-\theta)q$. Simple calculations show that $\frac{b_1}{a_2} = \sqrt{\frac{1-\theta}{2\theta-1}}$, implying that $1/2 < \theta < 1$. One might ask if $\vartheta = \eta$ would be possible. This is only possible if $\theta = 2/3$, implying that $q_1 = 2q_2$.

An extended version of equation (1) can serve as a basis for nonlinear dynamic simulation. A few comments are given in appendix A.

4. CONTROLLABILITY OF THE NONLINEAR DYNAMICAL SYSTEM

We now return to the dynamical system, described by equation (1). The purpose is not to investigate the best possible control strategy for the communicating vessel system (model predictive control, distributed PID-control, H-infinity control or some other approach to control), but rather to find out if this nonlinear system is at least possible to stabilize locally around the steady states $h_{1,0}, ..., h_{n,0}$. Let us change state and control variables:

$$h_k(t) = h_{k,0} + z_k(t), k = 1, ..., n \tag{15}$$

$$q(t) = q_0 + u(t) \tag{16}$$

Also introduce the positive coefficients

$$d_k = h_{k,0}, k = 1, ..., n \tag{17}$$

$$e_k = h_{k,0} - h_{k+1,0}, k = 1, ..., n-1 \tag{18}$$

$$\alpha_k = (a_k/A_k)\sqrt{2g}, k = 1, ..., n \tag{19}$$

$$\beta_k = (b_k/A_k)\sqrt{2g}, k = 1, ..., n-1 \tag{20}$$

$$\beta_{k-1,k} = (b_{k-1}/A_k)\sqrt{2g}, k = 1, ..., n-1 \tag{21}$$

We can now rewrite equation (1) as

$$\begin{aligned}
\frac{d}{dt}z_1(t) &= (u(t)+q_0)/A_1 - \alpha_1\sqrt{z_1(t)+d_1} - \\
&\quad \beta_1\sqrt{z_1(t)-z_2(t)+e_1} \\
\frac{d}{dt}z_2(t) &= \beta_{1,2}\sqrt{z_1(t)-z_2(t)+e_1} - \\
&\quad \alpha_2\sqrt{z_2(t)+d_2} - \beta_2\sqrt{z_2(t)-z_3(t)+e_2} \\
&\quad \vdots \\
\frac{d}{dt}z_{n-1}(t) &= \beta_{n-2,n-1}\sqrt{z_{n-2}(t)-z_{n-1}(t)+e_{n-2}} - \\
&\quad \alpha_{n-1}\sqrt{z_{n-1}(t)+d_{n-1}} - \\
&\quad \beta_{n-1}\sqrt{z_{n-1}(t)-z_n(t)+e_{n-1}} \\
\frac{d}{dt}z_n(t) &= \beta_{n-1,n}\sqrt{z_{n-1}(t)-z_n(t))+e_{n-1}} - \\
&\quad \alpha_n\sqrt{z_n(t)+d_n}
\end{aligned} \tag{22}$$

Equation (22) has an input affine structure, $\frac{d}{dt}z = f(z) + g(z)u$, where z is the state vector. The vector fields f and g are both continuous functions of state (but not time explicitly). In our application the vector field g is a constant column vector, having the first component $1/A_1$ and the rest being zeros. It is, due to the definition of state and control variables, obvious that $z = 0, u = 0$ constitutes an equilibrium point for the nonlinear system. The conditions for the vector field f to be well defined is:

$$z_k > -d_k, 1 \le k \le n \tag{23}$$
$$z_k < z_{k-1} + e_{k-1}, 2 \le k \le n \tag{24}$$

Denoting the subset of R^n where inequalities (23),(24) hold by Ω, the local controllability in Ω of the system (22) will be showed. One way to do so is to show that the vector fields $[g, ad_f g, ..., ad_f^{n-1} g]$ are linearily independent in Ω. Here, $ad_f g = [f, g] = (\nabla g)f - (\nabla f)g$, is the Lie bracket of f and g (∇f denotes the Jacobian of f) and $ad_f^k g = [f, ad_f^{k-1} g]$. See [8]. An indirect way of showing local controllability is directly to design a stabilizing controller for the nonlinear system, a controller that not necessarily has to be (in some sense) the best possible controller for the system. The structure of the communicating vessel system implies that, for row k, as most the states corresponding to $k-1, k, k+1$ are involved. This situation promotes the approach to control, known as back-stepping. See [7]. As back-stepping constitutes a well known control method for control input affine nonlinear systems, having this structure, it is sufficient to explain how the method will work. To further promote simplicity, suppose $n = 3$. The system is for $n = 3$ described by the three differential equations:

$$\frac{d}{dt}z_1(t) = (u(t)+q_0)/A_1 - \alpha_1\sqrt{z_1(t)+d_1} - \beta_1\sqrt{z_1(t)-z_2(t)+e_1} \tag{25}$$
$$\frac{d}{dt}z_2(t) = \beta_{1,2}\sqrt{z_1(t)-z_2(t)+e_1} - \alpha_2\sqrt{z_2(t)+d_2} - \beta_2\sqrt{z_2(t)-z_3(t)+e_2} \tag{26}$$
$$\frac{d}{dt}z_3(t) = \beta_{2,3}\sqrt{z_2(t)-z_3(t))+e_2} - \alpha_3\sqrt{z_3(t)+d_3} \tag{27}$$

If in equation (27), z_2 is formally considered as the control input, a control policy is to be derived that results in the feedback system $\dot{z}_3(t) = -\nu_3 z_3(t)$ where $\nu_k > 0, k = 1, 2, 3$. This implies that $\sqrt{z_2 - z_3 + e_2} = \beta_{2,3}^{-1}[-\nu_3 z_3 + \alpha_3\sqrt{z_3 + d_3}]$ or more explicitly $z_2 = z_3 - e_2 + [\beta_{2,3}^{-2}[-\nu_3 z_3 + \alpha_3\sqrt{z_3(t)+d_3}]^2$, which expressions can be inserted in equation (26):

$\dot{z}_2 = \beta_{1,2}\sqrt{z_1 - z_2 + e_1} - \alpha_2\sqrt{z_2 + d_2} - \beta_2\sqrt{z_2 - z_3 + e_2}$
The right hand side is a function of z_1, z_2, z_3, where z_3 already is secured to exponentially approach zero. Again, assuming that z_1 is the control input, a control policy is to be derived that results in the feedback system $\dot{z}_2(t) = -\nu_2 z_2(t)$. Then we have an expression for z_1 in terms of z_2, z_3, both approaching zero exponentially, to be inserted into equation (25). Finally, the real control input u is found to result in the feedback system $\dot{z}_1(t) = -\nu_1 z_1(t)$. The resulting feedback system is hence

$$\dot{z}_1(t) = -\nu_1 z_1(t) \tag{28}$$
$$\dot{z}_2(t) = -\nu_2 z_2(t) \tag{29}$$
$$\dot{z}_3(t) = -\nu_3 z_3(t) \tag{30}$$

where ν_1, ν_2, ν_3 are positive design parameters, free of choice. Exactly the same approach can obviously be applied for $n = 4$ or any arbitrary order, resulting in, using matrix/vector notation,

$$\dot{z}(t) = -Nz(t) \tag{31}$$
$$N = diag[\nu_1, ..., \nu_n] \tag{32}$$

As N is a positive definite matrix, the feedback state equation is exponentially stable. In other words, the nonlinear communicating vessels system is locally controllable in Ω.

Remark 1: Assume that an input affine nonlinear system is locally controllable in a set Ω. The corresponding linearized system in the neighborhood of an operating point in Ω is in general not controllable in the linear sense.

Remark 2: An assumption of major importance made, not previously commented on, is that the state vector z is assumed to be known at every time t. The practical implication of this assumption is either that every component of the state vector can be accurately measured, or that from more restricted measurements, for example the scalar output $y = z_1$, the state vector z can be reconstructed by an observer. The design of nonlinear observers is, however, outside the scope of this paper.

5. PHYSICAL ANALOGY TO THE LINEARIZED DYNAMICAL COMMUNICATING VESSELS SYSTEM

The linearized dynamical model, corresponding to the nonlinear model of equation (1), can be written as equation (12), but with the right hand zeros replaced by $\frac{d}{dt}(A_1\Delta h_1(t)), ..., \frac{d}{dt}(A_n\Delta h_n(t))$. The $\vartheta_k, k = 1, ..., n$ and the $\eta_k, k = 1, ..., n-1$, defined be equations (10) and (11), again represent the flow conductances. For example in the case $n = 3$ we get:

$$dt(A_1\Delta h_1) = \Delta q - (\vartheta_1 + \eta_1)\Delta h_1 + \eta_1\Delta h_2 \tag{33}$$
$$dt(A_2\Delta h_2) = \eta_1\Delta h_1 - (\vartheta_2 + \eta_1 + \eta_2)\Delta h_2 + \eta_2\Delta h_3 \tag{34}$$
$$dt(A_3\Delta h_3) = \eta_2\Delta h_2 - (\vartheta_3 + \eta_2)\Delta h_3 \tag{35}$$

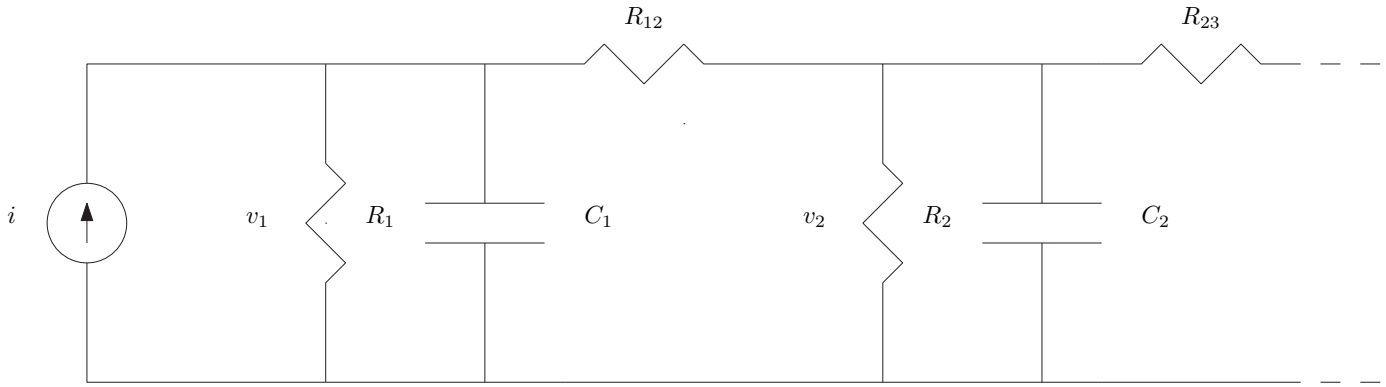

Fig. 2. The electric network corresponding to the communicating vessels system

Now, consider the time-invariant linear system from another physical area than fluid mechanics, lumped electrical networks or more specifically the RC-type circuit depicted in figure 2. To promote comparison, a circuit with three capacitors (dynamic elements) is chosen as an example.

The ideal current source i is an external system input and the voltages v_1, v_2, v_3 over the capacitors are possible state variables. The system model is directly a consequence of the well known laws of Kirchoff and Ohm. See for example [9], or numerous other books on basic electric circuit theory.

$$0 = i - v_1/R_1 - C_1\dot{v}_1 - (v_1 - v_2)/R_{12} \quad (36)$$
$$0 = (v_1 - v_2)/R_{12} - v_2/R_2 - C_2\dot{v}_2 - (v_2 - v_3)/R_{23} \quad (37)$$
$$0 = (v_2 - v_3)/R_{23} - v_3/R_3 - C_2\dot{v}_2 \quad (38)$$

If resistances are replaced by conductances, $G_1 = 1/R_1, ...,$ we get the resulting circuit model:

$$dt(C_1v_1) = i - (G_1 + G_{12})v_1 + G_{12}v_2 \quad (39)$$
$$dt(C_2v_2) = G_{12}v_1 - (G_2 + G_{12} + G_{23})v_2 + G_{23}v_3 \quad (40)$$
$$dt(C_3v_3) = G_{23}v_2 - (G_3 + G_{23})v_3 \quad (41)$$

Obviously the models (33)-(35) and (39)-(41) coincide exactly with respect to mathematical structure. The differences are due to the choices of parameter notation only. For example the vessel cross sectional areas $A_1, A_2, ...$ correspond to capacitances $C_1, C_2, ...$ The conclusion is that analysis of linearized dynamical models of communicating vessels can alternatively be carried out by analysis of the above kind of electric circuits. For example, the transfer function from a small input flow perturbation Δq to the perturbation in the first vessel level Δh_1, can be exactly interpreted as the transfer function from external input current i to voltage v_1. In the electrical case the transfer function is the network input impedance Z(s).

$$\Delta H_1(s) = G(s)\Delta Q(s) \quad (42)$$
$$V_1(s) = Z(s)I(s) \quad (43)$$

6. SOME BASIC PROPERTIES OF LINEARIZED COMMUNICATING VESSELS SYSTEMS

In section 4 it was pointed out that local stability of a nonlinear system does not in general guarantee stability for the linearized system, having the structure $\dot{x}(t) = Ax(t) + Bu(t)$, where x and u denotes the state vector and the control input of the linearized system. Controllability of a time-invariant linear system of order n is secured if the matrix $S = [B, AB, ..., A^{n-1}B]$ has full rank. For a scalar u, this is the case, if the determinant of S is non-zero. See [10] or [11].

Consider an n-dimensional extension of the model (33)-(35), it is obvious that the A-matrix will have a banded structure, resulting in an upper triangular controllability matrix S, which is full rank as all diagonal elements are non-zero. Hence the linearized communicating vessel system is controllable.

Consider the same state space model as above, but having an output. For example, choose the first vessel liquid level Δh_1 as the output. In the electric analogy this output corresponds to the first capacitor voltage v_1. From an applicative perspective, this choice can be justified as the level closest to the liquid source is likely to be easily measured.

The question to be answered is if the full state vector can be reconstructed from this output, or in other words if the system is observable. The equation relating the output y to the state x and the input u is $y = Cx + Du$, where in our application $C = [1, 0, ..., 0], D = 0$. Observability of a time-invariant linear system of order n is secured if the matrix $O^T = [C^T, A^TC^T, ..., (A^T)^{n-1}C^T]$ has full rank. Again, see [10] or [11].

It turns out that the observability matrix O is lower triangular, which is full rank as all diagonal elements are non-zero. Hence the linearized communicating vessel system, having the first state as the output, is observable. This means that, having accurate knowledge of the first state vector component, the other components can be estimated by an observer such as a Kalman filter. See, for example, [12].

It is then concluded that the linearized communicating vessel system as well as the corresponding electric circuit, are both controllable and observable. Hence these systems are minimal order, implying that the corresponding transfer function $G(s) = C(sI - A)^{-1}B + D$ has no common pole or zero factors to be canceled.

It can also be noted that the transfer function is strictly proper as the matrix D is zero (the output is not directly dependent of the input). See [10].

7. AN ASYMPTOTIC STUDY OF LINEARIZED COMMUNICATING VESSELS SYSTEMS

In this section the following additional assumptions are made to promote further analysis:

1. The conductances $\vartheta_k = \vartheta, \eta_k = \eta$ are k-independent.

2. The vessel areas $A_k = A$ are equal and k-independent.

3. The corresponding electric parameters are k-independent. It is assumed that all capacitances are C, the resistors shunting them are all R_1 and the resistors connecting two neighboring parallel circuits are all R_2.

Consider the input impedance Z_n in the Laplace domain, where n is the system order, equal to the number of capacitors (exactly corresponding to the number of tanks in the linearized communicating vessels system).

For $n = 1$ and $n = 2$ we have:

$Z_1(s) = \frac{R_1}{1+sCR_1}$, $Z_2(s) = \frac{R_1(R_1+R_2+sCR_1R_2)}{(1+sCR_1)(2R_1+R_2+sCR_1R_2)}$

For two communicating vessels ($n = 2$) we have:

$G_2(s) = \frac{\vartheta+\eta+sA}{(\vartheta+sA)(\vartheta+2\eta+sA)}$

For reasonably low orders, transfer functions are not too cumbersome to give. For larger numbers, they are impractical to use. For simulations, state-space models are more practical to use. However, for very large orders this will also fail. One might ask if the sets of transfer functions $[G_1, G_2, ..., G_n], [Z_1, Z_2, ..., Z_n]$ will converge to transfer functions G or Z as n approaches infinity. Consider the electrical case. Assuming the existence of such an input impedance, nothing would change if yet another sub system, R_1, R_2, C was similarly connected to the already countably infinite order system. The input impedance would remain to be Z, resulting in the equality

$$Z(s) = \frac{\frac{R_1}{1+sCR_1}(R_2 + Z(s))}{\frac{R_1}{1+sCR_1} + R_2 + Z(s)} \tag{44}$$

Solving for Z, we obtain the expression

$$Z(s) = \frac{R_2}{2}[\sqrt{1 + \frac{4R_2/R_1}{sCR_1 + 1}} - 1] \tag{45}$$

In the communicating vessels case the transfer function can then be written

$$G(s) = \frac{1}{2\eta}[\sqrt{\frac{s + (\vartheta/A)(1 + 4\vartheta/\eta)}{s + \vartheta/A}} - 1] \tag{46}$$

The corresponding impulse response can directly be obtained from tables of Laplace transform pairs. See for example [13].

$$g(t) = \frac{\vartheta^2}{A\eta^2} e^{-[\frac{\vartheta}{A} + \frac{2\vartheta^2}{\eta A}]t}[I_0(\frac{2\vartheta^2 t}{\eta A}) + I_1(\frac{2\vartheta^2 t}{\eta A})] \tag{47}$$

Here $I_0(x), I_1(x)$ denotes the modified Bessel functions of the first kind and of orders zero and one, respectively. It can be shown that the function $e^{-x}(I_0(x) + I_1(x))$ is lower and upper bounded and hence $g(t)$, due to the extra factor $e^{-(\vartheta/A)t}$, is an exponentially decreasing function. This implies that the step response is bounded and the system is input to output stable. However, we would as well establish passivity of the linear time-invariant (LTR) systems (45) and (46), differing only in parametrization.

It is well known that electric lumped linear RC-networks (RL- and RLC-networks as well) are passive and actually dissipative. See for example the book [14], where the concepts of positive realness and strictly positive realness are used, concepts that for LTR-systems largely coincide with passive and dissipative. See [7], [8].

Consider the sequence of impedances $[Z_1(s), Z_2(s), ..., Z_n(s)]$, where each element represents a dissipative or strictly positive real rational transfer function. Letting n approach infinity, the sequence approaches a non-rational limit transfer function, which is obviously outside the sequence. We will now show that it is strictly positive real or dissipative.

Theorem: A transfer function $h(s)$ is strictly positive real (SPR) if and only if

(1) h(s) is an input to output stable transfer function

(2) the real part of $h(s)$ is strictly positive along the imaginary $j\omega$-axis: $Re[h(j\omega)] > 0, \forall\omega \geq 0$

For proof, see [8].

We have already showed (1) input to output stability of the transfer function, but (2) remains to be shown. The transfer function has the structure $g(s) = \sqrt{\frac{s+a+b}{s+a}} - 1$, where a and b are positive constants. Instead of analyzing $g(j\omega)$, we analyse g with respect to the scaled frequency $\nu = \omega/a$. Introducing $\mu = b/a$ and $\gamma = \nu^2 + 1 + \mu$, we have

$g(j\nu) = \sqrt{\frac{j\nu+1+\mu}{j\nu+1}} - 1 = \sqrt{\frac{\sqrt{\gamma^2+\mu^2\nu^2}}{\nu^2+1}} e^{-j\arctan(\frac{\mu\nu}{\gamma})} - 1$

Letting $\theta = -\arctan(\frac{\mu\nu}{\gamma})$, we have to show that

$Re[g(j\nu)] = \sqrt{\frac{\sqrt{\gamma^2+\mu^2\nu^2}}{\nu^2+1}}\cos(\theta/2) - 1 > 0$ implying that

$\frac{\sqrt{\gamma^2+\mu^2\nu^2}}{\nu^2+1}(1 + \cos\theta) > 2$

As $|\theta| < \pi/2$ we can use that $\cos\theta = 1/\sqrt{1 + \tan^2\theta}$:

$1 + \cos\theta = 1 + 1/\sqrt{1 + (\frac{\mu\nu}{\gamma})^2} = \frac{\gamma+\sqrt{\gamma^2+\mu^2\nu^2}}{\sqrt{\gamma^2+\mu^2\nu^2}}$

Inserting this expression into the inequality and multiplying by $\nu^2 + 1$ we get

$\gamma + \sqrt{\gamma^2 + \mu^2\nu^2} > 2(\nu^2 + 1)$

However 2γ is a lower bound of the left hand side and an upper bound of the right hand side of the inequality. Consequently it holds that $Re[g(j\nu)] > 0$, implying that $g(s)$ is strictly positive real and the limit transfer function hence dissipative.

8. CONCLUSIONS

A sequence of cylindrical vessels is assumed to be fed by an external liquid flow from one end, where each vessel communicates with its left and right neighbor as well as having its own outlet. The system states are the liquid levels of each vessel. A system model based on the Bernoulli equation is given. A systematic way of obtaining the steady states for an arbitrary long sequence of such vessels is presented, based on fractions between channel cross sectional areas. Conditions for equal output flows and for equal differential flow conductances are given and found to exclude each other.

The controllability of this nonlinear system, using the external flow as the control input and assuming the state to be known, is discussed. Controllability is established by the design of a nonlinear controller, based on the back-stepping approach. The resulting feedback system is locally exponentially stable.

The linearized system model (with respect to the steady state) is shown to be mathematically analogue to an electrical RC-network, having exactly the same state equation structure. The transfer function from small perturbations in the input flow to the corresponding variations in, for example, the first vessel liquid level, is mathematically identical to the electrical input impedance relating the input current to the input voltage. Controllability and observability of the linearized system is shown as well.

It is a fact that impedances made up by finite R and C combinations, not only are input to output stable but also strictly positive real functions. In the special case of equal shunt resistances, series resistances and capacitances in each link (corresponding to each vessel) the resulting impedance, as the number of links (vessels) approaches infinity, is obtained. This impedance function is not possible to describe on state-space form, but is shown to be input to output stable and moreover strictly positive real.

REFERENCES

[1] Stefanov, M., Potroz, M., Kim, J., Lim, J., Cha, R. and Nam, M.-H. (2013). The Primo Vascular System as a New Anatomical System. Journal of Acupuncture and Meridian Studies. Vol. 6, Issue 6, Dec. 2013, Pages 331-338.

[2] Quintero, R.A., Martinez, J.M., Lopez, J., Bermudez, C., Becerra, C., Morales, W. and Arroyo, J. (2005). Individual placental territories after selective laser photocoagulation of communicating vessels in twin-twin transfusion syndrome. American Journal of Obstetrics and Gynecology 192, 1112-8.

[3] Astrom, K.J. (1975). Flow Systems. (Report TFRT; Vol. 7087). Department of Automatic Control, Lund Institute of Technology (LTH).

[4] Zhou, F., Peng, H., Zeng, X., Tian, X. and Wu, J. (2017). Modeling and Control Approach to Coupled Tanks Liquid Level System Based on Function-Type Weight $RBF - ARX$ Model. Asian Journal of Control. Vol. 19, Issue 2, Mar. 2017, Pages 692-707.

[5] De Luca, R. and Faella, O. (2017). Communicating Vessels: a nonlinear dynamical system. Revista Brasileira de Ensino de Fisica. Vol. 39, No 3, 2017.

[6] Khalil, H. (2002). Nonlinear Systems (third edition). Prentice-Hall, Inc. Upper Saddle River, NJ 07458.

[7] Yang, W.-J. and Masubuchi, M. (1970). Dynamics for Process and System Control. Gordon and Breach, Science Publishers, Inc., 150 Fifth Avenue, New York, N.Y. 10011.

[8] Slotine, J.-J. E. and Li, W. (1991). Applied Nonlinear Control. Prentice-Hall, Inc. Englewood Cliffs, NJ 07632.

[9] Dorf, R. C. and Svoboda, J. A. (2011). Introduction to Electric Circuits. John Wiley and Sons (ASia). Pte Ltd.

[10] Rugh, W. R. (1996). Linear System Theory (second edition). Prentice-Hall, Inc. Englewood Cliffs, NJ 07458.

[11] Brocket, R. W. (1970). Finite Dimensional Linear Systems. John Wiley and Sons, Inc.

[12] Skogestad, S. and Postlethwaite, I. (2005). Multivariable Feedback Control. John Wiley and Sons Ltd.

[13] Abramowitz, M. and Stegun, I. (1964). Handbook of Mathematical Functions. National Bureau of Standards. Applied Mathematics Series, 55.

[14] Hazony, D. (1963). Elements of Network Synthesis. Reinhold Electrical Engineering Sciences Textbook Series. Chapman and Hall Ltd, London.

Appendix A. SIMULATION ASPECTS

Consider the nonlinear communicating vessels model given by equation (1). Letting $q = q_1$ in the first equation, adding of a new external input q_2 in the second, q_3 in the third and so on, will result in a multi input system. It is from now on not secured that, for example, $\sqrt{h_{n-1} - h_n}$ is well defined. Instead, replace all terms having square roots operating on differences between variables by, for example, $\delta_{n-1,n}\sqrt{|h_{n-1} - h_n|}$, where $\delta_{n-1,n} = 1$ for $h_{n-1} > h_n$, $\delta_{n-1,n} = -1$ for $h_{n-1} < h_n$ and $\delta_{n-1,n} = 0$ for $h_{n-1} = h_n$. All factors $\delta_{n-1,n}$ have to be decided on in each step of numerical integration. One or more external inflows may in addition be negative, due to liquid being pumped out of vessels.

Data based self-optimizing control: machine learning approaches

Ana Carolina Spindola Rangel Dias*, Maurício Bezerra de Souza Jr. *, José Carlos Costa da Silva Pinto **, Johannes Jäschke***

**Programa de Engenharia de Processos Químicos e Bioquímicos, Escola de Química, Universidade Federal do Rio de Janeiro.*
***Programa de Engenharia Química, COPPE, Universidade Federal do Rio de Janeiro.*
**** Department of Chemical Engineering, Norwegian University of Science and Technology*

(e-mail: johannes.jaschke@ntnu.no)

Abstract: Chemical processes are complex, coupled systems, and it is not obvious how to operate them optimally. High competitiveness and strict safety laws encourage the use of intelligent methods to assure safety and improve operational efficiency and profit. The controlled variable (CV) selection step is important and directly affect the operational performance. It is usually calculated only once and remains constant over longer periods of the operation.

Self-optimizing control (Skogestad, 2000) is a framework for finding controlled variables that result in a near-optimal operation with acceptable loss. Typically, the self-optimizing CV selection is based on a process model to evaluate the optimal solution of the operation. The CV is obtained either selecting single measurements or using a linear combination of measured process variables that drives the process to near the optimum when kept at a constant setpoint, and maintains it there, even in presence of disturbances.

However, sometimes a reliable model of the process may not be available. More recently new proposals have appeared in the literature presenting alternative solutions based on measurement data instead a model. We present and compare different methods for finding self-optimizing controlled variables, that are based on partial least squares regression and artificial neural networks, and apply them on the Van de Vusse reactor as a case study.

Keywords: Self-optimizing control, Economical optimal operation, Artificial neural networks, Partial least squares regression, Controlled variables selection.

References:

Jäschke, J., Cao, Y. and Kariwala, V., 2017. Self-optimizing control–A survey. Annual Reviews in Control, 43, pp.199-223.

Jäschke, J. and Skogestad, S., 2013. Using process data for finding self-optimizing controlled variables. IFAC Proceedings Volumes, 46(32), pp.451-456.

Skogestad, S., 2000. Plantwide control: The search for the self-optimizing control structure. Journal of process control, 10(5), pp.487-507.

CONTROL STRATEGIES TO SLUGGING SUPPRESSION IN DEEP AND ULTRA-DEEPWATER WELLS

Diehl F.C., Machado T.O., Campos M.C.M.M., Farenzena M., Trierweiler J.O.

In the petroleum industry, a brownfield is a production stage of maturity where the production plateau has been reached and starts to slowly decline. At this phase of the field depletion it is common to face multiphase flow problems such as limit cycles which causes undesirable oscillations in the well's flowrate and pressure. This phenomenon, called slugging, might be still worse when the wells are located in deep and ultra-deepwater areas once this installations require longer pipelines to transport the reservoir fluids to the surface facilities. In this work three control strategies are tested in OLGA simulator in order to maximize oil production without slugging: (1) linear PID; (2) nonlinear PID; and (3) linear MPC-PID. All these strategies can be used to suppress slugging, however while the nonlinear PID allowed reaching lower pressures in the well, which means more oil produced, the MPC-PID allowed more smooth acting and transitions toward low pressures. Finally, the MPC-PID strategy was applied in a real ultra-deepwater well resulting in 10% of oil increasing.

Abstract for the Nordic Process Control Workshop, DTU, Copenhagen 22-23. August 2019.

Title: **Practical control of a Four-Product Dividing Wall Column**

Authors: Goran Lukač[a], Ivar J. Halvorsen[b], Žarko Olujić[c], Igor Dejanović[a]

[a] University of Zagreb, Faculty of Chemical Engineering and Technology, Zagreb, Croatia
[b] SINTEF Digital, Mathematics and Cybernetics / NTNU, Dept. of Chemical Engineering, both in Trondheim, Norway
[c] Retired, The Hague, the Netherlands

In the search for improved energy efficiency, the Dividing Wall Column (DWC) is an attractive technical solution for separation by distillation. There are now over 300 DWC-installations world-wide and there are savings in the range from 15-30% in both heat consumption and capital costs. Most of these are three-product columns. However, the concept can also be applied for more products, and the potential savings are even higher, up to 50%. There is still reluctance in the industry and uncertainty in design and control are the usual explanations. The general four-product DWC is more complex internally, as there may be required with up to three extra liquid and vapor splits. However, for a certain class of feed compositions it is possible to simplify the internals structure and obtain four-product separation without compromising the overall energy savings (Halvorsen et.al. 2011). Dejanović et.al. (2011) have showed how to do the full hydraulic design.

This presentation focuses on a simulation study of control performance for the column in Figure 1 in a practical industrial setting. That is, using conventional controllers with feedback mainly from temperature measurements (Lukač, et.al. 2019). The input data and product specifications were based on a real industrial case of a reformate fractionation complex. Three control structures were proposed, and their performance analysed regarding maintaining product specifications, settle times after introduction of disturbances and energy demand. Results show that the controllers can effectively maintain all four product qualities within their limits in all cases, having relatively quick response and settle times. The temperature points must be selected with some care and it must be ensured that all internal sub-column profiles are stabilized. There are two vapor splits in this column, however, as in most industrial three-product installations, these can be left at design values and do not need to be actively manipulated for the expected feed property variations.

Figure 1. Four-product DWC with two partition walls.

The key result is that control is feasible with the standard type of controllers that are available in all commercial process control systems. This should contribute to reduced uncertainty on how to operate a four-product DWC in practice. It is not too complex, but it must be done right.

I.J. Halvorsen, S. Skogestad, I. Dejanović, Lj. Matiješević, Ž Olujić, Multi-product dividing wall columns: a simple and effective assessment and conceptual design procedure, Chem. Eng. Trans., 25 (2011), pp. 611-616, 10.3303/CET1125102

I. Dejanović, Lj. Matijašević, H. Jansen, Olujić Ž, Designing a packed dividing wall column for an aromatics processing plant. Ind. Eng. Chem. Res., 50 (9) (2011), pp. 5680-5692

G. Lukač, I.J. Halvorsen, Ž. Olujić, I. Dejanović, On controllability of a fully thermally coupled four-product dividing wall column, Chemical Engineering Research and Design, Volume 147, 2019, Pages 367-377, https://doi.org/10.1016/j.cherd.2019.04.041.

Combining Data Analytics and Scheduling

Iiro Harjunkoski

Aalto University, School of Chemical Technology, Kemistintie 1, 02150 Espoo, Finland
ABB AG, Corporate Research Germany, Wallstadter Str. 59, 68526 Ladenburg, Germany
(Tel: +49(0)6203-716014; e-mail: iiro.harjunkoski@de.abb.com)

Abstract: There is a lot of hype ongoing on big data analytics (Qin, 2014) and machine learning. Among others, AIChE conference has also arranged topical conferences on the topic, and for a good reason. Most companies collect continuously data from sensors that is stored for a certain time but never actually used, unless there is a need for post analytics as part of trouble shooting (Yidan et al., 2016). One attempt to create true value from the data is to use it proactively to improve the quality and actuality of planning. Nevertheless, often a schedule that is based on statistical average data is outdated already by the time it gets sent to the plant floor and due to the hierarchical planning structures, it is very difficult to quickly adapt a schedule to changing conditions. This is a challenge that has also been looked into in integration of scheduling and control studies (Touretzky et al., 2017). The presented project SINGPRO will merge Big Data platforms, machine learning and data analytics methods with process planning and scheduling optimization. The goal is to create online, reactive and anticipative tools for more sustainable and efficient operation.

Keywords: Scheduling, analytics, machine learning, optimization

The currently employed classical mathematical optimization models (Harjunkoski et al., 2014) are often limited by fixed parameter sets, which are commonly updated off-line and represent only statistical averages. Such parameters could be estimated much more precisely in an on-line fashion using Big Data technologies. By creating collaboration interfaces between scheduling optimization, big data analytics and machine learning, the process related decision-making loop will become much more agile, self-aware and flexible.

With sophisticated data analytics methods, one can embed to the overall key performance indicators (KPI) also all information about the process, e.g., tracking abnormal situations (anomaly detection), individual process equipment performance degradations (predictive maintenance), anticipated process timings (prediction of process behavior) and scenario simulation (e.g., artificial intelligence AI planning). Such an approach will help to select the best production strategies in order to maintain, e.g., production and energy efficiency as well as sustainability in rapidly changing market situations through data-driven self-adaptive scheduling models. The topic of data-driven models has already been investigated in other domains (Van der Aalst et al., 2004) and tools become available for the process industry (Wilson and Sahinidis, 2017). A good perspective on this topic is given in Venkatasubmaranian (2019). It can be expected that Industrial Internet of Things (IIoT) provides the needed seamless connectivity, cloud computing infrastructure and service-based business models to realize this vision.

In this presentation, we aim at using available data proactively to improve the quality and actuality of planning instead of relying on static data that do not reflect current operation conditions. This can be seen as a way of supporting the integration of scheduling and control. However, instead of defining workflows between the levels, we aim to provide more accurate estimates in advance to reduce the mismatch between planning and online operations. We have studied cases of merging Big Data platforms, machine learning and data analytics methods with process planning and scheduling optimization and will provide an overview of the first promising results. We will also show results that can improve the estimation of processing times, leading to more robust schedules and examples where using historical operational data allows us to exclude some decisions leading to smaller scheduling problems. Finally, the process data can also be used in estimating equipment conditions leading to better approaches that combine operational and maintenance scheduling optimization. The examples show that by creating collaboration interfaces between scheduling optimization, big data analytics and machine learning the process related decision-making loop can become more agile, self-aware and flexible.

REFERENCES

Harjunkoski, I., Maravelias, C. T., Bongers, P., Castro, P. M., Engell, S., Grossmann, I. E., . . . Wassick, J. (2014). Scope for industrial applications of production scheduling models and solution methods. Computers and Chemical Engineering, 62, 161-193. doi:10.1016/j.compchemeng.2013.12.001

Qin, S. J. (2014), Process data analytics in the era of big data. AIChE J., 60, 3092-3100. doi:10.1002/aic.14523

Touretzky, C. R., Harjunkoski, I., & Baldea, M. (2017). Dynamic models and fault diagnosis-based triggers for closed-loop scheduling. AIChE Journal, 63(6), 1959-1973. doi:10.1002/aic.15564

Venkatasubramanian, V. (2019). The promise of artificial intelligence in chemical engineering: Is it here, finally? AIChE Journal, 65(2), 466-478.

W. Van der Aalst, T. Weijters, L. Maruster, (2004). Workflow mining: Discovering process models from event logs", Knowledge and Data Engineering IEEE Transactions on, vol. 16, no. 9, 1128-1142

Wilson, Z. T., & Sahinidis, N. V. (2017). The ALAMO approach to machine learning. Computers and Chemical Engineering, 106, 785-795. doi:10.1016/j.compchemeng.2017.02.010

Yidan Shu, Liang Ming, Feifan Cheng, Zhanpeng Zhang, Jinsong Zhao (2016), Abnormal situation management: Challenges and opportunities in the big data era. Computers & Chemical Engineering, 91m 104-113. doi:10.1016/j.compchemeng.2016.04.011

A new mid-ranging control strategy

Tore Hägglund

Department of Automatic Control, Lund University, Box 118,
SE-22100 Lund, Sweden (e-mail: tore.hagglund@control.lth.se)

1. MID-RANGING CONTROL

Mid-ranging control is a control strategy that is used when there are more than one manipulated variable available to control a process variable. Mid-ranging control handles the redundancy by coordinating the roles of the different manipulated variables. The most common approach is to introduce valve position controllers (VPC) that control the steady-state position of manipulated variables. In this presentation, some drawbacks of the VPC approach are pointed out, and a new control structure that lacks these drawbacks is presented. Instead of using valve position controllers, the new strategy uses feedforward control to obtain the desired steady-state values of the manipulated variables.

2. VALVE POSITION CONTROL (VPC)

The mid-ranging control problem and the valve position control solution are illustrated by the block diagram in Figure 1. For simplicity, we restrict the presentation to the case of two manipulated variables, u_1 and u_2, that control one process variable, y.

The goal of the control is that process output y should follow a setpoint y_{sp}, and that control signal u_1 should be close to a setpoint u_{sp} in steady-state. Since the main goal is the control of y, process P_1 and controller C_1 are chosen so that they form a fast and precise feedback loop. Controller C_2 is the valve position controller that controls u_1 to its setpoint u_{sp}.

Controller C_1 is normally a PI controller and it can be tuned in standard ways. Controller C_2 must, however, be tuned conservatively so that it does not disturb the other loop too much. The idea is that the VPC controller should adjust the output from C_1 slowly in the background.

The VPC approach is a simple and the most common way to treat the mid-ranging control problem, and it works well in many applications. There are, however, some drawbacks associated with the approach that limits its use, namely

(1) It is common that there is a relatively large pump or valve in P_2. In these cases, it is likely that stick-slip motion that destroys the control precision occurs.
(2) u_{sp} is often chosen to be close to a saturation limit of u_1. In these cases, the control error in the VPC loop may become small, leading to sluggish control.
(3) There are two controllers that influences y, but still no redundancy since C_2 controls u_1 and not y.

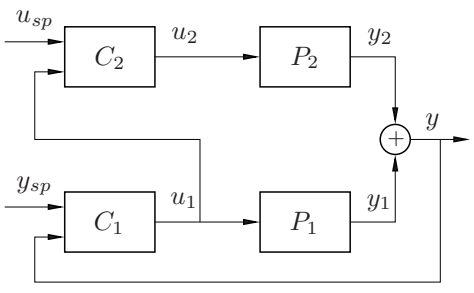

Fig. 1. The valve position control approach.

3. THE FEEDFORWARD MID-RANGING CONTROL STRATEGY

The new mid-ranging control structure is presented in Figure 2. As for the VPC approach, given in Figure 1, process P_1 and controller C_1 form the fast and precise feedback loop. Controller C_2 is no longer a VPC, but also this controller takes y as input and y_{sp} as setpoint. Thus, both controllers act on the same signals. To avoid stick-slip motion, integral action is not introduced in this controller.

The mid-ranging of u_1 is obtained by adding a feedforward signal to C_2. Feedforward signal u_3 is obtained in the following way. Control signal u_1 is first passed through a deadzone, where the user has to specify parameters u_{low} and u_{high}, that define an acceptable region for the stationary value of u_1. The deadzone is introduced to avoid stick-slip motion. The output from the deadzone is fed to a third controller, C_3, with setpoint equal to zero. The output from C_3, u_3, is the feedforward signal that is added to controller C_2. Controller C_3 is a PI controller.

In the presentation it is shown that the new mid-ranging control strategy lacks the three drawbacks associated with the VPC approach. Design methods for the controllers and simulation results are also presented.

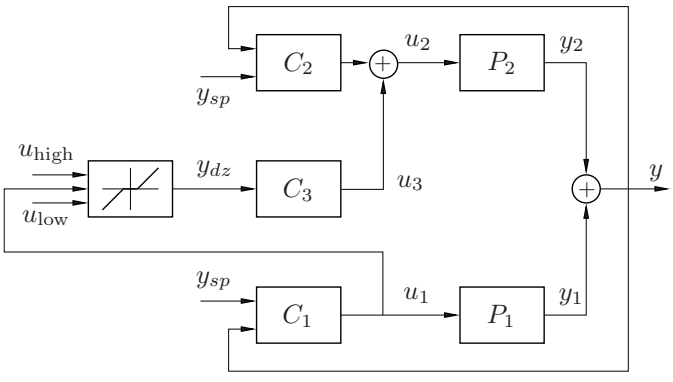

Fig. 2. The feedforward mid-ranging control approach.

Stochastic Differential Equations and Nonlinear Model Predictive Control

John Bagterp Jørgensen, **Dimitri Boiroux**,
Tobias K. S. Ritschel, **Niels Kjølstad Poulsen**, **Henrik Madsen**

Department of Applied Mathematics and Computer Science,
Technical University of Denmark, DK-2800 Kgs. Lyngby, Denmark

Abstract: The algorithm for state estimation in the form of filtering and prediction is central to the performance of a model predictive control system. In the paper, the filtering and prediction algorithms are based on a continuous-discrete stochastic system. In this representation, the dynamics is described by stochastic differential equations with a diffusion term that is affected by standard Wiener processes, and the observations are nonlinear mappings of the state corrupted by Gaussian noise. The model parameters, as well as the hyper parameters that describe the distribution, are estimated using a prediction-error-method based on maximum likelihood (ML) and maximum a posteriori (MAP) criteria and gradient based numerical optimization routines. The experimental conditions for estimating the parameters are determined by solution of an experimental design optimization problem. The filtering and prediction algorithm obtained by systematic experimental design and parameter estimation is used for predictive control. We use this method for nonlinear model predictive control of 1) the temperature in an adiabatic continuous-stirred tank reactor with exothermic reaction, 2) the glucose concentration in people with type 1 diabetes, and 3) for the biomass, substrate, and dissolved oxygen concentration in a U-loop reactor that is used for single cell protein production.

Keywords: Stochastic differential equations, Model predictive control, State estimation, Parameter estimation, Prediction-error-method, Experimental design

Functional modelling view on process operations

Sten Bay Jørgensen[1], Morten Lind[2], Niels Jensen[3]

[1]Department of Chemical and Biochemical Engineering, Technical University of Denmark, DK-2800 Kgs.Lyngby, Denmark

[2]Department of Electrical Engineering, Technical University of Denmark, DK-2800 Kgs.Lyngby, Denmark

[3]Safepark, Kannikestræde 14, DK-3550 Slangerup, Denmark

Process modelling knowledge plays an important role in the planning and safe execution of process operations. When mishaps do occur model knowledge again is important for development of an understanding of the causes behind the events. The model knowledge is seemingly applied in many different ways as illustrated by the different names of the different model types and analysis tools. Consequently, it could be worthwhile to understand how these different representations of model knowledge are related. Thereby it could become possible to develop the different representations from a common base to ensure consistency between the applied knowledge in the different aspects of process operations.

This presentation addresses functional modelling for the purpose of the object system under investigation, where the purpose of functional modelling is to represent the relations between the system goal and the underlying phenomena. The object under investigation in this presentation is process operation. The role of different aspects of functional modelling within process operation is analyzed. The fundamental principles of functional modelling for the object under investigation are presented leading to:

The concept of Functional modelling hermeneutics defined as

1. translating the modelling goal into desired system properties,
2. identifying the needed theory to model the system to represent these properties
3. identifying the criteria for evaluation of system purpose and performance.

Different types of functional models are illustrated with a discussion of their relations to quantitative computational physicochemical models. It is demonstrated that functional modelling hermeneutics can be viewed as a common foundation for many different functional process model types applied in as diverse areas as monitoring, alarm handling, fault detection and consequence reasoning as well as for traditional simulation with computational physicochemical models.

Online Process Optimization with Active Constraint Set Changes using Simple Control Structures

Dinesh Krishnamoorthy, Sigurd Skogestad

Department of Chemical Engineering,
Norwegian University of Science and Technology (NTNU), Trondhiem, Norway
dinesh.krishnamoorthy@ntnu.no, skoge@ntnu.no

The primary objective of online process optimization, also known as real-time optimization (RTO), is to optimize the economic performance subject to satisfying constraints such as product specifications and operational limits. Online process optimization is traditionally based on rigorous steady-state mathematical models of the process that are used in a numerical optimization solver to compute the optimal inputs and setpoints. However, the main challenge with this approach is the need for mathematical models. Mathematical models are generally expensive to obtain and maintain. In addition, the required computation may be difficult to implement and may not converge to the optimal solution. Moreover, there is always plant-model mismatch due to lack of knowledge and/or model simplification. This may lead to suboptimal operation. Addressing the plant-model mismatch has been one of the main focus areas of RTO in the past four decades or so.

Online process measurements are used to cope with plant-model mismatch.The most obvious and common approach in traditional RTO is to update the model using the so-called two-step approach, where deviations between the model predictions and the measurements are used in the first step to update the model parameters. In the second step, the updated steady-state model is used to re-optimize the setpoints. The RTO layer generally has as degrees of freedom, the setpoints for the controlled variables (CV^{sp}) which is given to the control layer below. The control layer has degrees of freedom $\mathbf{u}$, which are the physical manipulated variables (MV), and in addition to achieving feasible operation, its main objective is to keep the outputs $\mathbf{y}$ or controlled variables (CV) at the optimal values computed by the RTO layer.

The main purpose of this presentation is to show how we can eliminate the RTO layer, even for the case when the set of constraints that are optimally active, changes with changing operating conditions. In other words, the objective is to indirectly move the optimization into the control layer.

For many simple processes, online *steady-state* process optimization with changes in active CV constraint regions can indeed be achieved by using simple feedback control structures, without having a separate online optimization layer. In particular, we show that changes in active constraint regions can be handled using simple logics such as selectors, without needing to identify the exact location of the active constraint regions *a priori*, nor using a detailed model online. When we have one manipulated variable (MV) controlling two controlled variable (CV), i.e. CV-CV switching, then minimum/maximum selectors can be used. Alternatively, when we have more than one candidate MV to control one controlled variable (CV), then split-range logic can be used. Split range control may also be used when MV-CV pairings need to be changed when a MV saturates. This presentation will particularly focus on CV-CV switching.

Some well known case studies are presented that demonstrate the effectiveness of the proposed control structures and how changes in the active constraint regions can be handled using simple control logics such as selectors.

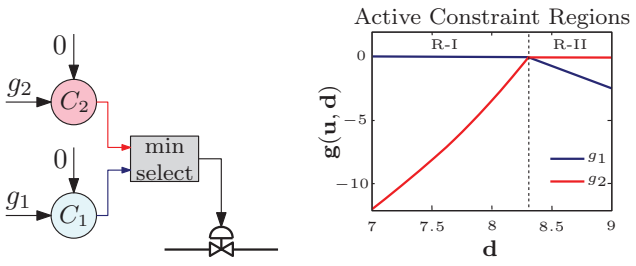

Figure 1: Schematic representation showing a minimum selector block used to switch between two constraints that are active in two different regions.

Gradient-free optimization of data center cooling using Extremum Seeking ⋆

R. Lucchese [*] **M. Lionello** [**] **M. Rampazzo** [**] **M. Guay** [***] **K. Atta** [*]

[*] *Department of Computer Science, Electrical and Space engineering, Luleå University of Technology, Sweden (e-mails:* {riccardo.lucchese|khalid.atta}@ltu.se*)*
[**] *Department of Information Engineering, University of Padova, Italy (e-mails:* {lionello|rampazzom}@dei.unipd.it*)*
[***] *Department of Chemical Engineering, Queen's University, Kingston, Canada. (e-mail:* guaym@queensu.ca*)*

Abstract: We consider the thermal management problem of provisioning the cooling airflow to data center rooms. Building on a virtual plant capturing the thermal behaviour of both the cooling equipment and the room-side heat load, we evaluate a 2D phasor-based Extremum Seeking Control (ESC) strategy that strives to satisfy the cooling demand while minimizing the cooling provisioning cost.

Keywords: Data center cooling, Phasor extremum seeking control.

1. INTRODUCTION

We consider an environmental control application employing a data center Indirect Adiabatic Cooling (IAC) unit [1,2]. The objective is to minimize the cooling power consumption, while letting the data-processing equipment operate within a safe temperature envelope. To this setting, we apply a two-dimensional phasor-based Extremum Seeking Control (ESC) strategy that manipulates the flow rates of the process-side air and water to optimize the overall cooling efficiency.

Toward faster convergence to the optimum, we propose a Newton-like acceleration of the phasor-based ESC [3]. The scheme is inspired by the work in [4], in which the steepest descent strategy of the classical perturbation based ESC is substituted by a Newton-like descent. Here, we make use of a phasor-based strategy by the first and second order derivatives of the plant's index are filtered from its representation on truncated Fourier basis. The proposed controller enjoys several desirable properties: *i*) it is *adaptive* with respect to changes in the environmental and workload conditions; *ii*) it is *plug-in*, since it requires updates to software only components; *iii*) it is *simple* to implement, since the optimal controls are learned on-line without the requirement of a detailed knowledge of the plant.

Statement of contributions. The contribution of this study is twofold:

- the analysis of a Newton-like ESC aimed at multivariable problems that builds on the phasor-based derivative estimator;
- the in silico validation of our approach in a relevant data center cooling application.

⋆ This work is partially funded by ProcessIT Innovations.

Organization of this manuscript. Section 2 introduces relevant background material. Section 3 discusses the estimation step in the phasor based ESC. Section 4 describes the proposed Newton-like approach. Section 5 demonstrates our design in simulation. Finally, Section 6 collects concluding remarks and future directions.

2. BACKGROUND MATERIAL

We consider a nonlinear control systems of the form

$$\Sigma \doteq \begin{cases} \dot{\boldsymbol{x}} = f(\boldsymbol{x}, \boldsymbol{\theta}) \\ y^{\mathrm{o}} = h(\boldsymbol{x}) \end{cases} \tag{1}$$

where $\boldsymbol{x} \in \mathbb{R}^n$ is the state, $\boldsymbol{\theta} \in \mathbb{R}^m$ is the control value, $y^{\mathrm{o}} \in \mathbb{R}$ is the scalar measured output, and the vector fields f, h are sufficiently smooth. In this context, the plant index y^{o} has the meaning of either a cost or a utility.

Assumption 1. There exists a sufficiently smooth function $\ell : \mathbb{R}^m \to \mathbb{R}^n$ such that

$$f(\boldsymbol{x}, \boldsymbol{\theta}) = \mathbf{0} \quad \Leftrightarrow \quad \boldsymbol{x} = \ell(\boldsymbol{\theta}). \tag{2}$$

Assumption 2. For each $\boldsymbol{\theta} \in \mathbb{R}^m$, the equilibrium point $\ell(\boldsymbol{\theta})$ is locally exponentially stable for the autonomous dynamics $\dot{\boldsymbol{x}} = f(\boldsymbol{x}, \boldsymbol{\theta})$ with constants uniform in $\boldsymbol{\theta}$.

Let $Q : \mathbb{R}^m \to \mathbb{R}$, $Q \doteq h \circ \ell$, denote the steady state value of the plant's index given the parameter. To ensure global convergence, we require the following characterization.

Assumption 3. The index Q is strongly convex with positive definite Hessian.

We stress that f, h in (1), ℓ in (2), and the steady state index Q are otherwise unknown. The control task is to optimize the plant operation by steering Σ along the profitable directions inferred from the continuous measurement of y^{o}. This entails to learn the optimal parameters online,

$$\boldsymbol{\theta}^* \in \underset{\boldsymbol{\theta} \in \mathbb{R}^m}{\operatorname{argmin}} \; Q(\boldsymbol{\theta}), \tag{3}$$

and then to bring the system operation near this optimum.

Here, we take an ESC controller to be a new dynamical system of the form

$$\begin{cases} \dot{\boldsymbol{\zeta}}(t) = f_{\text{esc}}\left(t, \boldsymbol{\zeta}(t), y^{\text{o}}(t)\right) \\ \dot{\widehat{\boldsymbol{\theta}}}(t) = \text{diag}\left(\boldsymbol{k}\right) h_{\text{esc}}\left(\boldsymbol{\zeta}(t), y^{\text{o}}(t)\right) \\ \boldsymbol{\theta}(t) = \widehat{\boldsymbol{\theta}}(t) + \text{diag}\left(\boldsymbol{a}\right) \boldsymbol{s}(t) \end{cases} \tag{4}$$

where:

- f_{esc} is the dynamics of the *direction finder* and h_{esc} a mapping of the internal state to the estimated descent direction;
- $\widehat{\boldsymbol{\theta}}$ is the estimated minimizer of (3) and $\boldsymbol{k} \in \mathbb{R}^m_{>0}$ a vector of integration gains affecting the convergence speed;
- $\boldsymbol{s} = \boldsymbol{s}(t) \in \mathbb{R}^m$ is a vector of additive sine waves
$$\boldsymbol{s}_k(t) = \sin(\omega_k t), \quad k = 1, \dots, m \tag{5}$$
with $\omega_1 < \omega_2 < \ldots < \omega_m$, while $\boldsymbol{a} \in \mathbb{R}^m_{>0}$ is a vector of perturbation amplitudes such that, for any choice of distinct indeces $k, v, z = 1, \dots, m$, there holds [5].: *i)* $\omega_k \neq 2\omega_j$, *ii)* $\omega_k \pm \omega_v \neq \omega_z$, and *iii)* $\omega_k \pm \omega_v \neq 2\omega_z$.

3. DERIVATIVE ESTIMATOR

Following [3], we approximate $y^{\text{o}}(t)$ by projecting the signal onto a truncated Fourier basis:

$$y^{\text{o}}(t) \approx \boldsymbol{\chi}(t)^\top \boldsymbol{\zeta}, \tag{6}$$

where $\boldsymbol{\chi}(t)$ is obtained by stacking the sine and cosine basis functions [1], and $\boldsymbol{\zeta}$ collects the corresponding Fourier coefficients. By assimilating $\boldsymbol{\zeta}(t)$ to a vector of state variables, we introduce the dynamical observer

$$\dot{\widehat{\boldsymbol{\zeta}}}(t) = L(t)\left(y^{\text{o}}(t) - \boldsymbol{\chi}^\top(t)\widehat{\boldsymbol{\zeta}}(t)\right), \tag{8}$$

where the entries of the gain are phase-shifted versions of the entries of $\boldsymbol{\chi}(t)$. Under the following noise modeling, $L(t)$ can be chosen as the unique, periodic, stabilizing, Kalman-Bucy gain associated to the dynamics [3]

$$\begin{cases} \dot{\boldsymbol{\zeta}}(t) = \boldsymbol{\varepsilon}_1(t) \\ y^{\text{o}}(t) = \boldsymbol{\chi}(t)^\top \boldsymbol{\zeta}(t) + \varepsilon_2(t) \end{cases} \tag{9}$$

where $\boldsymbol{\varepsilon}_1, \varepsilon_2$ are zero mean Gaussian random processes with covariances $V \doteq \text{var}\left(\boldsymbol{\varepsilon}_1\right)$ and $r \doteq \text{var}\left(\varepsilon_2\right)$. In particular, the optimal gain in the Kalman sense can be evaluated by solving a periodic Riccati Differential Equation (RDE):

$$\dot{P}(t) = V - rL(t)L^\top(t), \quad L(t) = r^{-1}P(t)\chi(t). \tag{10}$$

The state (8) can be shown to capture the derivatives' estimates up to fixed but unknown multiplicative factors. In particular the derivatives of Q can be estimated using:

$$(\widehat{\nabla Q})_k \doteq \frac{\widehat{\zeta}^{\text{s}}_k}{\boldsymbol{a}_k}\sqrt{1 + \left(\frac{\widehat{\zeta}^{\text{c}}_k}{\widehat{\zeta}^{\text{s}}_k}\right)^2} \approx (\nabla Q)_k,$$

$$(\widehat{\nabla Q})_k \doteq \frac{\widehat{\zeta}^{\text{s}}_k}{\boldsymbol{a}_k}\sqrt{1 + \left(\frac{\widehat{\zeta}^{\text{c}}_k}{\widehat{\zeta}^{\text{s}}_k}\right)^2} \approx (\nabla Q)_k \varrho^{\text{o}}_{\omega_k},$$

[1] For example, in the case $m = 1$:

$$\boldsymbol{\chi}(t) \doteq \begin{bmatrix} 1 & \sin(\omega t) & \cos(\omega t) & \sin(2\omega t) & \cos(2\omega t) \end{bmatrix}^\top. \tag{7}$$

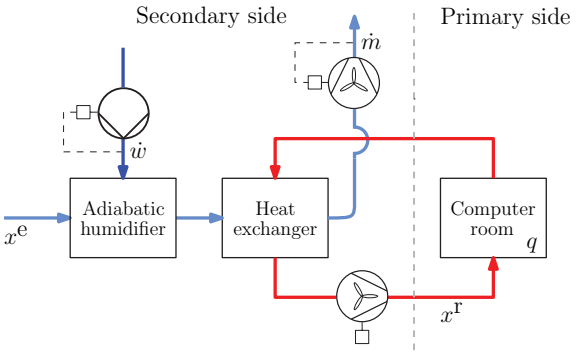

Figure 1. Overview of the indirect cooling setup: a *secondary* airflow (in light blue) transits through a cross-flow heat exchanger to recover thermal energy from an independent *primary* airflow (in red). A humidifier is used to enhance the recovery rate.

$$(\widehat{\boldsymbol{H}\boldsymbol{Q}})_{kk} \doteq -4\frac{\widehat{\zeta}^{\text{c}+}_{kk}}{\boldsymbol{a}_k^2}\sqrt{1 + \left(\frac{\widehat{\zeta}^{\text{s}+}_{kk}}{\widehat{\zeta}^{\text{c}+}_{kk}}\right)^2} \approx (\boldsymbol{H}\boldsymbol{Q})_{kk},$$

$$(\widehat{\boldsymbol{H}\boldsymbol{Q}})_{kv} \doteq (\widehat{\boldsymbol{H}\boldsymbol{Q}})_{vk} \doteq -2\frac{\widehat{\zeta}^{\text{c}+}_{kv}}{\boldsymbol{a}_k\boldsymbol{a}_v}\sqrt{1 + \left(\frac{\widehat{\zeta}^{\text{c}+}_{kv}}{\widehat{\zeta}^{\text{s}+}_{kv}}\right)^2} \approx (\boldsymbol{H}\boldsymbol{Q})_{kv}.$$

4. THE NEWTON-LIKE ESC

The Newton-like acceleration for the phasor ESC is derived by specializing the general scheme in (4). Specifically, we let:

- f_{esc} be the state-update law in (8), augmented with a Hessian inversion dynamics
$$f_{\text{esc}}\left(t, \begin{bmatrix} \widehat{\boldsymbol{\zeta}} \\ \boldsymbol{\Gamma} \end{bmatrix}, y^{\text{o}}\right) \doteq \begin{bmatrix} L(t)\left(y^{\text{o}}(t) - \boldsymbol{\chi}^\top(t)\widehat{\boldsymbol{\zeta}}(t)\right) \\ \omega_\Gamma\left(\boldsymbol{\Gamma} - \boldsymbol{\Gamma}\widehat{\boldsymbol{H}\boldsymbol{Q}}\boldsymbol{\Gamma}\right) \end{bmatrix} \tag{11}$$
where the state $\boldsymbol{\Gamma}$ of the RDE correspods to an estimate of $(\boldsymbol{H}\boldsymbol{Q})^{-1}$, and $\omega_\Gamma \in \mathbb{R}_{>0}$ is a tuning gain [6];
- h_{esc} as the Newton-like direction
$$h_{\text{esc}}(\widehat{\boldsymbol{\zeta}}) \doteq -\boldsymbol{\Gamma}\widehat{\nabla Q}. \tag{12}$$

It can be shown that the proposed Newton-like ESC enjoys staiblity properties similar to those of the classical perturbation-based multi-variable ESC. See [**?**] for details.

5. EXAMPLE: ON-LINE OPTIMIZATION OF AN INDIRECT ADIABATIC COOLING UNIT

We aim to minimze the power consumption of the Indirect Adiabatic Cooling (IAC) unit schematized in Figure 1. The system operates as follows. A stream of *primary* cooling air is supplied to the computer room where it absorbs the heat load produced by the electronic equipment before being recirculated through the hot-side of a main heat exchanger. An independent stream of air, known as *secondary* air, is circulated across the cold-side of the heat exchanger and then exhausted back to the environment. To enhance the unit's capacity, a humidifier injects pulverized water in the secondary airflow, translating its thermo-hygrometric properties across isenthalpic lines to lower temperatures.

The corresponding control problem considers two independent manipulable variables:

- $\dot{m}$, the volumetric flow rate of secondary air produced by the secondary fans;
- $\dot{w}$, the volumetric flow rate of water processed by the humidifier.

Therefore, $\boldsymbol{\theta}(t) = [\dot{m}(t) \;\; \dot{w}(t)]^\top$. Moreover, operating the room-side equipment safely induces a temperature requirement on the supply temperature x^{r},

$$x^{\mathrm{r}}(t) \leq \overline{x^{\mathrm{r}}}, \tag{13}$$

where $\overline{x^{\mathrm{r}}}$ is a constant threshold. Seeking the minimum power consumption, we consider the following smooth, convex, absorption index

$$p^{\mathrm{iac}}(\dot{m}, \dot{w}) \doteq p^{\mathrm{fan}}(\dot{m}) + p^{\mathrm{hum}}(\dot{w}), \tag{14}$$

and account for (13) by including a one-sided barrier in the final plant index:

$$y^{\mathrm{o}}(t) \doteq p^{\mathrm{iac}}(\dot{m}(t), \dot{w}(t)) + \lambda \left(\max\{0, x^{\mathrm{r}}(t) - \overline{x^{\mathrm{r}}}\}\right)^2. \tag{15}$$

We task the Newton-like ESC of Section 4 to optimize the cooling operations over a period of 9 hours. To evaluate the dynamic behavior, we design a numerical scenario including changes in the outdoor temperature and the room-side heat load. Specifically, at time $t_1 \approx 2$ hours we inject a sudden step in the heat load q, increasing it from 75 kW to 85 kW. At time $t_2 \approx 5$ hours we inject an additive ramp term in the outdoor temperature x^{e} which goes from 25 °C to 26 °C. The model used for simulation was developed for and calibrated on commercial IAC unit, using a First-Principle Data-Driven methodology [1] (and references therein). Moreover, we consider $\omega_1 = 0.0762\,\mathrm{rad\,s^{-1}}$, $\omega_2 = 0.0967\,\mathrm{rad\,s^{-1}}$, $\boldsymbol{a}_1 = 150\,\mathrm{m^3\,h^{-1}}$, $\boldsymbol{a}_2 = 10\,\mathrm{L\,h^{-1}}$, $\boldsymbol{k} = -10^{-5} \cdot [1 \;\; 6]^\top$, $\lambda = 25\,\mathrm{kW\,°C^{-2}}$, and $\overline{x^{\mathrm{r}}} = 21\,°\mathrm{C}$.

The simulation results are summarized in Figure 2. We observe significant differences between the optimization objective (14) and the actual power consumption (15) when the temperature constraint (13) is active. Since the dynamics of the supply temperature induces higher phase-lags than the actuator dynamics, the barrier term in (15) injects significant harmonic distortions, affecting the accuracy of the derivative estimation. Moreover, the barrier renders a non-convex index, with an optimal $\boldsymbol{\theta}^*$ different from that of (14), and potentially multiple optimizers. Nevertheless, throughout the testing, the controller is able to update the manipulable variables, adaptively with the operating conditions, bringing the system's operation near the optimal settings.

6. CONCLUSIONS

We propose a multi-variable Newton-like implementation of the phasor ESC, and demonstrate its effectiveness a calibrated model of a data center IAC unit.

We stress that Newton-like strategies come with strict requirements that in practice are not easily satisfied (for instance, strict convexity or concavity of the index). On the one hand, Newton-like strategies enable faster convergence rates compared to simpler schemes. On the other hand, slow variations in the parameters are typically required to moderate any estimation errors, making the potential benefits generally hard to achieve.

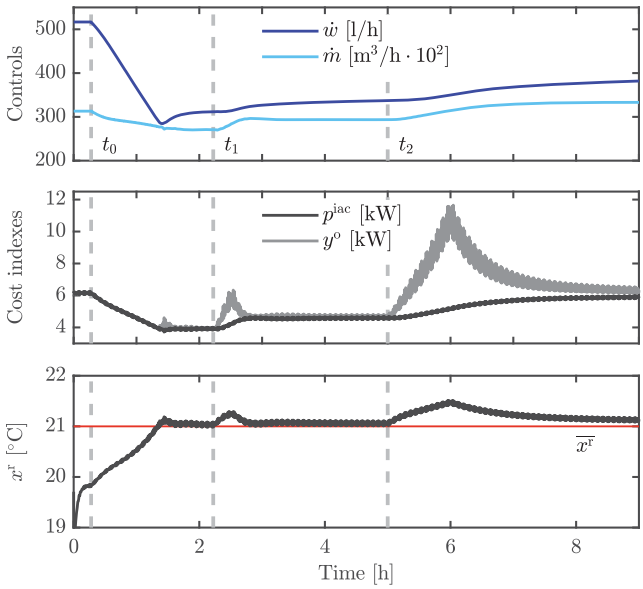

Figure 2. Simulated optimization scenario involving the IAC unit and the proposed Newton-like ESC. The manipulable inputs (in the top panel) are updated online to minimize the plant index (in the middle panel). The supply temperature (bottom panel) is regulated in a neighborhood of $\overline{x^{\mathrm{r}}}$. The ESC starts operating at time t_0. Changes in the room-side heat load q and the outdoor temperature x^{e} are injected at times t_1 and t_2 (see the text for the details).

As highlighted by our numerical example, future directions of prominent interest include a formal address of problems with output constraints.

REFERENCES

[1] A. Beghi, L. Cecchinato, G. Dalla Mana, M. Lionello, M. Rampazzo, and E. Sisti, "Modelling and control of a free cooling system for data centers," *Energy Procedia*, 2017.

[2] R. Lucchese, M. Lionello, M. Rampazzo, and A. Johansson, "On economic cooling of contained server racks using an indirect adiabatic air handler," in *IEEE Conference on Control and Decision (submitted)*, 2019.

[3] K. T. Atta, A. Johansson, and T. Gustafsson, "Extremum seeking control based on phasor estimation," *Systems & Control Letters*, 2015.

[4] W. Moase, C. Manzie, and M. Brear, "Newton-like extremum-seeking for the control of thermoacoustic instability," *IEEE Trans. Automat. Contr.*, 2010.

[5] K. T. Atta, A. Johansson, and M. Guay, "On the Generalization and Stability Analysis of Pareto Seeking Control," *IEEE Control Systems Letters*, 2018.

[6] A. Ghaffari, M. Krstić, and D. Nešić, "Multivariable newton-based extremum seeking," *Automatica*, 2012.

Virtual sensing in marine systems ⋆

Mikael Manngård, Wictor Lund, Jerker Björkqvist, Hannu T. Toivonen

Faculty of Science and Engineering, Åbo Akademi University. Biskopsgatan 8, FIN-20500 Åbo, Finland

Abstract: In this work, virtual sensing methods for estimation of unknown inputs and states of a ship propulsion system is presented. Dynamical models of the propulsion system together with indirect measurements are used to estimate torque and angular velocities at various locations of the system. A case study where a simulation model of the propulsion system of a hybrid ship is used to demonstrate the performance of the proposed methods.

Keywords: Virtual sensor, input-and-state estimation, marine systems

Energy efficient and reliable operation of modern ships relies heavily on the availability of high-quality data. Tasks such as automatic control, predictive maintenance and fault diagnostics on ships are all dependent on sensing data. However, obtaining the required data by installing sensors in all desired locations is not only impractical due to the high installation cost, but sometimes also impossible due to the physical constraints of the system. Virtual sensing techniques, which rely on indirect measurements and dynamical models of the system, have thus been used as additions to physical sensors (Hsieh, 2009, 2006; Gillijns and De Moor, 2007; Manngård et al., 2019).

In this work, the virtual sensing problem is formulated as a simultaneous input-and-state estimation problem. A fixed-lag Kalman-type smoother for estimating the unknown inputs and states in have been derived. Furthermore, by relying on real-time convex optimization, we have shown that robustness can be enforced on the estimates. We present a case study where torque contributions from the propellers and engine-generator sets, as well as angular velocities from different components on the driveline, are estimated.

⋆ This work is was done withing the Business Finland funded projects Reboot IoT Factory and Integrated Energy Solutions to Smart and Green Shipping (INTENS).

REFERENCES

Gillijns, S. and De Moor, B. (2007). Unbiased minimum-variance input and state estimation for linear discrete-time systems. *Automatica*, 43(1), 111–116.

Hsieh, C.S. (2006). Optimal filtering for systems with unknown inputs via unbiased minimum-variance estimation. In *TENCON 2006-2006 IEEE Region 10 Conference*, 1–4. IEEE.

Hsieh, C.S. (2009). Extension of unbiased minimum-variance input and state estimation for systems with unknown inputs. *Automatica*, 45(9), 2149–2153.

Manngård, M., Lund, W., Keski-Rahkonen, J., Nänimainen, J., Saarela, V.P., Björkqvist, J., and Toivonen, H.T. (2019). Estimation of propeller torque in azimuth thrusters. *Submitted manuscript.*

Hybrid modelling and control framework for particle processes

Rasmus Fjordbak Nielsen*, Krist V. Gernaey*, Seyed Soheil Mansouri*

** Process and Systems Engineering Centre, Department of Chemical Engineering, Technical University of Denmark, 2800 Kgs. Lyngby, Denmark (e-mail: rfjoni@kt.dtu.dk, kvg@kt.dtu.dk, seso@kt.dtu.dk).*

1. INTRODUCTION

Particle processes are essential parts in both upstream and downstream processes in many chemical and biochemical productions. The complex dynamics of these processes have in the meantime made it difficult to monitor and control these processes to satisfactory level. With recent developments within real-time on-line image acquisition from particle processes and the breakthroughs within the field of machine learning, today there is an opportunity to monitor these processes with more sophistication.

In this work, a novel hybrid modelling framework is presented which can be used to predict the evolution in particle size distribution using advanced image analysis. This is done by combining a deep neural network for phenomena rate estimation with a generic population balance model (see model structure in Figure 1). This way one can couple the phenomena kinetics observed to a range of measured and controlled process variables, without assuming any specific rate expressions or input variables. Thereby, the framework is generic and can be applied to a wide range of particle processes, and take into account more input-parameters than used in conventional white-box modelling approaches.

Combined with on-line imaging of the particle process, the generated process model can be used for process control, using discrete-time model predictive control. At the same time, the hybrid model can be continuously trained and improved in real-time during process operation, forming a platform for self-learning process control in particle processes.

2. MODEL FRAMEWORK

In modelling of particle processes, the particle phenomena rates can be difficult to model and predict due to their multivariable and nonlinear dependencies of a large number of process variables, and as phenomena rates cannot be directly measured. Here we suggest a framework where a number of measured process variables (x), controlled process variables (y) and the time-derivative of the controlled process variables (dy/dt) are fed to a deep neural network, which outputs predictions of the phenomena rates. The phenomena rates are then provided to a first-principle model, based on a population and mass balance model, providing with predictions of the future size-distribution, which is a direct or indirect measure in many particle processes.

By using this model structure, we integrate all available knowledge into one approach, and enable the possibility of continuously training and improving the model.

The modelling framework has been implemented in the TensorFlow framework developed by Google Inc, which allows for rapid training due to the implementation of Automatic Differentiation, meaning that tasks like model training, predictions and optimizations can be carried out in real-time.

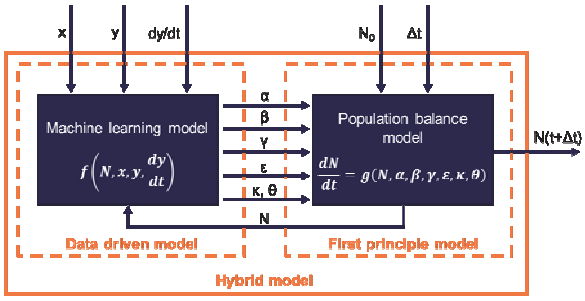

Fig. 1. Proposed model framework for modelling of a generic particle process

3. CONTROL STRATEGY

With the currently commercially available fast, non-invasive and robust on-line imaging and analysis of particle suspensions, we here suggest a parallelized model training and control approach as shown in Figure 2. For each sampling cycle, a data point is saved to the training-set, which is then used to train the model and solve a MPC optimization problem in parallel processes. This will form continued process verification, as recommended by the FDA (2019), operated fully automatic and at the same time be used to refine the process control both intra-batch and inter-batch.

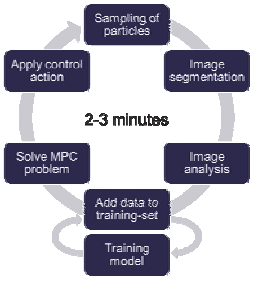

Fig. 2. Proposed control strategy loop

4. CURRENT STATUS AND FUTURE WORK

Until now, the modelling framework has been tested on two cases of crystallizations, showing to provide good predictions of the process dynamics. The proposed control strategy is now to being applied for a crystallization study, and planned for cases of flocculation and fermentations.

REFERENCES

FDA (2019), Quality Considerations for Continuous Manufacturing Guidance for Industry, Draft Guidance, CDER

Experimental Application of a Radial Basis Functions Based Control Strategy for a Pharmaceutical Crystallization Process

Merve Öner[1], Frederico Montes[1], Stuart M. Stocks[3], Zoltan K. Nagy[2], Gürkan Sin[1]

[1] Process and Systems Engineering Center (PROSYS), Department of Chemical and Biochemical Engineering, Technical University of Denmark, Building 229, 2800 Kgs. Lyngby, Denmark
[2]Crystallization and Particle Technology Systems Engineering (CryPT-Sys), School of Chemical Engineering, Purdue University, 480 Stadium Mall Drive, West Lafayette, IN 47907, USA
[3]LEO Pharma A/S, Industriparken 55, 2750 Ballerup, Denmark

Keywords: Pharmaceutical crystallization, process control, surrogate modeling, radial basis functions (RBF), polynomial chaos expansions (PCE)

Abstract

In pharmaceutical manufacturing, crystallization is the most preferred technique in downstream processing to recover crystal products. Crystal quality attributes such as crystal size distribution, purity, and polymorphic form, which are critical for not only following unit operations, but also therapeutic properties of the formulated product, are determined by the operating conditions of crystallizers. Therefore, control of a crystallization process is critically and essentially the control of quality attributes. Traditionally, crystallization processes are operated based on a pre-defined recipe of a process variable such as a temperature trajectory for a cooling crystallization system, and the quality of the crystal product is tested only at the end of the process. Quality by testing (QbT) approach leads to high profit loss since batch-to-batch variations of crystal quality attributes are unavoidable, due to the absence of control actions taken during the process in order to avoid effects of any disturbances available in the system through *e.g.* feedback signals coming from solid-state attributes or supersaturation. However, consistency of a process outcome is highly dependent on a robust process control strategy. In literature, emergence of the latest generation of process analytical technology (PAT) tools, mechanistic understanding and modeling of underlying mechanism of crystallization process and incentives by regulatory mechanism have accelerated the efforts on the development of advanced process control strategies in order to achieve desired product quality, so called quality by control (QbC). State of the art crystallization control strategies can be classified into two main groups as model free and model based. Model free methods such as direct nucleation control (DNC) or supersaturation control (SSC) are simple and found many applications, they might require some investigations on the determination of a robust set point as well as some efforts on online sensor calibration. Model based control strategies utilize real time crystallization process simulations to predict the effects of inputs and disturbances on the process output, whose performance is strictly dependent on the complexity and accuracy of the

implemented model as well as speed of solution time. However, often a simple but reliable control strategy is required in the pharmaceutical industries to achieve a fast and successful transition from laboratory to pilot scale crystallization operation. Therefore, in this work we developed a Radial Basis Functions Network (RBF) based control strategy and showed experimental application on a pharmaceutical batch cooling crystallization process. A reference trajectory of particle counts measured by FBRM is followed by manipulating and updating the temperature profile during the experiment time. Performance of the proposed control strategy based on RBF was evaluated with different training data techniques and in the presence of disturbances in the system such as initial concentration and seed specifications.

Acknowledgment
We would like to thank the Danish Council for Independent Research (DFF) for financing the project with grant ID: DFF-6111600077B.

Self-Optimizing Control of a Continuous Pharmaceutical Manufacturing Plant

David P. Piñeiro[1,2], Anastasia Nikolakopoulou[2], Johannes Jäschke[3], Truls Gundersen[1] and Richard D. Braatz[2]

[1]Energy and Process Engineering, Norwegian University of Science and Technology, Trondheim, Norway
[2]Department of Chemical Engineering, Massachusetts Institute of Technology, Cambridge, MA
[3]Chemical Engineering, Norwegian University of Science and Technology, Trondheim, Norway

Abstract: The pharmaceutical industry is increasing its use of continuous manufacturing, which enables easier scale-up, faster time-to-market, and tighter control over product quality [Plumb, 2005]. Continuous operation is well suited for the application of plantwide control approaches such as self-optimizing control (SOC), where the goal is to find a set of controlled variables (CVs) which, when kept at constant setpoints, indirectly lead to near-optimal operation [Skogestad, 2000, Jaschke et al., 2017].

The main idea of SOC is to control optimal invariants, which are process variables whose optimal setpoints are insensitive to disturbances and measurement noise. The ideal SOC variable would be the gradient of the objective function, where the necessary condition for optimality is enforced by controlling the gradient to zero. In real processes, where the gradient cannot be measured directly, selecting self-optimizing controlled variables is equivalent to finding good approximations of the gradient using single measurements or combinations, often linear, of measurements.

An SOC structure is able to track the optimal steady-state operating point of the plant closely in the presence of uncertainty, without the need for re-optimization. In hierarchical control structures which have time-scale separation between the supervisory control and optimization layers, SOC at the supervisory layer can ensure optimal operation when disturbances impact the process, without waiting for setpoint updates given by the upper level optimization layer. Only in the presence of unmodeled disturbances or when large disturbances move the process far away from the nominal operating point, a new setpoint is computed from the optimizer to correct for the steady-state loss of optimality.

This work explores how self-optimizing control can be applied to the continuous-flow synthesis of atropine, and appears to be the first application of self-optimizing control (SOC) to a continuous pharmaceutical manufacturing plant reported in the literature.

This study employs an improved version of a recently published first-principles model of the continuous flow synthesis of atropine [Nikolakopoulou et al., 2019], which is an active pharmaceutical ingredient (API) with a variety of therapeutic uses, including the treatment of heart rhythm problems. The model was constructed from the process flowsheet and experimental results reported by [Bedard et al., 2017]. The Environmental factor (E-factor, defined by the ratio of the mass of waste per mass of product) is used as the objective function to find the optimal operating point of the plant. The main sources of uncertainty considered when designing the control structure include perturbations in the process variables (disturbances), parametric model uncertainty, and sensor noise.

The controlled variables are selected in two steps. First, local methods [Halvorsen et al., 2003, Kariwala et al., 2008, Alstad et al., 2009, Kariwala and Cao, 2009] are used to screen promising candidate controlled variables around the nominal operating point, where the plant is expected to operate most of the time. These local methods rely on a linearized model of the plant and a quadratic approximation of the objective function. The performance of a given control structure is quantified in terms of the loss of optimality, i.e., the difference between the value of the objective function resulting from constant setpoint control using that particular control structure and the value of the objective function resulting from truly optimal operation [Halvorsen et al., 2003]. The sets of controlled variables are selected by systematically minimizing the average loss of optimality with respect to the given objective function (in this case, the E-factor). In a second step, these preliminary candidate controlled variables are then validated over the entire operating envelope using the original nonlinear model of the plant and Monte Carlo simulations for independent and normally distributed scenarios of disturbances and measurement noise realizations. It was found that near-optimal operation can be achieved by controlling a linear combination of flow rate

and concentration measurements to constant setpoints, with only small losses of optimality for all of the model parametric uncertainties, disturbances, and measurement noise considered in this case study.

Keywords: Self-Optimizing Control, Control Structure Design, Plantwide Control, Pharmaceutical Manufacturing

References

Alstad, V., Skogestad, S., and Hori, E. S. (2009). Optimal measurement combinations as controlled variables. *Journal of Process Control*, 19(1):138–148.

Bedard, A.-C., Longstreet, A. R., Britton, J., Wang, Y., Moriguchi, H., Hicklin, R. W., Green, W. H., and Jamison, T. F. (2017). Minimizing E-factor in the continuous-flow synthesis of diazepam and atropine. *Bioorganic & Medicinal Chemistry*, 25(23):6233–6241.

Halvorsen, I. J., Skogestad, S., Morud, J. C., and Alstad, V. (2003). Optimal selection of controlled variables. *Industrial & Engineering Chemistry Research*, 42(14):3273–3284.

Jaschke, J., Cao, Y., and Kariwala, V. (2017). Self-optimizing control – A survey. *Annual Reviews in Control*, 43:199–223.

Kariwala, V. and Cao, Y. (2009). Bidirectional branch and bound for controlled variable selection. Part II: Exact local method for self-optimizing control. *Computers & Chemical Engineering*, 33(8):1402–1412.

Kariwala, V., Cao, Y., and Janardhanan, S. (2008). Local self-optimizing control with average loss minimization. *Industrial & Engineering Chemistry Research*, 47(4):1150–1158.

Nikolakopoulou, A., von Andrian, M., and Braatz, R. D. (2019). Supervisory control of a compact modular reconfigurable system for continuous-flow pharmaceutical manufacturing. In Proceedings of the *American Control Conference*. in press.

Plumb, K. (2005). Continuous processing in the pharmaceutical industry: Changing the mindset. *Chemical Engineering Research Design*, 83(6):730–738.

Skogestad, S. (2000). Plantwide control: The search for the self-optimizing control structure. *Journal of Process Control*, 10(5):487–507.

Model-based monitoring of pH gradients in a pilot-scale lactic acid bacteria fermentation

Robert Spann[1], Krist V. Gernaey[2], Gürkan Sin[2]

[1] Chr. Hansen, Boege Allé 10-12, 2970 Hoersholm, Denmark

[2] Process and Systems Engineering Center (PROSYS), Department of Chemical and Biochemical Engineering, Technical University of Denmark, Søltofts Plads, Building 229, 2800 Kgs. Lyngby, Denmark

Abstract

There is an increasing interest in process analytical technology (PAT) tools for on-line monitoring and control of bioprocesses. In large-scale bioprocesses, heterogeneous process conditions occur due to imperfect mixing. An aerotolerant *Streptococcus thermophilus* batch cultivation in a 700-L bioreactor was employed as a case study. These cells are used in the dairy industry as starter cultures, e.g., for cheese and yoghurt production. The production target of the cultivation is thus the cells, which needs to be optimized. However, pH gradients that occur in large vessels affect the biomass growth and modelling them is key for the understanding and improvement of the production process. A mechanistic bioprocess model describing the biomass growth and lactate production is coupled with a chemical model that predicts the pH in the cultivation broth and a compartment model that accounts for the mixing in the bioreactor. Utilizing these models in a soft sensor enabled the monitoring of the critical quality attributes and critical process parameters, such as the biomass growth and the pH gradients respectively. A Monte Carlo simulation within the soft sensor considering model parameters' and measurements' uncertainties was utilized to quantify the risk of not achieving the target biomass production in real time. Such tools will help biotechnological companies to optimize the process, e.g., by model-based control of the agitation or model-based design of the bioreactor to minimize pH gradients and maximize productivity.

Keywords: lactic acid bacteria (LAB) fermentation, modelling, soft sensor, risk assessment, pH gradient

Nonlinear Model Predictive Control of Wastewater Treatment for Smart, Cost Efficient Aeration

P. A. Stentoft*,, A.K. Vangsgaard*, T. Munk-Nielsen***

**Krüger A/S, Veolia Water Technologies, Søborg, Denmark, (e-mail: akv@kruger.dk, thm@kruger.dk, pas@kruger.dk)*
*** Department of Applied Mathematics and Computer Science, Technical University of Denmark (e-mail:past@dtu.dk)*

Abstract: The Activated Sludge Process (ASP) is essential in municipal wastewater treatment. This is because it removes nutrients and carbon from the incoming wastewater before it is discharged back to environment. While the ASP is important, it also requires large amounts of electricity. Furthermore the discharged nutrients are subject to taxation. This implies that control is crucial to minimize costs and to secure satisfactory treatment. This study presents a novel model predictive control strategy to control an ASP with alternating operation. This means, that the aeration equipment is switching between on and off in controlled cycles to secure good conditions (aerobic/anaerobic) for the nutrient removing bacteria. The strategy uses discretely observed stochastic differential equations to predict the effect of control actions on the nutrient concentrations. The model parameters and states are estimated using maximum likelihood and updated with an Extended Kalman Filter. This is done in real-time with measurements from sensors located directly in the process tanks. The setup secures that changes in the biomass, inflow to the plant etc. are quickly adapted in the model and hence the model provides reliable predictions on horizons up to 24 hours ahead. The optimal control is estimated by minimizing an objective function over a 24 hours prediction horizon. We investigate one objective function (i) which describes the total costs as nutrient taxes and electricity consumption with variable prices. Furthermore we test an objective function (ii) which estimates the total environmental impact, here defined as eutrophication related to the discharge of nutrients and global warming potential related to the electricity production method and emissions from the biological processes (in the form of nitrous oxide). The strategy is tested with data from two wastewater treatment plants in Denmark and electricity price data from the largest power market in Scandinavia (run by Nord Pool a/s). Results from simulations using (i) indicate that costs can be reduced by approximately 25% on a small wastewater treatment plant as compared with the currently installed rule-based control. The reduction in cost is caused firstly by the ability of the MPC to find the best balance between taxes and electricity consumption and, secondly, by the prioritization of electricity consumption in periods when electricity prices are low. Results from (ii) show that it is possible to reduce environmental impact. However it is sensitive to the weights on the different impacts which must be specified in the objective function, and hence these needs to be determined with caution.

Energy Savings using MPC on a TES unit for Heat Exchange in Industrial Clusters ⋆

Mandar Thombre, Johannes Jäschke

Department of Chemical Engineering, Norwegian University of Science & Technology , NO-7491 Trondheim, (e-mail: mandar.thombre@ntnu.no).

Abstract: An industrial cluster refers to multiple process plants located in the same geographical area, facilitating the sharing of utilities, infrastructure and services (Chertow, 2007). Surplus heat recovery is an especially attractive proposition for such industrial clusters since it presents an opportunity for flexible energy exchange within the cluster, with plants representing both sources and sinks of surplus heat. A prominent operational challenge for surplus heat exchange between multiple plants is the temporal decoupling between the availability of surplus heat and its demand. Thermal energy storage (TES) is a viable option to resolve this issue (Mir et al., 2016), since it offers operating flexibility to heat recovery by creating a buffer between the supply and demand of surplus heat, thereby reducing peak energy requirements.

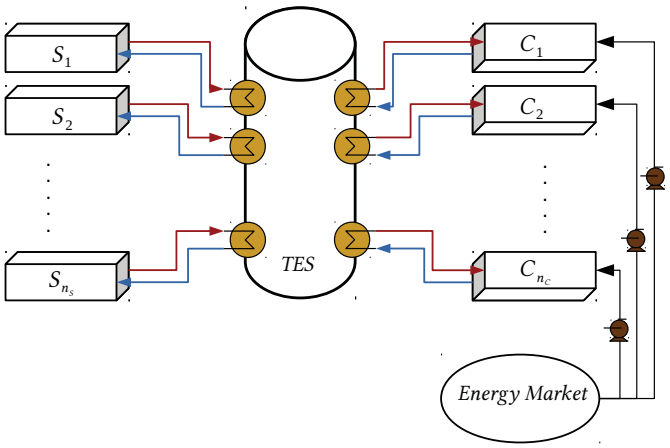

In this work, we propose an model predictive control (MPC) scheme for coordinating the heat exchange in an industrial cluster with a TES unit. We compare this with a corresponding case without TES, and demonstrate that use of a TES unit along with optimal control leads to higher energy-efficiency and significant energy savings. An industrial cluster system with a hot water tank for TES is shown in the figure. The various plants act as sources $(S_1, \ldots, S_{nS})$ or sinks $(C_1, \ldots, C_{nC})$ of the heat in the TES tank. A common practice in case of excess demand is to purchase electricity directly from the market, or to burn fossil fuels using boilers, to heat up the required process streams. Not only are these "peak-heating" sources of energy expensive, significantly increasing the operating costs in the cluster, but they also lead to higher carbon emissions. The economic objective then is to minimize this peak-heating while satisfying the consumer-side heat demand.

We consider that the cumulative surplus heat supply and demand in the cluster are equal over a 24-hour period, but that the supply and demand profiles are asynchronous. In the case without TES, this leads to large heat wastage in case of excess supply and large peak-heating in case of excess demand. It is shown that by using the MPC framework along with storage, the surplus heat in the cluster is used to charge up the TES unit during periods of low demand, and that this stored energy is subsequently used in a low-supply/high-demand scenario. In addition, we quantitatively demonstrate the improved energy-savings obtained via the use of TES, by comparing the total dumped heat and the total peak-heating required in the two cases.

Keywords: model predictive control, thermal energy storage, industrial cluster

REFERENCES

Chertow, M.R. (2007). "Uncovering" Industrial Symbiosis. *Journal of Industrial Ecology*, 11(1), 11–30.

Mir, L., Gasia, J., and Cabeza, L.F. (2016). Thermal energy storage for industrial waste heat recovery: A review. *Applied Energy*, 179, 284 – 301.

⋆ This work is partly funded by HighEFF - Centre for an Energy Effcient and Competitive Industry for the Future. The authors gratefully acknowledge the financial support from the Research Council of Norway and user partners of HighEFF, an 8 year Research Centre under the FME-scheme (Centre for Environment-friendly Energy Research, 257632).

Discovery through process data analytics

Nina Thornhill[1]

[1]ABB/RAEng Professor of Process Automation, Department of Chemical Engineering, Imperial College London

Process plants may have thousands of measurements. They also have intricate connections that mean the measurements are not independent of one other. The talk will describe research that has helped with the complicated challenges of generating insights from these measurements to improve process performance. As an example, I will show how data analytics revealed the widespread consequences of slugging flow on a North Sea oil and gas platform. I will give some opinions about how process data analytics fit into the wider context of autonomous operation and artificial intelligence, and will speculate about research trends in the next few years. I am very grateful to ABB Corporate Research for supporting my post at Imperial College from 2007 until now. ABB collaborators and I have also worked with other industrial and academic partners in several European Marie Skłodowska-Curie projects.

Proceedings of the 22nd Nordic Process Control Workshop
August 2019, Kgs. Lyngby, Denmark

Linear-quadratic differential game control: two ways to ensure solvability

Vladimir Turetsky *

* *Ort Braude College of Engineering, Karmiel, Israel*
(e-mail: turetsky1@braude.ac.il)

Abstract:
A control, based on the linear-quadratic differential game, is a conventional tool in various applications. It is well known that this control becomes infeasible for some combinations of penalty coefficients of the cost functional, because the corresponding differential game does not satisfy the solvability condition. One way to guarantee the solvability is reducing the control penalty coefficient. However, in some practical examples, the penalty coefficient is fixed and cannot be reduced. It is proved that for given penalty coefficients, a sufficiently small control time interval can be chosen in such a way that the game on this interval is solvable. This allows employing a receding horizon control scheme. Simulation results are presented.

Keywords: differential game, solvability condition, Riccati equations, receding horizon.

1. INTRODUCTION

Linear-quadratic differential game (LQDG) is formulated for a linear dynamic system, whereas its cost functional is quadratic with respect to the state and control variables. It was solved by Ho et al. (1965) in the case of no state variable in the integral term of the cost functional. The solution in more general case was obtained by Zhukovskii (1970). The LQDG solution is based on the matrix Riccati differential equation (MRDE). In contrast with the one-side linear-quadratic optimization problem (Letov (1960); Kalman (1960)), the MRDE, associated with the LQDG, can have conjugate points on the game time interval, where its solution "blows up" (tends to infinity). As a rule, this leads to a non-existence of the LQDG solution on the entire game time interval.

Despite possible non-solvability, an LQDG based control became a conventional tool in a wide variety of robust control problems in conditions of uncertainty and conflict, including missile guidance (Shinar and Shima (2012)), disturbance rejection (Pachter and Pham (2010)), trajectory tracking (Turetsky et al. (2014); Turetsky (2016a)), robotics (Gu (2008)), etc. By linearization, the LQDG control can be applied for non-linear systems (Turetsky (2016b); Bhargav et al. (2018)).

The verifiable solvability condition for a generalized LQDG was derived by Shinar et al. (2008). In order to guarantee the fulfilment of this condition at a prescribed time interval, one should choose sufficiently small penalty coefficients in the cost functional. However, the values of the penalty coefficients can be determined by some technical constraints and cannot be reduced according to the solvability condition. In this paper, it is shown that for given penalty coefficients, a sufficiently small final time can be chosen in such a way that the game is solvable on the reduced time interval. It allows exploiting the LQDG control repeatedly at subsequent time intervals as in the receding horizon control scheme (Kwon and Han (2006)).

2. PREVIOUS RESULT: SOLVABILITY CONDITION

Let us consider the generalized LQDG for a linear system

$$\dot{x} = A(t)x + B(t)u + C(t)v,\ x(t_0) = x_0, \quad t_0 \le t \le t_f, \tag{1}$$

where $x \in \mathbb{R}^n$ is the state vector, $u \in \mathbb{R}^r$ and $v \in \mathbb{R}^s$ are the minimizer's and the maximizer's controls, respectively; t_0 and t_f are the prescribed initial and final time instants; the matrix functions $A(t)$, $B(t)$ and $C(t)$ are continuous. The cost functional is

$$J_{\alpha\beta} = G(x(\cdot)) + \alpha \int_{t_0}^{t_f} |u(t)|^2 dt - \beta \int_{t_0}^{t_f} |v(t)|^2 dt, \tag{2}$$

where

$$G(x(\cdot)) \triangleq \sum_{i=1}^{K} |D(t_i)(x(t_i) - y(t_i))|^2 + \sum_{j=1}^{L} \int_{a_j}^{b_j} |D(t)(x(t) - y(t))|^2 \, dt, \tag{3}$$

$t_i \in (t_0, t_f]$, $i = 1, \ldots, K$, are prescribed time instants; $(a_j, b_j) \subset [t_0, t_f]$, $j = 1, \ldots, L$, are non-intersecting intervals; $y(t)$ and $D(t)$, $t \in [t_0, t_f]$, are n-vector and $n \times n$-matrix functions, continuous for $t \in [a_j, b_j]$, $j = 1, \ldots, L$; $\alpha, \beta > 0$ are the control penalty coefficients of the players. Note that the state term of (2) can be represented as a Lebesgue-Stilties integral over properly defined mixed discrete/continuous measure:

$$G(x(\cdot)) = \int\limits_{[t_0,t_f]} |D(t)(x(t) - y(t))|^2 \, dm(t). \quad (4)$$

Remark 1. If $G(x(\cdot))$ is small, this means that the system tracks the function $y(t)$ in the sense of the space $L_2([t_0, t_f], m)$. It was proved (see, e.g., Turetsky et al. (2014); Turetsky (2016a)) that, subject to some additional conditions, the minimizer's optimal LQDG control also guarantees the smallness of $G(x(\cdot))$.

For $t \in [t_0, t_f]$, let us define two families of compact, self-adjoint, positive definite operators mapping $L_2^n[t_0, t_f], m(\cdot)]$ into itself:

$$\mathcal{F}_k(t; t_0, t_f) f(\cdot) = \int\limits_{[t,t_f]} F_k(t, \eta, \nu) f(\nu) dm(\nu), \quad k = u, v, \quad (5)$$

where

$$F_u(t, \eta, \nu) =$$

$$D(\eta) \left(\int\limits_t^{\min(\eta,\nu)} \Phi(\eta, \tau) B(\tau) B^T(\tau) \Phi^T(\nu, \tau) d\tau \right) D^T(\nu), \quad (6)$$

$$F_v(t, \eta, \nu) =$$

$$D(\eta) \left(\int\limits_t^{\min(\eta,\nu)} \Phi(\eta, \tau) C(\tau) C^T(\tau) \Phi^T(\nu, \tau) d\tau \right) D^T(\nu), \quad (7)$$

$\Phi(t, \tau)$ is the fundamental matrix of (1), i.e.,

$$\dot{\Phi}(t, \tau) = A(t)\Phi(t, \tau), \quad \Phi(\tau, \tau) = I_n. \quad (8)$$

Define the operator

$$\mathcal{F}_{\alpha\beta}(t; t_0, t_f) = \frac{1}{\beta}\mathcal{F}_v(t; t_0, t_f) - \frac{1}{\alpha}\mathcal{F}_u(t; t_0, t_f). \quad (9)$$

Let $\lambda_{\alpha\beta}^{(k)}(t; t_0, t_f)$, $k = 1, 2, ...$, be the eigenvalues of $\mathcal{F}_{\alpha\beta}(t; t_0, t_f)$, and

$$\lambda^* = \lambda^*(\alpha, \beta, t_0, t_f) \triangleq \sup_k \sup_{t \in [t_0,t_f]} \lambda_{\alpha\beta}^{(k)}(t; t_0, t_f). \quad (10)$$

Theorem 1. (Shinar et al. (2008)). The LQDG (1) – (2) is solvable if

$$\lambda^*(\alpha, \beta, t_0, t_f) < 1. \quad (11)$$

Remark 2. If (11) holds, then for any position $(t, x) \in [t_0, t_f] \times \mathbb{R}^n$, the saddle point of the LQDG are given by

$$u^0(t, x) = -\frac{1}{\alpha} B^T(t) \Phi^T(t_f, t) \Big(2R_{\alpha\beta}(t)\Phi(t_f, t)x + r_{\alpha\beta}(t) \Big), \quad (12)$$

$$v^0(t, x) = \frac{1}{2\beta}(t) C^T(t) \Phi^T(t_f, t) \Big(2R_{\alpha\beta}(t)\Phi(t_f, t)x + r_{\alpha\beta}(t) \Big), \quad (13)$$

where the matrix function $R_{\alpha\beta}(t)$ and the vector function $r_{\alpha\beta}(t)$ satisfy some impulsive Riccati and linear differential equations, respectively. The non-solvability of the LQDG means that the corresponding Riccati equation does not have the solution on the entire control interval.

3. SOLVABILITY BY CHOOSING α

The following theorem is, in a sense, inverse to Theorem 1.

Theorem 2. Let $t_0 \geq 0$, $t_f > t_0$ and $\beta > 0$ be fixed. Let

$$\mathrm{Ker}\mathcal{F}_u(t; t_0, t_f) \subseteq \mathrm{Ker}\mathcal{F}_v(t; t_0, t_f), \quad t \in [t_0, t_f]. \quad (14)$$

Then there exists $\alpha^* = \alpha^*(t_0, t_f, \beta) > 0$ such that (11) holds for all $\alpha \in (0, \alpha^*)$.

This result implies a common implementation practice which is to choose a (sufficiently small) α in (2) for given t_0, t_f and β which ensures (11) at the prescribed time interval.

Example 3.1. Scalar system with simple motions. Consider an LQDG for the scalar system

$$\dot{x} = u + v, \quad (15)$$

with the pure integral functional

$$G(x(\cdot)) = \int\limits_{t_0}^{t_f} x^2(t) dt. \quad (16)$$

The LQDG cost functional is

$$J_{\alpha\beta} = \int\limits_{t_0}^{t_f} x^2(t) dt + \alpha \int\limits_{t_0}^{t_f} u^2(t) dt - \beta \int\limits_{t_0}^{t_f} v^2(t) dt, \quad (17)$$

In this example,

$$\mathcal{F}_u(t; t_0, t_f) f(\cdot) = \mathcal{F}_v(t; t_0, t_f) f(\cdot) = \int\limits_t^{t_f} [\min(\eta, \nu) - t] \, f(\nu) d\nu. \quad (18)$$

For $\alpha \leq \beta$, the operator $\mathcal{F}_{\alpha\beta}$, given by (9), has non-positive eigenvalues, thus providing the LQDG solvability. For $\alpha > \beta$, due to Turetsky and Glizer (2016), the eigenvalues of this operator are

$$\lambda_{\alpha\beta}^{(k)}(t; t_0, t_f) = \frac{4(1/\beta - 1/\alpha)(t_f - t)^2}{(2k - 1)^2\pi^2}, \; k = 1, 2, ..., \quad (19)$$

yielding

$$\lambda^* = \frac{4(1/\beta - 1/\alpha)(t_f - t_0)^2}{\pi^2}. \quad (20)$$

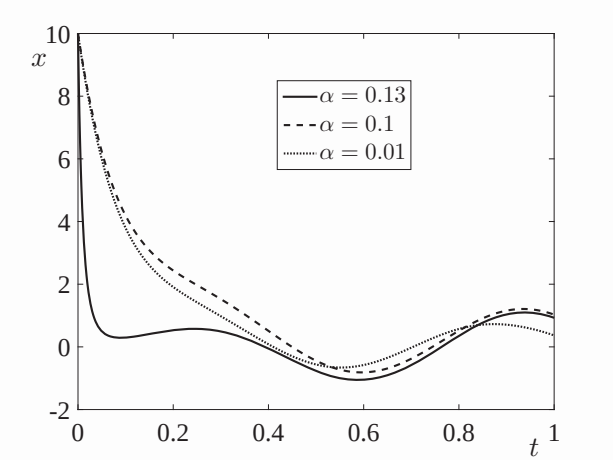

Fig. 1. Trajectories $x(t)$

Thus, the critical value α^* from Theorem 2 is

$$\alpha^* = \begin{cases} \dfrac{1}{\frac{1}{\beta} - \frac{\pi^2}{4(t_f-t_0)^2}}, & \beta < \dfrac{4(t_f-t_0)^2}{\pi^2}, \\ \infty, & \beta \geq \dfrac{4(t_f-t_0)^2}{\pi^2}. \end{cases} \tag{21}$$

In Fig. 1, three trajectories $x(t)$ are depicted for $t_0 = 0$, $t_f = 1$, $\beta = 0.1$, $v(t) = 10\sin 10t$, and for different values of $\alpha < \alpha^* = 0.1328$.

Example 3.2. Inverted pendulum. The inverted pendulum (see, e.g., Åström and Murray (2010)) is described by the differential equations

$$\begin{aligned} \dot{z}_1 &= z_2 \\ \dot{z}_2 &= a\sin z_1 - bz_2 + c_1\cos z_1 U + c_2 \cos z_1 V, \end{aligned} \tag{22}$$

where x_1 is the pendulum angle, U and V are external forces playing the roles of the control (minimizer) and the disturbance (maximizer), respectively. Define for the system (22) the functional

$$G_{\rm ip}(z(\cdot)) = \int_0^2 [z_1(t) - \pi/10]^2 dt + \int_3^5 [z_1(t) - \pi/10]^2 dt + [z_1(2.5) - \pi/4]^2. \tag{23}$$

This functional is the particular case of (3) for $D = [1, 0]$, $L = 2$, $a_1 = t_0 = 0$, $b_1 = 2$, $a_2 = 3$, $b_2 = t_f = 5$, $K = 1$, $t_1 = 2.5$. It represents the objective of the first player to keep the pendulum angle constant ($\pi/10$) on the intervals $[0, 2]$ and $[3, 5]$, and to set the angle to $\pi/4$ for $t = 2.5$.

This system is feedback linearizable (Isidori (1989)). The linearized system is obtained by the trivial transformation $x = z$ (Turetsky (2016b)):

$$\begin{aligned} \dot{x}_1 &= x_2 \\ \dot{x}_2 &= u + v, \end{aligned} \tag{24}$$

where

$$u = a\sin z_1 - bz_2 + c_1\cos z_1 U, v = c_2\cos z_1 V. \tag{25}$$

Consider the LQDG for (24) with the functional

$$J_{\alpha\beta} = G_{\rm ip}(x(\cdot)) + \alpha\int_{t_0}^{t_f} u^2(t)dt - \beta\int_{t_0}^{t_f} v^2(t)dt, \tag{26}$$

In the LQDG (24), (26),

$$\mathcal{F}_u(t;t_0,t_f)f(\cdot) = \mathcal{F}_v(t;t_0,t_f)f(\cdot) = \mathcal{F}(t;t_0,t_f)f(\cdot) = \int_{[t,t_f]} F(t,\eta,\nu)f(\nu)dm(\nu), \tag{27}$$

where

$$F(t,\eta,\nu) = \int_t^{\min(\eta,\nu)} (\eta-\tau)(\nu-\tau)d\tau = \varphi(\eta,\nu,\min(\eta,\nu)) - \varphi(\eta,\nu,t), \tag{28}$$

$$\varphi(\eta,\nu,\xi) = \frac{\xi^3}{3} - \frac{\eta+\nu}{2}\xi^2 + \eta\nu\xi. \tag{29}$$

For $\alpha \leq \beta$, the operator $\mathcal{F}_{\alpha\beta}$, given by (9), is non-positive, i.e., the condition (11) is valid and the LQDG is solvable.

Let $\bar{\lambda}^{(k)}_{\alpha\beta}(t;t_0,t_f)$, $k = 1, 2, ...$, be the eigenvalues of the positive definite operator (27). Then, for $\alpha > \beta$, the condition (11) becomes

$$\left(\frac{1}{\beta} - \frac{1}{\alpha}\right)\bar{\lambda}^* < 1, \tag{30}$$

where

$$\bar{\lambda}^* = \lambda^*(\alpha,\beta,t_0,t_f) = \sup_k \sup_{t\in[t_0,t_f]} \bar{\lambda}^{(k)}_{\alpha\beta}(t;t_0,t_f). \tag{31}$$

It can be directly shown that the second supremum in (31) is attained for $t = t_0$, i.e.,

$$\bar{\lambda}^* = \lambda^*(\alpha,\beta,t_0,t_f) = \sup_k \bar{\lambda}^{(k)}_{\alpha\beta}(t_0;t_0,t_f). \tag{32}$$

Thus, the critical value α^* from Theorem 2 is

$$\alpha^* = \begin{cases} \dfrac{\bar{\lambda}^*\beta}{\bar{\lambda}^* - \beta}, & \beta < \bar{\lambda}^*, \\ \infty, & \beta \geq \bar{\lambda}^*. \end{cases} \tag{33}$$

The value of $\bar{\lambda}^*$ is the maximal solution of the Sturm-Liouville problem

$$\mathcal{F}(t_0;t_0,t_f)f(\cdot) = \lambda f(\cdot), \tag{34}$$

which, due to (23) and (27) – (29), becomes for $t_0 = 0$:

$$\int_0^2 \varphi(\eta,\nu,\min(\eta,\nu))f(\nu)d\nu + f(2.5) +$$

$$\int_3^5 \varphi(\eta,\nu,\min(\eta,\nu))f(\nu)d\nu = \lambda f(\eta), \quad \eta\in[0,5]. \qquad (35)$$

We treat the problem (35) numerically by replacing the integrals with their quadrature approximation. To this end, define the same grids over $\eta \in [0,5]$ and $\nu \in [0,5]$ consisting of $2N+1$ points: $\eta_i = \nu_i = i\Delta$, $i = 1,...,N$, $\eta_{N+1} = \nu_{N+1} = 2.5$, $\eta_{N+1+i} = \nu_{N+1+i} = 3 + i\Delta$, $i = 1,...,N$, where $\Delta = 2/N$. Then, applying the right-hand rectangles approximation yields

$$\Delta\sum_{j=1}^{N}\varphi(\eta_i,\nu_j,\min(\eta_i,\nu_j))f(\nu_j) +$$
$$\varphi(\eta_i,\nu_{N+1},\min(\eta_i,\nu_{N+1}))f(\nu_{N+1}) +$$
$$\Delta\sum_{j=1}^{N}\varphi(\eta_i,\nu_{N+1+j},\min(\eta_i,\nu_{N+1+})))f(\nu_{N+1+j}) =$$
$$\lambda f(\eta_i), \quad i = 1,...,2N+1. \qquad (36)$$

Let us define the vector $\hat{f} = (f(\eta_1),...,f(\eta_{2N+1}))^T \in \mathbb{R}^{2N+1}$, and the $(2N+1)\times(2N+1)$ matrix H with the elements

$$H_{ij} = c_j\varphi(\eta_i,\nu_j,\min(\eta_i,\nu_j)), \quad i,j = 1,...,2N+1, \quad (37)$$

where

$$c_j = \begin{cases} \Delta, & j \neq N+1, \\ 1, & j = N+1. \end{cases} \qquad (38)$$

Then the equation (36) becomes

$$H\hat{f} = \lambda\hat{f}. \qquad (39)$$

Thus, the value $\bar{\lambda}^*$ is approximated by the maximal eigenvalue λ_N^* of the matrix H for large N. In Table 1, the values of λ_N^* are shown for $N = 5$, 10, 50, 100, 500, 1000, 5000, 10000. In the third column of the table, the differences between the current and the previous values are shown. The table demonstrates the convergence of λ_N^* for $N\to\infty$.

Table 1. Maximal eigenvalues of the matrix H

N	λ_N^*	$\lvert\Delta\lambda_N^*\rvert$
5	57.3897	
10	53.7866	3.6031
50	51.0031	2.7835
100	50.6613	0.3418
500	50.3889	0.2724
1000	50.3549	0.0340
5000	50.3277	0.0272
10000	50.3243	0.0034

Let us set $\bar{\lambda}^* \approx \lambda_{10000}^* = 50.3243$. Then, for $\beta = 0.1$, $\alpha^* = 0.1002$.

In Fig. 2, the trajectories $z_1(t)$ are depicted for $t_0 = 0$, $t_f = 5$, $x_0 = (0.5, 0)^T$, $a = b = c_1 = 1$, $c_2 = 10$, $V(t) = \sin(5t)$, and for different values of $\alpha < \alpha^*$. It is seen that for smaller values of α, the tracking of $y(t)$ is more accurate.

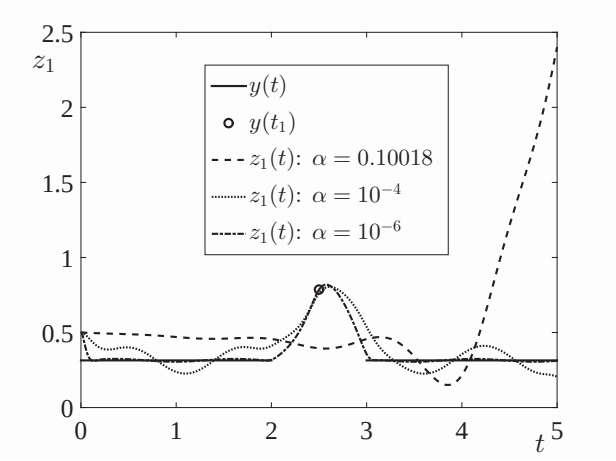

Fig. 2. Trajectories $z_1(t)$

4. SOLVABILITY BY CHOOSING CONTROL INTERVAL

For some technical reasons, the penalty coefficient α can be fixed in such a way that (11) is not satisfied, and it cannot be reduced according to Theorem 2. In such a case, one alternatively can reduce the control interval.

Theorem 3. Let $t_0 \geq 0$ $\alpha > 0$ and $\beta > 0$ be fixed. Let for some $T > t_0$,

$$\mathrm{Ker}\mathcal{F}_u(t;t_0,t_f) \subseteq \mathrm{Ker}\mathcal{F}_v(t;t_0,t_f), \quad t\in[t_0,T]. \qquad (40)$$

Then there exists $t_f^* = t_f^*(t_0,\alpha,\beta) \in (t_0,T]$ such that (11) holds for all $t_f \in (t_0,t_f^*)$.

This result allows constructing a suboptimal LQDG control in the receding horizon fashion. Assume that the LQDG is unsolvable on $[t_0,t_f]$ for given values of α and β. Let us divide the interval into $M = M(t_0,t_f,\alpha,\beta)$ subintervals $t_0 < t_1 < ... < t_M = t_f$ satisfying

$$t_{i+1} \leq t_f^*(t_i,\alpha,\beta), \quad i = 0,...,M-1. \qquad (41)$$

This condition guarantees that the LQDG is solvable on each subinterval $[t_i,t_{i+1}]$, $i = 0,...,M-1$.

In this section, we present two simplified examples of the implementation of Theorem 3. In both examples, $K = 0$ (there are no discrete measure points in the functional (3)) and $L = 1$ ((3) contains a single integral term over the whole interval $[t_0,t_f]$). Moreover, in these examples (as in Examples 3.1 – 3.2), $\mathcal{F}_u(t;t_0,t_f) = \mathcal{F}_v(t;t_0,t_f)$.

Example 4.1. Scalar system with simple motions.

Due to (20), the critical value t_f^* in the LQDG (15), (17), is

$$t_f^*(t_0,\alpha,\beta) = t_0 + \frac{\pi}{2\sqrt{1/\beta - 1/\alpha}}. \qquad (42)$$

In Fig. 3, the trajectory $x(t)$, generated by a suboptimal LQDG control for $t_0 = 0$, $t_f = 5$, $\alpha = 0.15$, $\beta = 0.1$, $v(t) = 10\sin 10t$, $M = 8$, is depicted. In this example $t_{i+1} - t_i = 0.4 < t_f^* - t_i = 0.8604$, $i = 0, ..., 7$, and the LQDG is solvable on each subinterval.

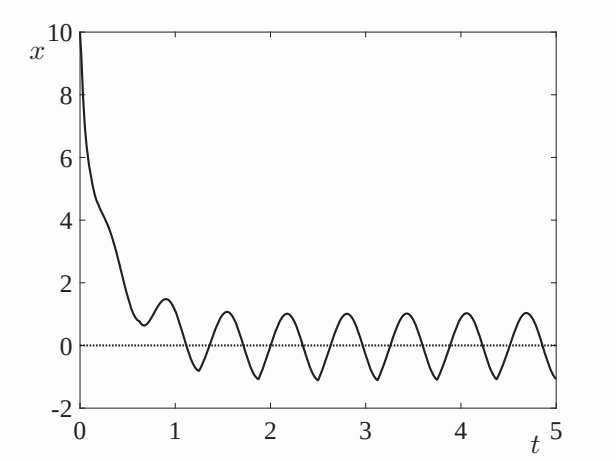

Fig. 3. Trajectory $x(t)$ by suboptimal LQDG control

Example 4.2. Inverted pendulum.

Consider the problem for the inverted pendulum (22) with the functional

$$G^0_{\rm ip}(z(\cdot)) = \int_0^{t_f} z_1^2(t)dt. \qquad (43)$$

As in Example 3.2, by the feedback linearization, the problem is reformulated into the LQDG for the system (24) with the cost functional

$$J_{\alpha\beta} = G^0_{\rm ip}(x(\cdot)) + \alpha \int_0^{t_f} u^2(t)dt - \beta \int_0^{t_f} v^2(t)dt. \qquad (44)$$

Similarly to Example 3.1, the maximal eigenvalue λ^* of $\mathcal{F}_{\alpha\beta}(t; 0, t_f)$ is equal to the maximal eigenvalue of $\mathcal{F}_{\alpha\beta}(0; 0, t_f)$

$$\mathcal{F}_{\alpha\beta}(0; 0, t_f)f(\cdot) = \left(\frac{1}{\beta} - \frac{1}{\alpha}\right) \int_0^{t_f} \varphi(\eta, \nu, \min(\eta, \nu))d\nu, \qquad (45)$$

where the function $\varphi(\eta, \nu, \xi)$ is given by (29). As in Example 3.1, we approximate λ^* by the maximal eigenvalue of the matrix H^0

$$H^0_{ij} = \left(\frac{1}{\beta} - \frac{1}{\alpha}\right) \Delta^0 \varphi(\eta_i, \nu_j, \min(\eta_i, \nu_j)), \quad i, j = 1, ..., N, \qquad (46)$$

where $\Delta^0 = t_f/N$, $\eta_i = i\Delta^0$, $\nu_j = j\Delta^0$, $i, j = 1, ..., N$.

In Fig.4, the approximate values of λ^* for $N = 1000$ are depicted as a function of $t_f \in [0.5, 2]$ for $\alpha = 0.15$, $\beta = 0.1$. In this example, the critical value $t_f^* = 1.38$.

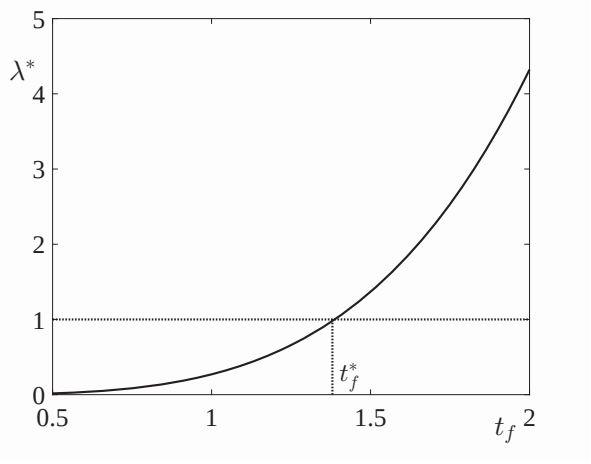

Fig. 4. Approximate values of λ^* for $\alpha = 0.15$, $\beta = 0.1$

In Fig. 5, the trajectory $z_1(t)$, generated by a suboptimal LQDG control for $t_0 = 0$, $t_f = 5$, $\alpha = 0.15$, $\beta = 0.1$, $v(t) = \sin 5t$, $M = 4$, is depicted. It is seen that the LQDG control is feasible on each of subintervals, but the tracking is not accurate.

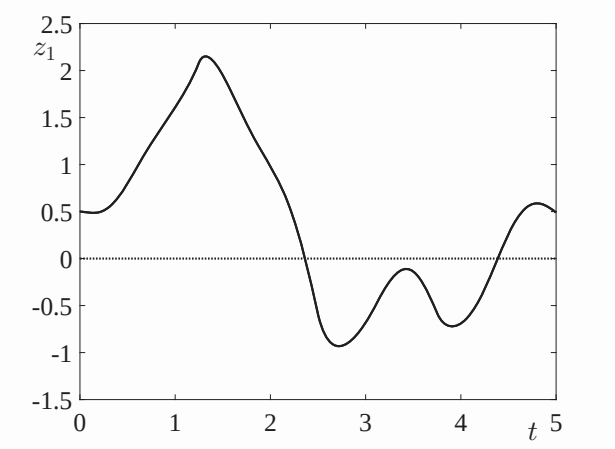

Fig. 5. Trajectory $z_1(t)$: suboptimal LQDG control for $\alpha = 0.15$, $\beta = 0.1$

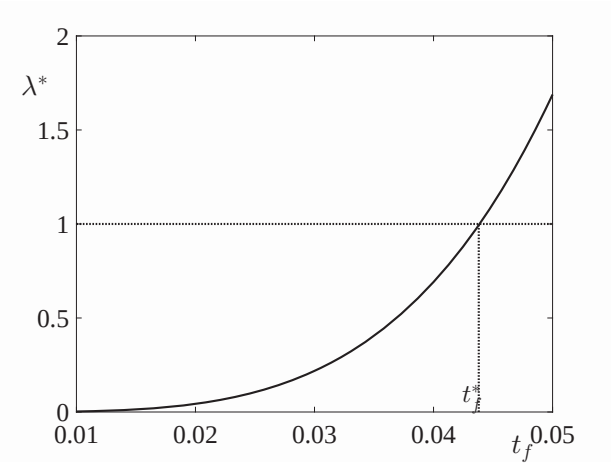

Fig. 6. Approximate values of λ^* for $\alpha = 1.5 \cdot 10^{-7}$, $\beta = 10^{-7}$

In order to improve the tracking accuracy, we consider the case where $\alpha = 1.5 \cdot 10^{-7}$, $\beta = 10^{-7}$. For these values, the

LQDG is also unsolvable on the interval $[0, 5]$. In Fig. 6, the approximate values of λ^* for $N = 1000$ are depicted as a function of $t_f \in [0.01, 0.05]$ for these small values of α and β. In this example, the critical value $t_f^* = 0.0438$. The resulting trajectory $z_1(t)$ for $M = 200$, is shown in Fig. 7. It is seen that now, the tracking is accurate enough.

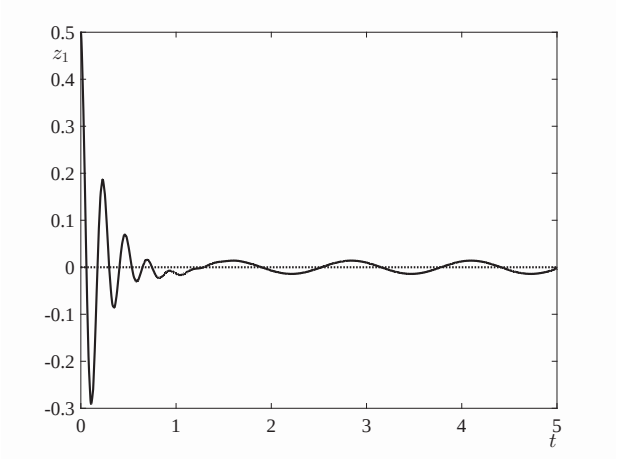

Fig. 7. Trajectory $z_1(t)$: suboptimal LQDG control for $\alpha = 1.5 \cdot 10^{-7}$, $\beta = 10^{-7}$

5. CONCLUSIONS

Two approaches are proposed to ensure the solvability of the linear-quadratic differential game with the generalized cost functional. The solvability condition was previously derived in a form of the condition on the maximal eigenvalue of some compact self-adjoint operator in a functional Hilbert space. In the first approach, the solvability is guaranteed by choosing a sufficiently small control penalty coefficient of the LQDG cost functional. In the second approach, the solvability condition is provided by a small enough control interval. This yields a suboptimal control scheme in the fashion of a receding horizon control. Two examples are presented. The first deals with the scalar system with simple motions. In this example, the required operator eigenvalues are calculated analytically and the corresponding analytical conditions on the penalty coefficient and on the control interval are derived. In the second example, the control problem for the inverted pendulum is considered. After the feedback linearization, the problem is reformulated as a linear-quadratic differential game. The solvability condition is treated numerically. In both examples, the simulation justifies the theoretical results.

REFERENCES

Bhargav, J., Turetsky, V., and Shima, T. (2018). Linear-quadratic robust path tracking for a Dubins vehicle. In *Proceedings of the European Control Conference*, 2101 – 2106.

Gu, D. (2008). A differential game approach to formation control. *IEEE Transactions on Control Systems Technology*, 16(1), 85 – 93.

Ho, Y.C., Bryson, A.E., and Baron, S. (1965). Differential games and optimal pursuit-evasion strategies. *IEEE Transactions on Automatic Control*, 10, 385 – 389.

Isidori, A. (1989). *Nonlinear Control Systems*. Springer-Verlag, London, 2 edition.

Kalman, R. (1960). Contributions to the theory of optimal control. *Boletin de la Sociedad Matematica Mexicana*, 5, 102 – 119.

Kwon, W.H. and Han, S.H. (2006). *Receding Horizon Control: Model Predictive Control for State Models*. Advanced Textbooks in Control and Signal Processing. Springer London.

Letov, A. (1960). Analytical controller design, I – III. *Automation and Remote Control*, 21, 303 – 306, 389 – 393, 458 – 461.

Pachter, M. and Pham, K.D. (2010). Discrete-time linear-quadratic dynamic games. *Journal of Optimization Theory and Applications*, 146.

Åström, K.J. and Murray, R.M. (2010). *Feedback Systems: An Introduction for Scientists and Engineers*. Princeton University Press, Princeton, NJ, USA.

Shinar, J. and Shima, T. (2012). Differential game-based interceptor missile guidance. In S.N. Balakrishnan, A. Tsourdos, and B.A. White (eds.), *Advances in Missile Guidance, Control, and Estimation*, volume 5 of *Automation and Control Engineering*, 307 – 342. CRC Press.

Shinar, J., Turetsky, V., Glizer, V., and Ianovsky, E. (2008). Solvability of linear-quadratic differential games associated with pursuit-evasion problems. *International Game Theory Review*, 10, 481 – 515.

Turetsky, V. (2016a). Robust route realization by linear-quadratic tracking. *Journal of Optimization Theory and Applications*, 170(3), 977 – 992.

Turetsky, V. (2016b). Robust trajectory tracking for a feedback linearizable nonlinear system. *IFAC - PapersOnLine*, 49(18), 540 – 545.

Turetsky, V. and Glizer, V.Y. (2016). Cheap control robust tracking: insight by solving the problem with simple motions. In *Proceedings of the 24th Mediterranean Conference on Control and Automation, June 2016, Athens, Greece*, 1059 – 1064.

Turetsky, V., Glizer, V., and Shinar, J. (2014). Robust trajectory tracking: differential game/ cheap control approach. *International Journal of Systems Science*, 45(11), 2260 – 2274.

Zhukovskii, V.I. (1970). Analytic design of optimum strategies in certain differential games. I. *Automation and Remote Control*, 4, 533 – 536.

Transformed Manipulated Variables for Decoupling and Perfect Disturbance Rejection ⋆

Cristina Zotică * **Sigurd Skogestad** *

* *Department of Chemical Engineering, Norwegian University of Science and Technology, N-7491, Trondheim, Norway (e-mail:Sigurd.Skogestad@ntnu.no)*

Abstract: The objective of this work is to find new transformed manipulated variables (MVs) for nonlinear systems which give decoupling and perfect feedforward control for disturbances (at least at steady-state). To start, we assume that we can write the model with the outputs, y, (controlled variables-CVs) separated from the inputs, u, (MVs) and disturbances, d, as in: $g(\dot{y}) + g_{ss}(y) = f(u, d, y)$. We can now introduce as new transformed input variables (v) the right hand side ($v = f(u, d, y)$), where we assume can measure the disturbances. We further assume that the g-function on the left hand side is independent of u and d, or at least that the steady-state part g_{ss} is independent of u and d. We can then obtain a decoupled system, which is also independent of disturbances (d).
The key idea is now to use decentralized SISO controllers for y using v as MVs. Then, we can find the actual input u based on based on given values of the transformed inputs v and disturbances d by using a calculation block or cascade control (the latter uses feedback as an indirect calculation block). In the first alternative, SISO controllers give v, and a nonlinear calculation block solves algebraic equations which explicitly gives u as a function og v and d. The calculation block also handles the decoupling, and feedforward action from the disturbance d. The block diagram for this approach is shown in Fig.1.

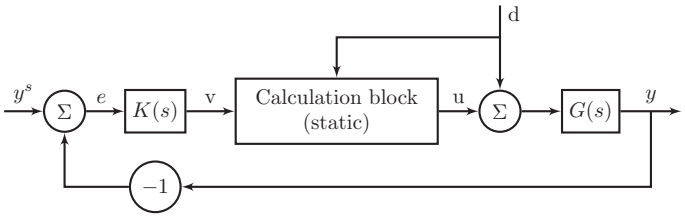

Fig.1. Decoupling and perfect disturbance rejection using a calculation block

This method is similar to feedback linearization, which implies transforming a nonlinear system into a linear system by changing the inputs or outputs. The difference is that we consider a system with equal inputs (u) and output (y), we include systems nonlinear in the inputs (u), and we also measure the disturbance (d).
As an example, we consider controlling the flow and temperature in a mixing process, and we investigate how this method handles coupling and plant-model mismatch.

Keywords: process control, decoupling, disturbance rejection

⋆ This publication has been partly funded by HighEFF - Centre for an Energy Efficient and Competitive Industry for the Future, an 8-years' Research Centre under the FME-scheme (Centre for Environment-friendly Energy Research, 257632). The authors gratefully acknowledge the financial support from the Research Council of Norway and user partners of HighEFF.

implified Model of CHO-cultivation in Bioprocess Library for Modelica – some experience

J. P. Axelsson

Vascaia AB, 112 51 Stockholm, Sweden (e-mail: jan.peter.axelsson@vascaia.se)

Abstract: A simplified dynamic model describing fedbatch cultivation of Hybridoma CHO is analyzed in a continuous perfusion cultivation setup. The model is evaluated in a qualitative way and compared with the literature and leads to suggestions of improvements of the model. A tentative way to account for multiple steady states in continuous operation is also discussed. The simulations were done in Modelica and the implementation was done in the framework Bioprocess Library.

Keywords: Biotechnology, Model-reduction, Simulation.

1. INTRODUCTION

There is a need for simplified modelling for bioprocesses to facilitate operation and control design, Kroll et al (2017). CHO-cultures, and mammalian cultures in general, have more complex metabolism than micro-organisms and that affect the model complexity. Much modelling work for mammalian cell cultures are developed to support medium design and must cover a wide range of validity. In study of operation and control of a process the medium is usually fixed, and the modelling work can focus on a narrower range and could lead to simplified models.

Here I evaluate a simplified model Amribt et al (2013) that has been shown to be fruitful in applications of control of Hybridoma CHO-processes. The model is based on the more complex model Niu et al (2013) where analysis of metabolic bottle-necks facilitated model reduction, inspired by modelling work on yeast made in the 1980s. The simplified model has been used for optimal control design of fedbatch cultivation, Dewasme et al (2015).

2. RESULTS AND DISCUSSION

The model is here evaluated for another kind of operation namely continuous perfusion and investigated in a qualitative way using simulation. The model is mainly developed and validated for batch and fedbatch operation and the goal here is to discuss how well continuous operation also can be described and high-light limitations and suggest improvements.

The process model is described in Appendix A, B, C and D at the end of the paper. All simulations are done using Bioprocess Library with JModelica and Python, see sec 3.

2.1 Comparison fedbatch with batch cultivation

First, we take a look at a basic result from the original study by Amribt et al (2013). They showed that the optimal feed profile for a fed-batch culture with the model is indeed an exponential profile. Here continuous low feed rate was used, while in practice often a short period of feed once a day is used with similar results.

In Fig. 1 batch cultivation and fed-batch cultivation are compared. We see that fed-batch operation gives a culture with the same final cell concentration as batch but with considerably lower by-product formation lactate and ammonia. By-product formation can actually not be completely avoided. The prize is that fedbatch cultivation takes a little longer time and here about 15 percent.

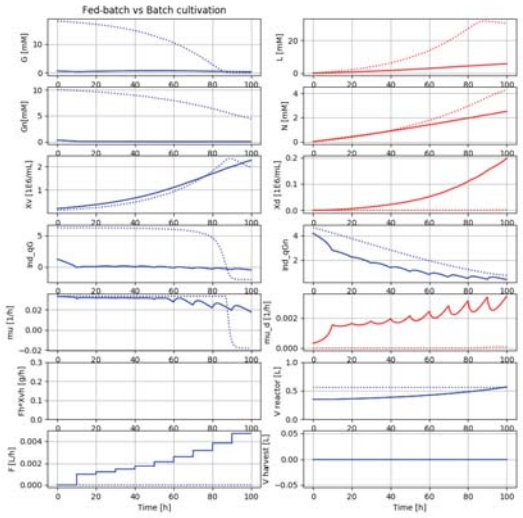

Fig. 1. Comparison of batch (dotted line) and fedbatch (solid line) cultivation of CHO-culture. Initial cell mass identical.

Paper accepted for 22th NPCW in Lyngby, Denmark, to be held August 22-23, 2019.

2.2 Perfusion cultivation and response to flow step changes

Results from response to change in perfusion rate from a low level to a higher level but still below maximal productivity level, is shown in Fig. 2. At time 500 hours, three different step changes in perfusion rate were tested. We see that a higher perfusion rate gives a higher cell concentration (and productivity) but also a higher level of by-product lactate. The re-circulation flow over the perfusion filter was 10x larger than the flow through the process all the time and the cell-concentration factor of the filter was ≈ 1.077 times, see Appendix C.

The simulation results are in accordance with expectations of CHO-cultures, but actually different to what is expected from a yeast culture. In this lower range of flow rates, the cell concentration would remain constant and no ethanol produced. At higher flow rates an increase would lead to decrease of cell concentration combined with increase in by-product ethanol formation

For CHO-cultures maintenance is not negligible as it is for yeast and many microbial cultures. The main reason viable cell concentration in a CHO-cultures goes up after the increase of perfusion rate is that the fraction of maintenance metabolism is smaller at higher growth rates. See text for B.3 in Appendix B.

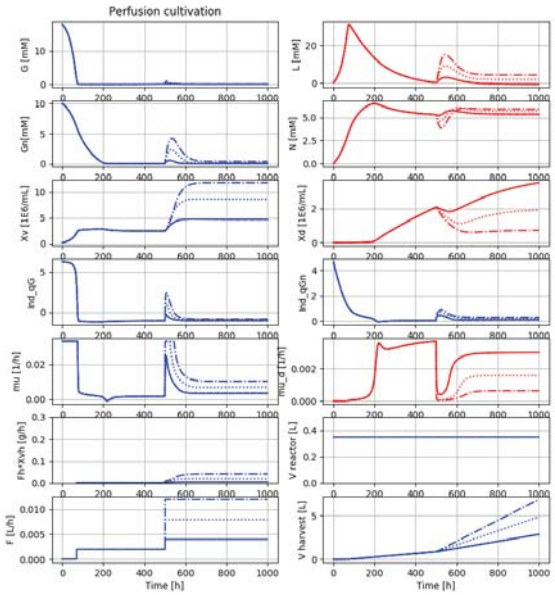

Fig. 2. Perfusion cultivation of a Hybridoma CHO-culture and response to increase in perfusion rate at time 500 h.

For even larger increases in perfusion rate the growth rate will saturate and the time to reach steady state in cell concentration will take much longer time. This is shown in Fig. 3 below.

The higher perfusion rate gives a culture with higher cell density but also higher levels of by-product lactate. The other by-product ammonium remains after the transient at around the same level.

The constructed indicator variables *Ind_qG_over* and *Ind_qGn_over* show that there is some margin to the bottle-necks for glucose but none for glutamine. During the transient starting at time 500 hours both bottle-necks saturate (=0) but after some time the metabolism comes down to the bottle-neck level, but for glutamine there remains a smaller over-flow metabolism. Therefore, the higher lactate level in steady state is due to the higher level of "aerobic glycolysis" at higher growth rate rather than over-flow, see Appendix A.

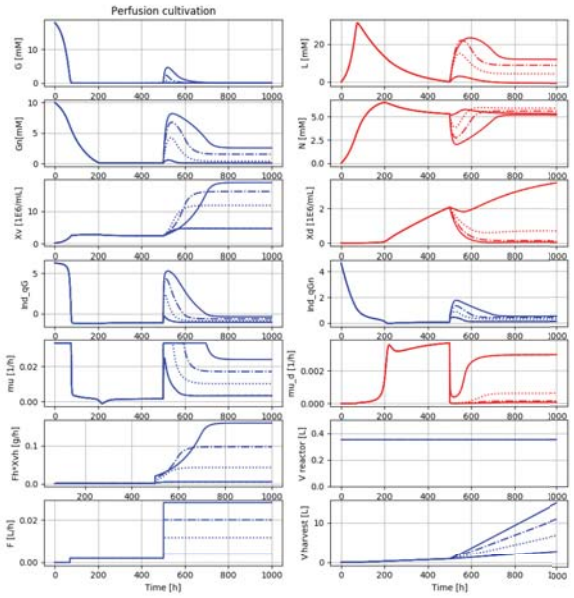

Fig 3. Perfusion cultivation of CHO-culture and response to larger increase in perfusion rate at time 500 h and the impact limited growth rate has.

2.3 Bandwidth limitation for control of cell concentration

From the previous section we understand that the limited growth rate set a limit on how fast we can increase the cell concentration to a new set-point, especially if the set-point is close to the maximal cell concentration of the medium.

It is interesting to further investigate control of the cell-concentration close to the maximal concentration using changes in perfusion rate.

In Fig. 4 we see the impact of small step-wise change of perfusion rate. The first small step up at time 700 hours shows increase of cell-concentration and productivity. The time reach steady state is about 50 hours.

The next step up shows initial increase of productivity followed by a slow trend to lower productivity than

Paper accepted for 22th NPCW in Lyngby, Denmark, to be held August 22-23, 2019.

before. The cell concentration shows immediately a decreasing trend, however. The explanation is that the perfusion rate here was set to a higher level than the maximal growth rate (plus cell-recycle rate) and that leads to a slow "wash-out" of the culture.

The following step down in perfusion rate stops the "wash-out" and the cell concentration recover to a high level and so do the productivity. The initial response in productivity is a clear drop, however.

The second step down and later back in perfusion rate shows the transient to a lower cell concentration as well as productivity, and then back. Here the response is back to what could be expected for a first order linear system.

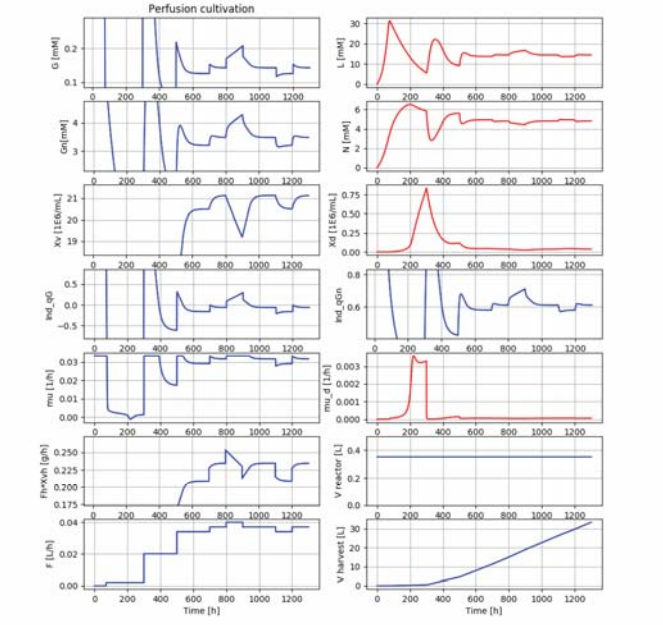

Fig. 4. Impact of small perfusion rate changes at high cell concentration around maximal productivity.

The example shows the difficulty of control of the process around a working point with maximal productivity and that there are inherent constraints on control performance.

Usually a working point for the perfusion reactor is set with some marginal to the maximal operating point, and here are several other factors involved in choosing a good working point.

2.4 Perfusion operation with ATF-filter and bleed

It is interesting to run CHO-cultures at very high cell densities at low growth rate, Clincke et al (2013). Here perfusion filter of ATF-type is often used and means that in principle "all" cells are re-circulated.

To avoid too low substrate levels and control the cell concentration level a separate bleed flow of cell broth is commonly used.

In Fig. 5. a perfusion cultivation with ATF filter is simulated. At time 500 hours the initial lactate level has come down to low levels and step change in perfusion rate brings the cell concentration up to a high level after about 100 hours.

At time 800 hours bleed flow is started and corresponding increase in feed rate is done while the perfusion rate is kept constant. We see that the cell concentration goes down and also the level of dead cells. This is partly due to better conditions for the cells and partly wash-out of the dead cells.

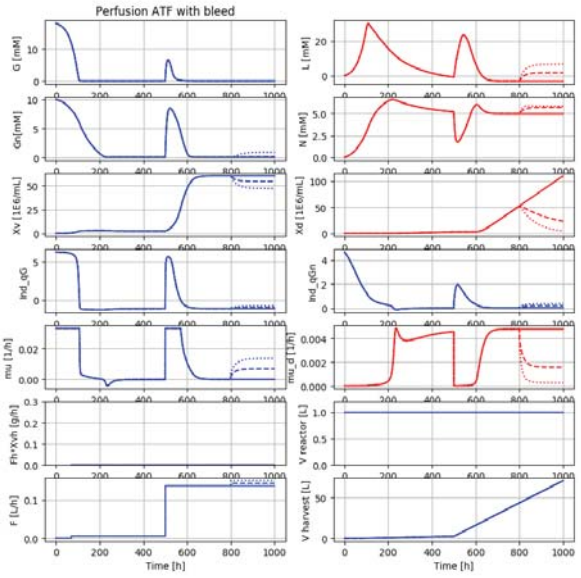

Fig. 5. High cell-density perfusion culture with ATF. Different bleed flow is tested at time 800 h.

The simulation results correspond qualitatively to what is expected. The substrate levels are however generally too low, but could perhaps simply be adjusted by the parameters K_G K_{Gn} in the Monod-expressions A.2a and A.2b.

2.5 Multiple steady states during continuous operation

It is well-known that CHO-cultures can exhibit multiple-steady states during continuous cultivation, see Europa et al (2000). The competing steady state to normal operation is a state with high lactate production and lower cell yield and recombinant product yield.

The simplified model does not account for inhibitory effects of high lactate levels (usually above 30 mM) but do account for inhibitory effects of high ammonia levels (above 3 mM). The model does not bring multiple steady states to continuous cultures.

Paper accepted for 22th NPCW in Lyngby, Denmark, to be held August 22-23, 2019.

A first idea to modify the model to account for lactate inhibition is to let high lactate levels decrease the metabolic bottle-necks. This idea was also briefly tested in the thesis work by Amribt (2014).

This idea of by-product inhibition of respiratory bottle-neck was successfully used to describe multiple-steady states during continuous cultivation of yeast with a similar bottle-neck model, Axelsson et al (1992), see also Appendix D.

For the simplified CHO-model this modification does indeed give multiple steady states in a chemostat, i.e. continuous cultivation without cell-recycle. Fig. 6 shows the effect of lactate inhibition. The mechanism used here was simply to decrease both the bottle-necks to 30% when lactate level > 8 mM, i.e. an exaggerated effect.

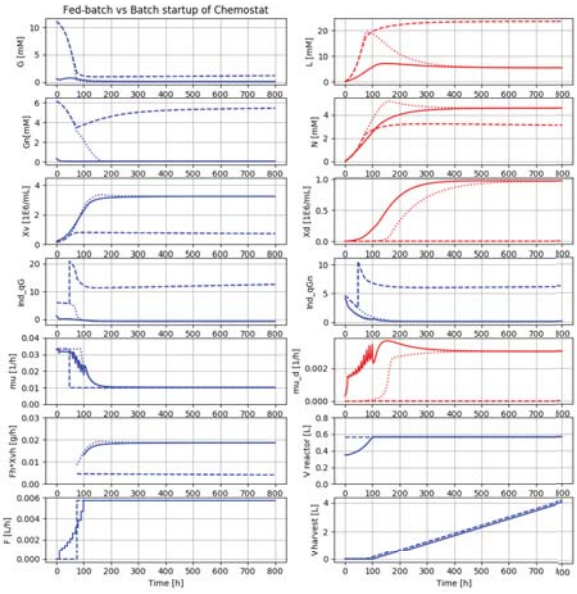

Fig. 6. Start-up of chemostat with batch or fedbatch and illustration of possible effect of lactate inhibition on the bottle-necks of glucose and glutamine metabolism. Fedbatch (solid line), batch (dotted line), batch with lactate inhibition (dashed line).

The dynamical behaviour is difficult to analyse. For some parameter settings we have chattering-solutions, due to the hard non-linearities in the model, data not shown.

Test of the impact of lactate inhibition in the culture when grown in a perfusion reactor setup, shows that this setup is less prone to multiple-steady states.

In Fig. 7 we see that lactate inhibition same as in previous example do give prolonged period of high lactate level when batch culture is used instead of fedbatch for start-up of perfusion but in converges back to the original steady state. For even stronger impact of lactate inhibition we can actually get multiple steady states.

The closer the stationary growth rate is to the maximal growth the more sensitive the system is to lactate inhibition to obtain multiple steady states. This is experience from several simulations, data not shown.

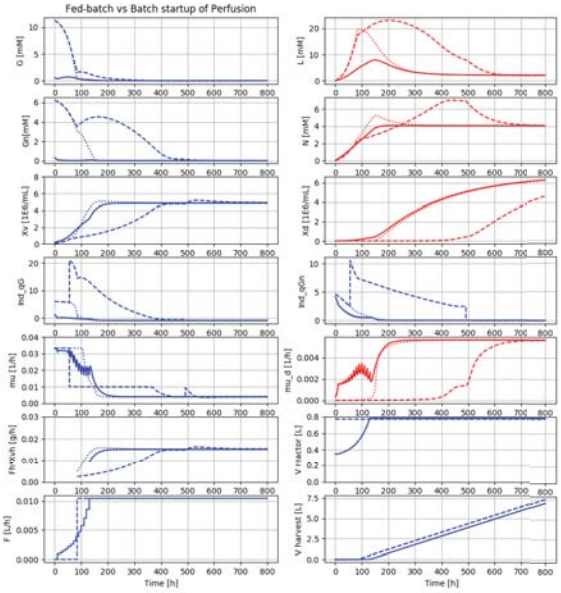

Fig. 7. Start-up of perfusion with batch or fedbatch and illustration of possible effect of lactate inhibition on the bottle-necks of glucose and glutamine metabolism. Fedbatch (solid line), batch (dotted line), batch with lactate inhibition (dashed line).

The rough analysis of the impact of lactate inhibition on multiple steady states could be extended to include impact of lactate on the growth yield described by the parameters *a* and *c*. In fact, analysis of a detailed model of the glycolysis show that it has multiple steady states, see Mulukutla et al (2015), and that may affect growth rate yield. There is a value to capture the multiple steady state phenomenon in a simplified model, I think.

There seems today to be a well-spread practice of how to start-up perfusion with CHO-cultures to avoid these problems. Using fedbatch instead of batch cultivation for start-up decreases the risk. Still here is a recent ambitious industrial interest from the pharmaceutical companies Lonza and Pfizer to understand it better and take patent on control strategies, Schmitt et al (2019).

3. IMPLEMENTATION IN MODELICA

The model Amribt et al (2013), was implemented with ease in Bioprocess Library for Modelica. The standard equipment in the library like pump, tank, reactor and filter was automatically adapted to the medium content with six compounds. We can in the Bioprocess Library framework easily switch between operation in fedbatch and perfusion mode as well as between different culture types, e.g. yeast and CHO etc. The flexibility of Bioprocess

Paper accepted for 22th NPCW in Lyngby, Denmark, to be held August 22-23, 2019.

Library has been greatly improved since it was first presented, Axelsson (2012). It has also been shown to integrate well with constrained-based genome-scale modelling, Axelsson (2018). Bioprocess Library is now developed in the direction to facilitate sensitivity analysis and support experimental work and a first simple example was presented recently Axelsson et al (2019).

The simulations were done in the open source software JModelica, Åkesson et al (2009) and scripts made in Python. The developed software Bioprocess Library for Modelica Axelsson (2012) is owned by the author but there is a student version with a permissive license.

4. CONCLUSION

The simplified model validated for fedbatch cultivation can be used also for perfusion cultivation and simulation results of transients agree well on a qualitative level. The model brings some insight into the steady state solutions dependence on yield parameters and medium composition in a way somewhat similar to microbial cultures. The model needs to be improved for very low substrate levels around maintenance needs, and some suggestions are made that need to be further investigated. Lactate consumption is not accounted for either and important for some CHO-strains. The model also lack description of inhibitory effects of high lactate levels and possibilities are here discussed that needs further work and should improve the understanding of multiple steady states. The language Modelica facilitated a flexible framework to study different kinds of process operation and change of cultures and medium with code re-use of code.

ACKNOWLEDGEMENT

The author thanks Dr Laurent Dewasme, University of Mons, Belgium, for sharing his knowledge around the simplified model by Amribt et al (2013) and Dr Andreas Castan, GE Healthcare, Sweden, for constructive comments on the paper.

REFERENCES

Amribt Z., Niu H., Tan W., Bogaerts P. (2013). "Macroscopic modelling of overflow metabolism and model-based optimization of hybridoma cell fed-batch cultures", *Biochem. Eng. Jour.*

Amribt Z. (2014) "Macroscopic modelling of hybridoma cell fed-batch cultures with overflow metabolism: model-based optimization and state estimation", *PhD thesis ULB*, *Belgium.*

Axelsson J. P, Münch T., Sonnleitner B. (1992). "Multiple steady states in continuous cultivation of yeast", *Proceedings of IFAC Modelling and Control of Biotechnical Processes, Keystone Colorado, March 29-April 2, 1992.*

Axelsson J. P. (2012). "Modelica library for simulation of bioprocesses", *Proceedings of the 17th NPCW*, Lyngby, Denmark, January 25-27 2012.

Axelsson J. P. (2018). "Integrating microbial genome-scale flux balance models with JModelica and the Bioprocess Library for Modelica, *Proceedings of the 21th NPCW*, Åbo, Finland, January 18-19, 2018.

Axelsson J. P. and Elsheikh A. (2019). "An example of sensitivity analysis of a bioprocess using Bioprocess Library for Modelica", *Proceedings of the 13th MODPROD Workshop*, Linköping, Sweden, February 5-6, 2019.

Clincke M-F., Mölleryd C., Zhang Y., Lindskog E., Walsh K., Chotteau V. (2013). "Very high density of CHO cells in perfusion by ATF or TFF in WAVE-bioreactor. Part I Effect of the cell density on the process". *AIChE journal.*

Dewasme L., Fernandes S., Amribt Z., Santos L. O., Bogaerts P., Vande Wouwer A. (2015). "State estimation and predictive control of fed-batch cultures of hybridoma cells", *J. Proc. Control*.

Europa A. F., Gambhir A., Fu P-C, Hu W-S (2000) "Multiple steady states with distinct cellular metabolism in continuous cultire of mammalian cells", *Biotech. Bioeng.*

Hu W.-S. (2103) *"Cell Culture Bioprocess Engineering"*, pg. 249-253, University of Minnesota.

Mulukutla B.-C., Yongky A., Grimm S., Daoutidis P., and Hu W.-S. (2015) "Multiplicity of steady states in glycolysis and shift of metabolic state in cultures mammalian cells". *Plos One.*

Kroll P., Hofer A., Ulonska S., Kager J., Herwig C. (2017). "Model-based methods in the biopharmaceutical process life-cycle", *Pharm. Res.*

Niu H., Amribt Z., Fickers W., Tan W., Bogaerts P. (2013). "Metabolic pathway analysis and reduction for mammalican cell cultures – towards macroscopic modeling", *Chem. Eng. Science.*

Schmitt J., Downey B., Beller J., Russell B., Quach A., Lyon D., Curran M., Mulukutla B. C., Chu C. "Forecasting and control of lactate bifurcation in Chinese hamster ovary cell culture processes". *Biotech. Bioeng.*

Åkesson J. Årzén K-E, Gäfvert M., Bergdahl T., Tummescheit H. (2009). "Modeling and Optimization with Optimica and JModelica.org – Languages and Tools for Solving Large-Scale Dynamic Optimization Problems", *Computers & Chemical Engineering.*

Appendix A. MODEL OF CHO-CULTURE

The model presented in Amribt et al (2013) is here briefly presented and parameter set 1 is used in the simulations.
I use a slightly different nomenclature using specific uptake and production rates instead of total flows. Basic properties of the models are shown, and some critic of the modelling is formulated.

The state variables chosen as masses of components in the medium. X_v and X_d concentrations of viable and dead cells respectively, G and Gn for substrates glucose and glutamine, and metabolic products are L for lactate and N for ammonia. The reactor liquid volume is V.

Note that what describe the cell is a static function that related medium concentrations to metabolic flows.

Paper accepted for 22th NPCW in Lyngby, Denmark, to be held August 22-23, 2019.

Mass balance gives the equations:

$$dVG/dt = -(q_G + m_G + q_{Gover})VX + G_{in}F_{in} - GF_{out} \quad (A.1a)$$
$$dVGn/dt = -(q_{Gn} + m_{Gn} + q_{Gnover})VX + Gn_{in}F_{in} - GnF_{out} \quad (A.1b)$$
$$dVX_v/dt = (aq_G + cq_{Gn})VX_v - \mu_d VX_v - X_v F_{out} \quad (A.1c)$$
$$dVX_d/dt = \mu_d VX_v - X_d F_{out} \quad (A.1d)$$
$$dVL/dt = (bq_G + 2q_{Gover} + 0.5q_{Gnover}) - LF_{out} \quad (A.1e)$$
$$dVN/dt = (dq_{Gn} + q_{Gnover}) - NF_{out} \quad (A.1f)$$
$$dV/dt = F_{in} - F_{out} \quad (A.1g)$$

Where the substrate uptake rates have upper limits $q_{G\,max1}$ and $q_{Gn\,max1}$ and described with Monod-type functions and including influence from Gn and N respectively

$$q_{G1}(G,Gn) = q_{G\,max\,1}\frac{G}{K_G+G}\frac{Gn}{K_{Gn}+Gn} \quad (A.2a)$$
$$q_{Gn1}(Gn,N) = q_{Gn\,max\,1}\frac{Gn}{K_{Gn}+Gn}\frac{K_N}{K_N+N} \quad (A.2b)$$

The part of substrate flows that go to cell growth is limited by $q_{G\,max2}$ and $q_{Gn\,max2}$. In case these bottle-necks are saturated the over-flow $q_{G\,over}$ and $q_{Gn\,over}$ go to by-product formation lactate and ammonia as described above in equation (1e-f). The flows are described by:

$$q_G = \min(q_{G1}, q_{G\,max\,2}) \quad (A.3a)$$
$$q_{Gn} = \min(q_{Gn1}, q_{Gn\,max\,2}) \quad (A.3b)$$
$$q_{Gover} = \max(0, q_{G1} - q_{G\,max\,2}) \quad (A.3c)$$
$$q_{Gover} = \max(0, q_{G1} - q_{G\,max\,2}) \quad (A.3d)$$

Note, however, that by-product formation take place already at low metabolic rates, but associated with cell-proliferation, before the mentioned bottle-necks are saturated and described by the parameters b and d. This phenomena is called "aerobic glycolysis" and characteristic for mammalian cell cultures. Thus the "metabolic bottle-neck" view is different from what we have for microbials like *S cerevisiae* and *E coli.*

Two practical dimensionless indicator variables for the degree of saturation of the bottle-necks are:

$$Ind\_q_{G\_over} = (q_{G1} - q_{G\,max\,2})/q_{G\,max\,2} \quad (A.4a)$$
$$Ind\_q_{Gn\_over} = (q_{Gn1} - q_{Gn\,max\,2})/q_{Gn\,max\,2} \quad (A.4b)$$

For value < 0 the bottle-neck is not saturated. These indicator variables are used in all diagrams.

Cell-death due to low substrate levels are described crudely by equation (A.1d) where

$$\mu_d = \mu_{d\,max}\frac{K_{Gd}}{K_{Gd}+G}\frac{K_{Gnd}}{K_{Gnd}+Gn} \quad (A.5)$$

The maintenance metabolic fluxes are the lowest thresholds. At this low level the cells just stay alive and do not proliferate. This maintenance substrate uptake is at a low level but must also decrease if the substrate concentration decrease. The modelling here is not that transparent and use two different mechanisms and altogether four parameters. The identifiability analysis did suggest to set m_{Gn} and K_{Gnd} to zero, see Amribt (2014) but I think here is more to do.

The first mechanism is that metabolic flows m_G and m_{Gn} are simply subtracted. These flows should not be constant but should decrease to zero at zero substrate levels. This is especially important for chemostat and perfusion studies that operate at low substrate levels.

The second mechanism that relate to maintenance is the modelling of cell-death. In equations (A.1c) we see that metabolic flux must satisfy

$$aq_{G+}cq_{Gn} > \mu_d \quad (A.6)$$

to have cell growth positive. This means that the total glucose and glutamine uptake q_{G1} and q_{Gn1} must be larger than m_G and m_{Gn} to obtain positive cell growth.

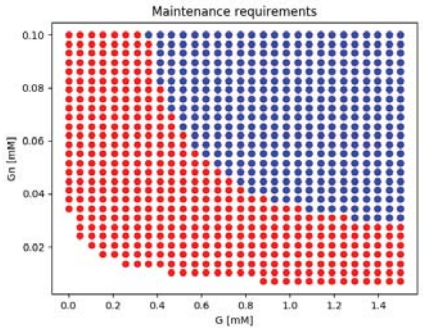

Fig. A. Illustration of maintenance requirement in terms of medium concentration G and Gn, provided $N=K_N=1.92$ mM. Growth rate positive (red dots) and maintenance requirements m_G and m_{Gn} met (blue dots).

Appendix B. PROPERTIES OF THE CHO-MODEL

The model in Appendix A has some clarifying properties that can be easily derived under simplifying assumptions.

Important is that cell growth is formulated as a sum of growth on glucose and glutamine (A.1c) and that different combinations of substrates may give the same growth rate. In vector form we can see specific growth rate μ as a scalar product of yields Y and metabolic rates q_S

$$\mu = Y \cdot q_S = \begin{pmatrix} a & c \end{pmatrix}\begin{pmatrix} q_{G(G,Gn)} \\ q_{Gn(Gn,N)} \end{pmatrix} \quad (B.1)$$

Thus, cell growth may change from dominated by glucose to glutamine and keep the same specific growth rate and the time to change is here considered negligible.

Paper accepted for 22th NPCW in Lyngby, Denmark, to be held August 22-23, 2019.

In Fig. B1 are level curves shown of specific growth rate μ for different combinations of metabolic rates q_G and q_{Gn}. Here the bottle-neck limits (A.3a) and (A.3b) are shown with a box. Cell maintenance requirements as well as cell death are here considered negligible in order to simplify.

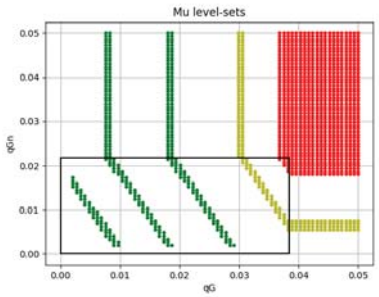

Fig. B1. Level sets of specific growth rate μ for various combination of metabolic rates q_G and q_{Gn}. Here μ=0.007, 0.014, 0.020 (green), 0.028 (yellow) and 0.033 (red) 1/h with a span of ± 0.0005 1/h.

Outside the box given by the maximal growth limits we have a different pattern of level curves of specific growth rate. Maximal specific growth rate is in the upper right corner of the box. The upper right quadrant also has maximal specific growth rate but with various degree of overflow metabolism.

The maximal viable cell growth rate μ_{max} of (used in section 2.1) provided cell death is negligible, i.e. $\mu_d = 0$ is

$$\mu_{\max} = \begin{pmatrix} a & c \end{pmatrix} \begin{pmatrix} q_{G\max 2} \\ q_{Gn\max 2} \end{pmatrix} \tag{B.2}$$

The cell concentration in a chemostat is constant under a large range of dilution rates and only dependent on the "yield properties" and medium concentrations. Thus, the CHO-culture model shows similar behaviour as a microbial culture, provided we set maintenance and cell death to zero, i.e. $m_G = m_{Gn} = \mu_{dmax} = 0$. Solving the mass balance for stationary solution gives then a solution independent of the dilution rate D provided the bottle-necks are not saturated.

$$X_v^0 = \begin{pmatrix} a & c \end{pmatrix} \begin{pmatrix} G_{in} \\ Gn_{in} \end{pmatrix} \tag{B.3}$$

If maintenance is not negligible, then the stationary solution shows lower values of X_v^0 for lower values of the dilution rate D. See also section 2.2.

The model provide some more insight into how the medium balance between glucose and glutamine affect growth.

In Fig. B2 we see results from continuous cultivation in chemostat at different growth rates (dilution rates) and what the metabolic rates q_G and q_{Gn} become. Results are given for three different media with different composition.

Thus Fig. B2. indicate that a medium containing glucose and glutamine should be balanced with the same proportion as the sizes of each metabolic bottle-neck to facilitate control of

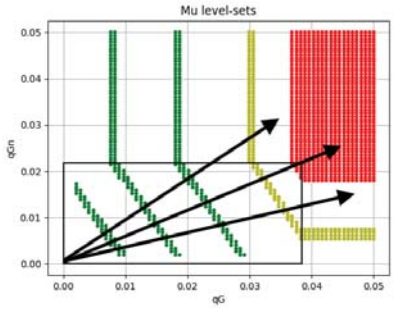

Fig. B2. Illustration of the impact of different medium composition on what growth rates can be obtained.

feed rate for high growth rates without over-flow metabolism. This holds for the ideal situation of negligible maintenance, cell-death and ammonia inhibition.

$$\begin{pmatrix} G_{in} & Gn_{in} \end{pmatrix} \sim \begin{pmatrix} q_{G\max 2} & q_{Gn\max 2} \end{pmatrix} \tag{B.4}$$

In this study $G_{in}/Gn_{in} = 15.0/9.0 \approx 1.67$ similar to what was used experimentally in Amribt et al (2013) and thus close to the ideal value 0.0384/0.0218 ≈1.76.

Needless to say, in practice in medium design there are several aspects to consider and the simplifying assumptions most likely do not hold. Still the bottle-neck view of CHO-metabolism provide some rough guide.

Appendix C. MODEL OF PERFUSION FILTERS

The setup for perfusion cultivation is shown in Fig. C below.

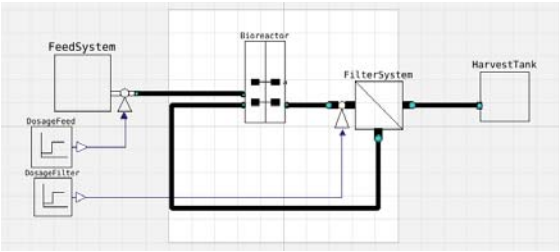

Fig. C. The setup for perfusion cultivation. The thick lines show tubes that transport liquid. The thin lines show electrical connections between control system and pumps

The perfusion filter is modelled very crudely as a filter where you can set the fraction of flow to the filtrate and the rest goes to retentate. Further, for each substance in the medium there is a parameter that describes fraction of substance to filtrate. The parameters for viable and dead cells are set to give a cell concentration factor of 1.077, i.e. retentate/inlet concentration. The other filter parameters are set to give the same concentration of substance in filtrate and retentate. Mass-balance gives then all the relations between concentration in the flows. See Hu et al (2013).

The ATF filter is simply modelled by setting the parameters for viable and dead cells so that all cells goes to the retentate.

Paper accepted for 22th NPCW in Lyngby, Denmark, to be held August 22-23, 2019.

Appendix D. MULTIPLE STEADY STATES

The results in section 2.5 is here analysed with respect to the relation between lactate inhibition on a metabolic bottle-neck and possible multiple steady states. For simplicity the analysis is limited to one bottle-neck $q_{Gn\ max2}$ affected by lactate. This bottle-neck is saturated already for lower growth rates compared to the maximal grow rate and therefore the system is sensitive to changes in this bottle-neck, while there is some margin for the glucose bottle-neck, see Fig. 6 and Fig. D2 below. This is partly due to the medium composition used and seems typical situation in production.

The analysis is similar to what was done for continuous yeast culture Axelsson et al (1992). The main difference is that the CHO-culture model is more complex than the yeast model and the analysis below is a computational procedure, with a similar graphical visualization Fig. D1, but with no further insight from analytical expressions.

The idea for a mechanism for multiple steady states for the CHO-culture in a chemostat is as follows. The steady state in a chemostat is controlled by the dilution rate and critically dependent on the metabolic bottle-necks. The lactate is present already at low dilution rates and increase for higher rates. Higher lactate levels have an inhibitory effect on the bottle-necks and may lock the culture in a state of high lactate production due to the lowered bottle-necks from inhibition by lactate.

The potential multiple steady states are shown in Fig. D1. For a give dilution rate $D=0.012\ 1/h$ the potential steady state lactate concentration L^0 is plotted in relation to a hypothetically lowered bottle-neck $KGnL*q_{Gn\ max2}$ with the fraction denoted $KGnL$ and derived from simulations. In the same diagram the simplified inhibitory effect of lactate on the metabolic capacity is also shown.

Where the lines cross in Fig. D1, steady states with lactate production are possible at the above given dilution rate, despite the fact that the dilution rate is below the critical level (≈0.034 1/h). Thus, three potential steady states are revealed with different levels of lactate. The lower and the higher are stable while the one in the middle is unstable. Note, that even with a gradual onset of lactate inhibition around 8 mM the middle steady state would be unstable.

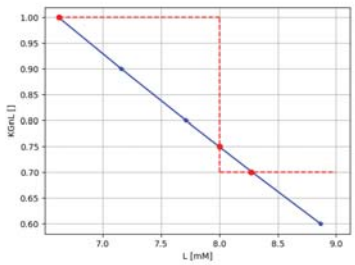

Fig. D1. Potential multiple steady states are encircled. The solid line shows the potential steady state lactate concentration for different fractions $KGnL$ of the metabolic bottle-neck for glutamine. The dashed red line is the inhibitory effect of lactate on the metabolic glutamine bottle-neck.

The dynamics of the system to reach steady state for different values of $KGnL$ are shown in Fig. D2. Note the slow recovery to the lower lactate level state and for $KGnL=0.7$ the process instead reaches the higher lactate level state, which also gives slightly lower cell concentration. The net cell growth rate is in steady state is not affected, but the balance between cell growth and cell death is changed in steady state.

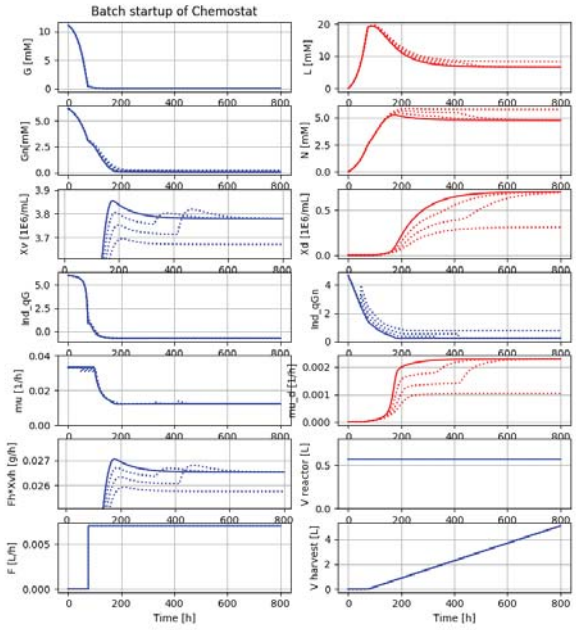

Fig. D2. The transient behaviour to reach steady state for the following values of $KGnL = 1.0, 0.9, 0.8$ and 0.7 (dotted lines). Lactate level > 8 mM has inhibitory effect for all.

With a dilution rate of the chemostat closer to the maximal rate, the sensitivity to lactate inhibition increasea and the margin for the competing “high lactate producing” steady state is smaller. Data not shown.

The complete analysis with lactate inhibition on both bottle-necks as shown in Fig. 6 is more complex. In this way the effect on the cell-concentration becomes larger. Mathematically here are for some parameter settings chattering solutions due to the hard non-linearities, that are important to consider and complicates analysis. Data not shown.

Needless to say, the modelling of lactate inhibition is here very crude and careful modelling would pave the way for an improved understanding. Hopefully, the rough analysis presented here give some tools for design of relevant experiments.

Paper accepted for 22th NPCW in Lyngby, Denmark, to be held August 22-23, 2019.

Physics-Aware Machine Learning in Multiphase Flow Estimation

Timur Bikmukhametov, Johannes Jäschke

Department of Chemical Engineering, Norwegian University of Science and Technology, 7491, Trondheim, Norway

Abstract

Accurate flowrate estimation in petroleum production is important for optimization, fiscal metering and allocation purposes [1]. An attractive solution to this problem is to use a mathematical model of the system which describes its behavior and allows to estimate the flowrates. This approach is called Virtual Flow Metering. During the last several years, it has become popular to use machine learning techniques for this purpose. The advantage of this approach is that it can provide accurate flow estimates at low computational cost and relative high accuracy and typically does not require deep understanding of the system features. However, due to its black-box nature, it is hard to interpret the algorithm outcomes which results in relatively rare usage of the method in the industry.

We propose an approach which allows to incorporate first principles modeling such as momentum equations into machine learning models, such that the algorithms become aware of the system physics a priori. This is different from the traditional machine learning Virtual Flow Metering where raw measurements are used directly [2]. The results show that it improves the accuracy of the algorithms as well as gives more explainable behavior which can help to develop more trust and employability in real production systems. We test this approach using gradient boosting regression trees [3], feed-forward and Long-Short-Term-Memory [4] neural networks. In addition, we propose an approach for tuning hyperparameters of the algorithms using Bayesian optimization techniques.

[1] Falcone, G., Hewitt, G. F., & Alimonti, C. (2009). Multiphase Flow Metering: Principles and Applications. Amsterdam: Elsevier.

[2] Al-Qutami, T., Ibrahim, R., Ismail, I., & Ishak, M. (2017) (Al-Qutami et al. 2017a) Development of Soft Sensor to Estimate Multiphase Flow Rates Using Neural Networks and Early Stopping. International Journal on Smart Sensing and Intelligent Systems, 10(1), 199-222. doi:10.21307/ijssis-2017-209.

[3] Chen, Tianqi, and Carlos Guestrin. "Xgboost: A scalable tree boosting system." In Proceedings of the 22nd international conference on knowledge discovery and data mining, pp. 785-794. ACM, 2016.

[4] Hochreiter, Sepp, and Jürgen Schmidhuber. "Long short-term memory." Neural computation 9, no. 8 (1997): 1735-1780.

Free-floating sensor devices as a tool for characterizing mixing performance in stirred vessels

Bisgaard, J[a,b] Huusom, J. K[b] Rasmussen, T[a] Gernaey, K. V[b]

[a)] *Freesense ApS, Copenhagen, Denmark*
[b)] *Process and Systems Engineering Center (PROSYS), Department of Chemical and Biochemical Engineering, Technical University of Denmark (DTU), Lyngby, Denmark*

Abstract: Process mixing in large-scale bioreactors remains a problem due to the inherent practical constraints of traditional process scale-up. Quantifying mixing in production scale quickly becomes a complicated task due to safety reasons and unfit process equipment. In addition, traditional tracer methods cannot take into account the rheological properties of the broth. This study presents a tool for data-based mapping of industrial fermentation processes, both in terms of characterizing mixing performance and measuring spatial gradients directly. The technology consists of a free-floating sensor device developed by Freesense ApS, which is robust, steam sterilizable and capable of measuring pH, temperature and pressure with sub-second response times. In the study, the mean circulation time of the devices has been derived from the pressure measurements at different conditions in a 600 L pilot vessel. The circulation times were then correlated to the mixing time determined by addition of pH tracer. The tracer response was measured with both fixed sensors and the sensor devices. The examined conditions include: Water agitated by Rushton turbine and pitch blade turbine, and xanthan solutions of 1.25 %wt and 2.5 %wt agitated by Rushton turbine. All cases were examined at four levels of power input.

Keywords: Free-floating sensor device, Flow follower, Process mixing, Mixing time, Circulation time, Stirred vessel, Macro-mixing

NPCW22 poster

Simulation and control of a secondary crushing circuit ⋆

Haroldo Ibarra * **Andreas Johansson** * **Thiago Euzébio** **
Vinicius Silva Moreira *** **Khalid Tourkey Atta** *

* *Luleå university of technology (e-mail: {haroldo.ibarra,andreas.johansson,khalid.atta}@ltu.se)*
** *Instituto Tecnológico Vale (e-mail: thiago.euzebio@itv.org).*
*** *Vale S.A. (e-mail: vinicius.silva.moreira@vale.com).*

Abstract: In this work, we present a simulator and a proposed control strategy for a secondary crushing circuit. The circuit consists of the basic components; crushers, screens, conveyor belts, and storage which are all modelled using Simulink. The simulator is based on a validated crusher model and exhibits a realistic behaviour. The work also includes a control strategy for the crushing circuit aimed at realtime maximization of the throughput.

Keywords: Cone Crushers, Model validation, Energy Model.

1. INTRODUCTION

Comminution (crushing and grinding) accounts for approximately 4% of the world's total energy consumption according to Pokrajcic (2008). Meanwhile, the environmental and social impacts from the production of tailings (e.g. due to overgrinding) can be significant and long-term (Franks et al. (2011)). However, crushing and grinding machinery represents capital intensive equipment and cannot be quickly replaced, even if more efficient models would be available. Hence, controlling the comminution chain to minimize energy consumption and waste, while maintaining sufficient production rate and quality is a well-motivated task. For this task, we focus on the cone crushers as a central component in the comminution chain. The cone-crusher is endowed with the ability to adjust the opening of the outlet (Closed Side Setting, CSS) and sometimes also the option of manipulating the eccentric speed. Hence, the importance of the cone crusher is that these manipulated variables enables it to control the performance of the whole comminution chain in order to obtain the appropriate material size. It can act as a regulator that can receive a wide range of materials with different properties and yet provide a consistent material to the later stage that can produce either a final product with specific sizes or input material to grinding circuits.

2. PLANT DESCRIPTION

Serra Leste is one of Vale's iron-ore processing plants located in the Amazon region in northern Brazil. The flow diagram of its secondary crushing stage can be seen in Fig. 3. The plant started its operation in 2014 and nowadays produces 6.0 million tons per year of sinter feed and natural pellets. The primary ore processed is high-quality compact hematite, which reaches 68% of iron content. Serra Leste does not have concentration equipment so the crushing circuits constitute the whole plant.

The cone crushers used in Serra Leste are from the Metso HP400 series. There are 2 cone crushers with fixed CSS of 38mm in the secondary crushing circuit, and another 2 cone crushers with fixed CSS of 25mm in the tertiary crushing circuit. In order to compensate for wear, maintenance technicians calibrate the CSS of the crushers once a week and replace mantle and bowl once a month.

One of the main problems of the plant is that, when only one crusher is active the material starts to overfill the silo placed before the crushers, and when two crushers are working, the level of the silo becomes too low and a security interlock is activated, which causes a series of more complicated problems. First, the interlock means that the feeders are stopped and will restart when a certain level of material in the silos is reached. However, stopping the feeders risks the crusher to run empty, which causes wear due to direct contact between bowl and mantle. A solution to stop the crusher simultaneously with the feeder is not feasible since the crusher must be empty is order to stop it which requires it to run in for a while after the feeder has been stopped, risking wear to occur and decreasing efficiency while it is being emptied, since it is not choke fed. In addition, turning off and on the crusher frequently is not desirable.

3. PLANT SIMULATOR

The plant simulator was developed using Simulink. It follows the structure of the crushing plant at Serra Leste and contains the main elements of a secondary crushing stage (cone crushers, silos, feeders, sieves and conveyor belts).

The conveyors generate realistic time delay between elements and have a fixed speed. Each silo has two outputs. The first silo capacity is 215 m^3 and for the second is 117

⋆ This work is financed by the program SIP|STRIM from Sweden's innovation agency VINNOVA and by Vale S.A. The efforts from Tero Onnela from Metso Minerals Inc., Finland are highly appreciated in providing the laboratory data and the discussions.

m^3. The sieve models are ideal, meaning that all material of 40 mm or less becomes an output of this stage and the rest is recirculated. The feeders are modelled like conveyors but with much shorter length and lower speed that can be changed to control the output of material from the silos.

The input of the simulation is a size distribution vector with the proportion of each size class. This vector is multiplied by a rate of mass per time.

The plant simulator can be seen in Fig. 4. It was implemented in Simulink and built by creating the basic elements of a secondary crushing stage, namely cone crushers, silos, feeders, screens and conveyor belts. The central element in the simulator is a crusher model (Atta et al., 2014) that predicts the outflow in terms of its size distribution given the size distribution and hardness of the input material and the CSS and rotational speed of the crusher.

The dynamics of the plant simulator are illustrated in Fig. 1 which shows the simulation results from a constant input of 110 t/h and the tonnes per hour that pass through the screen, meaning that are 40 mm or smaller and the ones that are bigger are recirculated, Note the drastic changes with approximately 200 s interval that are due to sudden changes in the size distribution of the recirculating load which is delivered from a conveyor with 200 s delay. The second part of this plot shows the level of material in the silos which never exceed the 3% for the time of the simulation. The plots in Fig. 2 show the cumulative particle size distribution (CSD) and particle size distribution (PSD) at time t=1000. In the simulator, the CSD and PSD plots are updated in real time.

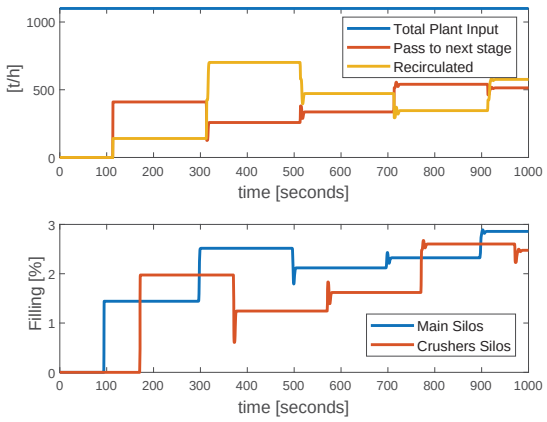

Fig. 1. Dynamic plant simulation

4. CONTROL STRUCTURE

4.1 Measurements

The objective is to find the best trade-off between throughput and particle size. What can be measured is the throughput by weight and level of the silos, but other negative indicators have to be taken into account, namely high pressure and high current that would require an increment in the CSS.

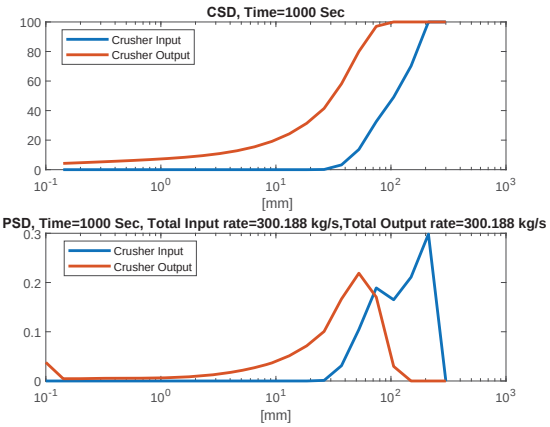

Fig. 2. Online CSD-PSD plots in the simulator

4.2 Control signals

The main idea is to control the throughput of the crushers. This can be done by changing the CSS and feeders speed. A larger CSS increases throughput but also results in larger particle size. Reducing the CSS has the opposite effect.

The speed of the feeders is controlled between 30 % and 70 % of their maximum value, 0.29 m/s for the screen feeders and 0.23 m/s for crusher feeders. If the speed were required to be lower than 30 % this would imply turning off the feeders as they cannot work below this limit.

If the silo before the crushers has reached an upper limit and the CSS is optimal, the feeders before the sieves could be slowed down, which would decrease the throughput of the stage instantaneously but would use the larger capacity silos a buffer to accumulate material for later use in the crusher.

4.3 Control objectives

The best scenario is to work with one crusher as much of the time possible to reduce energy consumption by turning off one crusher and controlling the feed rate and throughput of the other one. Only when the throughput is required to increase but the crusher has reached a limit for the CSS, the second crusher would be turned on. In the opposite case, if CSS is at minimum as well as the feeder speed, and there is still a warning of low level silos, then it is required to stop the feeder and later the crusher. Restart of the crusher would occur when certain level on the silos has been reached.

When considering online adjustable CSS or crusher speed, then more advanced control algorithms can be considered, such as the Finite State Machine. This type of algorithm has been used successfully to regulate CSS with the objective of improving the amount of saleable product while monitoring pressure (Hulthén and Evertsson, 2009). The objective is to monitor also the current and silo levels to improve particle size, throughput or finding a good trade-off between these two. Another option is to employ Extremum-Seeking Control for throughput maximization (Atta et al., 2013).

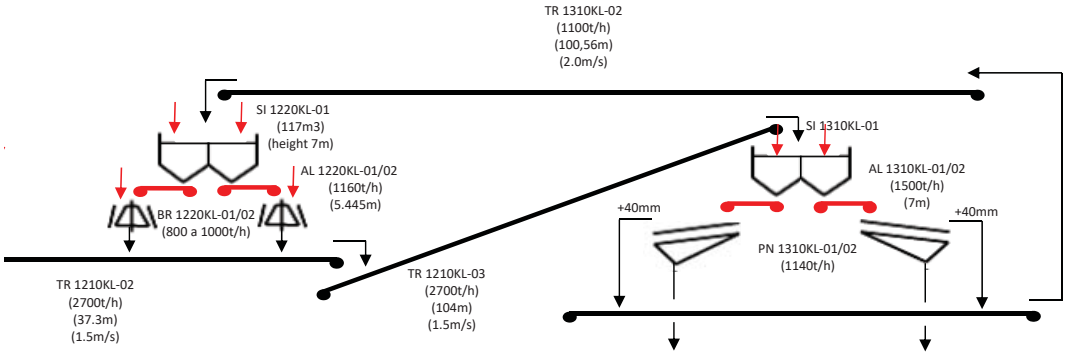

Fig. 3. Flow chart of the secondary crushing circuit at Serra Leste

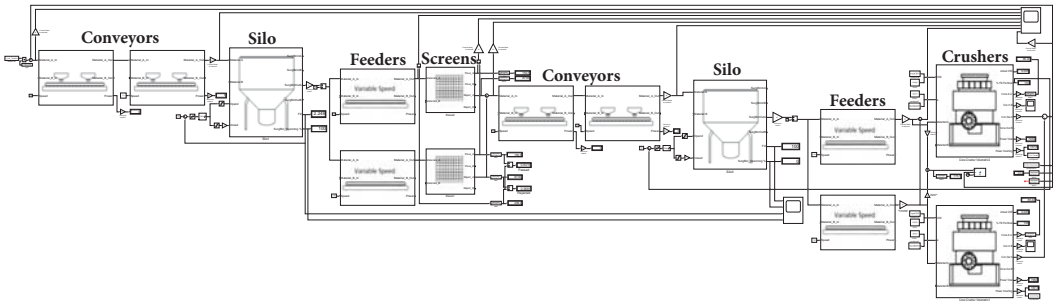

Fig. 4. Simulink simulator of the secondary crusher circuit. The figure is only intended to show the structure of the simulator, as most of the text is unreadable at this zoom level

REFERENCES

Atta, K.T., Johansson, A., and Gustafsson, T. (2013). Online optimization of cone crushers using extremum-seeking control. In *The 2013 IEEE Multi-conference on Systems and Control, Hyderabad, India*.

Atta, K.T., Johansson, A., and Gustafsson, T. (2014). Control oriented modeling of flow and size distribution in cone crushers. *Minerals Engineering*, 56, 81–90.

Franks, D., Boger, D., Côte, C., and Mulligan, D. (2011). Sustainable development principles for the disposal of mining and mineral processing wastes. *Resources Policy*, 36, 114–122.

Hulthén, E. and Evertsson, C.M. (2009). Algorithm for dynamic cone crusher control. *Miner Eng*, 22(3), 296 – 303. doi:https://doi.org/10.1016/j.mineng.2008.08.007. URL http://www.sciencedirect.com/science/article/pii/S0892687508002070.

Pokrajcic, Z. (2008). Energy efficient comminution circuits a modified grinding strategy and the selection of a target product size. In *2nd annual conference, Brisbane, Australia, November 2008*. CSRP08 (Centre for Sustainable Resource Processing).

Relay feedback excitation for identification of Fuel Cell performance parameters

Ivar J. Halvorsen and Federico Zenith, SINTEF Digital, Trondheim, Norway

Fuel cell technology is emerging as a zero-emission power generation alternative. Durability is a critical factor and it is therefore important to monitor degradation parameters that can be used for prognostics of remaining useful life and to take precautions to optimize the lifecycle. The Giantleap project is founded by EU through the Horizon 2020 programme and focuses on these issues for automotive applications in Fuel-Cell Electric buses. One interesting parameter is the so-called low frequency intercept resistance (LFR). From basic studies of performance degradation, it has been observed that changes in this parameter correlate well with ageing, making it an interesting indicator to measure (Pivac et.al., 2018). A key issue is that dynamic excitation is needed to identify this parameter, since it is not observable in steady state. It is simply the low frequency point of the Nyquist diagram of the Fuel Cell impedance where the phase crosses through zero while passing from positive to negative phase angle. In a laboratory, this can be measured by performing Electrochemical Impedance Spectroscopy (EIS). However, this requires special equipment and is not practical (or possible) to do for a fuel cell stack that is an integrated component in an application.

In the control community, the celebrated relay feedback excitation method (Åström and Hägglund, 1995) is used to directly identify the ultimate- gain and frequency of an unknown process: the result can e.g. be used for tuning of PID controllers. Here, this excitation technique is adapted to obtain direct identification of the interesting low frequency intercept point (Halvorsen et. al., 2019). Results from simulations and from testing on fuel cell stacks will be presented. The simple relay excitation method can be implemented as a software component in typical fuel cell control systems without any extra hardware equipment.

References:

Ivan Pivac, Dario Bezmalinović, Frano Barbir, Catalyst degradation diagnostics of proton exchange membrane fuel cells using electrochemical impedance spectroscopy, International Journal of Hydrogen Energy, Volume 43, Issue 29, 2018, Pages 13512-13520, https://doi.org/10.1016/j.ijhydene.2018.05.095

Aström, Karl Johan, Hägglund ,Tore. PID controllers: theory,design, and tuning, vol. 2. , NC: Instrument society of America Research Triangle Park; 1995

Ivar J. Halvorsen, Ivan Pivac, Dario Bezmalinović, Frano Barbir, Federico Zenith, Electrochemical low-frequency impedance spectroscopy algorithm for diagnostics of PEM fuel cell degradation, International Journal of Hydrogen Energy, 2019, In Press, https://doi.org/10.1016/j.ijhydene.2019.04.004

Digital Twin platform for pharmaceutical process using deep-learning and reinforcement learning algorithm

Soonho Hwangbo[1] and Gürkan Sin[1,*]
[1]Process and Systems Engineering Center (PROSYS), Department of Chemical and Biochemical Engineering, Technical University of Denmark, Building 229, DK-2800 Kgs. Lyngby, Denmark

gsi@kt.dtu.dk

Abstract

This study aims to design an optimal and smart separation process of pharmaceuticals based on uncertainty analysis and reinforcement learning. Research on the separation of pharmaceuticals has been consistently investigated on purpose of a better performance. However, few studies have implemented uncertainty analysis considering thermodynamic parameters and operating conditions and conducted an intelligent operating planning. This research precisely suggests two-phase strategy for designing pharmaceutical separation. The first phase encompasses deterministic thermodynamics and transport properties, and uncertainty analysis thereof. The second stage is related to a smart operating planning. Deep reinforcement learning is taken into account based on results from the first stage in order to balance the system flexibility. Liquid-liquid extraction column as a separation process is applied and results show the feasibility of an advanced separation framework of pharmaceuticals. This study purposes to design a novel extraction process in pharmaceutical industry based on uncertainty analysis and reinforcement learning. Thermodynamics property modelling, solubility modelling, solvent screening, and uncertainty analysis are consecutively examined to design the feasible LLE process of pharmaceuticals. Afterwards reinforcement learning is considered to suggest the optimal operating planning based on the results from uncertainty analysis. Moreover, the proposed two-phase framework of the LLE process would be extended to other processes in downstream process.

Acknowledgement

We would like to thank the Danish Council for Independent Research (DFF) for financing the project under the grant ID: DFF-6111600077B.

References

[1] Fernandes P. The global challenge of new classes of antibacterial agents: an industry perspective. Current opinion in pharmacology. 2015;24:7-11.
[2] Henderson P, Islam R, Bachman P, Pineau J, Precup D, Meger D. Deep reinforcement learning that matters. Thirty-Second AAAI Conference on Artificial Intelligence2018.
[3] Frutiger J, Andreasen J, Liu W, Spliethoff H, Haglind F, Abildskov J, et al. Working fluid selection for organic Rankine cycles–Impact of uncertainty of fluid properties. Energy. 2016;109:987-97.

A Python Toolbox for Model Predictive Control

Marcus Krogh Nielsen, **Dimitri Boiroux**, **Steen Hørsholt**, **Jakob Kjøbsted Huusom**, **John Bagterp Jørgensen**

Department of Applied Mathematics and Computer Science, Technical University of Denmark, DK-2800 Kgs. Lyngby, Denmark

Abstract: We present a Python toolbox for linear and nonlinear model predictive control. The toolbox contains methods for realization of transfer function matrices related to deterministic and stochastic inputs as a discrete time linear state space model with deterministic and stochastic inputs. The linear model predictive controller consists of a Kalman filter and a constrained optimal control problem with linear dynamics and constraints. The objective function may contain ℓ_2 as well as ℓ_1 weighted output deviation terms, input deviation terms, rate-of-movement , as well as linear and quadratic economic terms. The toolbox also allows for nonlinear model predictive control of continuous-discrete stochastic nonlinear systems using a continuous-discrete extended Kalman filter and an optimal control problem implemented using the simultaneous method and IPOPT. Real-time implementation is supported using OPC UA. We demonstrate the toolbox by simulation for a modified four-tank systems and in real-time for the laboratory scale four-tank system at the Technical University of Denmark.

Keywords: Python, Model predictive control, Four-tank system, Realization, OPC UA

Proceedings of the 22nd Nordic Process Control Workshop
August 2019, Kgs. Lyngby, Denmark

On the allowable uncertainty in control configuration selection

Riccardo Lucchese * **Wolfgang Birk** *

* *Department of Computer Science, Electrical and Space engineering, Luleå University of Technology, Sweden.*
E-mails: riccardo.lucchese | wolfgang.birk@ltu.se

Abstract: We consider Control Configuration Selection (CCS) problems in the presence of uncertainty. Our analysis focuses nominal plants given as Transfer Functions (TFs) and an additive perturbation model to capture uncertainty. The discussion is tailored to the Relative Gain Array (RGA) measure proposed by Bristol in 1966 and later popularized by several authors. Within this setting, we propose an algorithmic approach to estimate an allowable perturbation radius for which the nominal control configuration remains the preferred one. We benchmark our strategy using an example from the literature, demonstrating its effectiveness.

Keywords: Robust control configuration selection, Relative Gain Array.

1. INTRODUCTION

Control Configuration Selection (CCS) is the branch of automatic control studying the design of distributed and sparse control structures. A subfield of this larger topic is concerned with forming decisions on which feedback loops are needed to attain desired control performance and closed-loop stability properties. Within this context, Interaction Measures (IMs) are formal tools to evaluate channel interactions and inform the promising configurations starting from a model of the plant. In practice, however, models are affected from uncertainty which arises from approximations, unaccounted phenomena such as time-varying environmental conditions, and even part failures. Understanding the amount of uncertainty tolerated by a given configuration is then of paramount importance van de Wal and de Jager (2001).

Uncertain CCS have been investigated by several authors, especially in the context of the RGA. Tight bounds on the RGA elements for 2×2 plants are developed in Chen and Seborg (2002). The authors moreover apply a statistical argument to derive a loose bound addressing higher dimensional plants. Kariwala et al. (2006) list necessary and sufficient conditions for detecting sign changes in the relative gains. However, the algorithm becomes computationally impractical as the plant dimension grows. Moaveni and Sedigh (2008) bound the entries of the Hankel interaction matrix for uncertain linear systems in state space form. Castaño Arranz and Birk (2016) evaluate the Σ_2 and Participation Matrix measures over a worst-case TF envelope induced by multiplicative uncertainty. Other works consider non-parametric uncertainty models. For instance, in Kadhim et al. (2015) the set of perturbed plants is inferred from experimental trials. We stress that all the previous strategies offer generally loose bounds that require a careful interpretation of the results.

Here we propose an algorithmic randomized strategy to quantify the amount of uncertainty that may be tolerated by a nominal plant model, providing a quantitative basis for understanding the robustness of a CCS decision. The basic intuition is to employ a finite sampling of the CCS protocol over the set of uncertain plants. Its practical value lies in both its simplicity and the independence from a specific CCS protocol.

2. BACKGROUND

Let $\mathcal{L}^{q\times m}$ be the set of TFs with m inputs and q outputs. Throughout this document we focus on a special element, $G \in \mathcal{L}^{q\times m}$, that we refer to as the *nominal plant*. A generic element in $\mathcal{L}^{q\times m}$ is denoted by $\widetilde{G}$ and is referred to as *perturbed plant*. The vectorization of the matrix $\widetilde{G}$ is the $q \cdot m$ vector $\mathrm{vec}\left(\widetilde{G}\right)$. The unvectorization of a $q \cdot m$ vector into a $q \times m$ matrix is denoted using $\mathrm{unvec}\left(\mathrm{vec}\left(\widetilde{G}\right)\right) \doteq \widetilde{G}$.

A control configuration for G is a $q \times m$ matrix ξ with a "1" in position (i, j) if the j-th input is used to regulate the i-th output, and a "0" otherwise. The set of all a priori plausible configurations is

$$\Xi^{q\times m} \doteq \{0, 1\}^{q\times m}. \tag{1}$$

Uncertainty is encoded in the finite-dimensional unit ball

$$\Delta_{\boldsymbol{w}} \doteq \left\{\boldsymbol{\delta} \in \mathbb{R}^h : \|\boldsymbol{\delta}\|_{\boldsymbol{w},\infty} \leq 1\right\}, \tag{2}$$

where the norm on the right-hand side is the composition of a scaling operation with weights $\boldsymbol{w} \in \mathbb{R}^h_{>0}$ and the usual L^∞ norm:

$$\|\boldsymbol{\delta}\|_{\boldsymbol{w},\infty} \doteq \|\mathrm{diag}\,(\boldsymbol{w})\,\boldsymbol{\delta}\|_\infty\,. \tag{3}$$

Notice that $1/\boldsymbol{w}_i$, $i = 1, \ldots, h$, $\boldsymbol{w}_i \neq 0$, is the maximum *extent* along the i-th axis of an arbitrary element $\boldsymbol{\delta} \in \Delta_{\boldsymbol{w}}$.

Our methodology builds on top of three ingredients:

i) a generator function $\pi : \Delta_{\boldsymbol{w}} \to \mathcal{L}^{q\times m}$ that associates the uncertainty description to the uncertain plant models;

ii) a selection protocol $S : \mathcal{L}^{q\times m} \to \Xi^{q\times m}$ that gives the preferred control configuration for a given (perturbed) plant;
iii) a sampling strategy that approximates the allowable uncertainty radius (see Problem 4 and Section 4).

Example 1. Define the following set of perturbed plants under an additive uncertainty model Grosdidier et al. (1985); Skogestad and Postlethwaite (2007)

$$\Pi(\rho) \doteq \{\pi(\rho\boldsymbol{\delta}) : \boldsymbol{\delta} \in \Delta_{\boldsymbol{w}}\}, \tag{4}$$

where the generator takes the form

$$\pi(\boldsymbol{\delta}) \doteq G + \mathrm{unvec}\,(\boldsymbol{\delta}), \tag{5}$$

and the scaling factor ρ is interpreted as a normalized *radius*, contracting the maximum perturbation amplitude:

$$\Pi(\rho') \subseteq \Pi(\rho), \quad 0 < \rho' < \rho \leq 1. \tag{6}$$

Example 2. The RGA is an IM operating on gain matrices sampled from a TF Bristol (1966). For the plant $G \in \mathcal{L}^{q\times m}$, the frequency dependent RGA is defined as:

$$\left(\mu(G(\boldsymbol{j}\omega))\right)_{ij} \doteq \left\| \left(G(\boldsymbol{j}\omega) \circ G(\boldsymbol{j}\omega)^{-\dagger}\right)_{ij} \right\|, \tag{7}$$

where $\boldsymbol{j}$ is the imaginary unit, $\circ$ is Hadamard's entry-wise product, the $q \times m$ matrix $G(\boldsymbol{j}\omega)$ is required to be invertible, and $\cdot^{-\dagger}$ denotes the inverse transpose. Within the scope of *input/output pairing* problems, we consider the RGA-number selection protocol [1] (see Skogestad and Postlethwaite (2007)):

$$\xi^\star = S(G) \doteq \begin{cases} \underset{\xi\in\Xi^{q\times m}}{\operatorname{argmin}} \|\mu(G) - \xi\|_1 \\ \text{subject to:} \\ \xi \mathbf{1}_m = \mathbf{1}_m \end{cases} \tag{8}$$

where the constraint limits the search space to those ξ for which exactly one input is paired to each output.

3. PROBLEM STATEMENT

Definition 3. (Robust CCS). Let $G \in \mathcal{L}^{q\times m}$ be the nominal plant, S be the selection protocol, ρ a given radius in $]0, 1]$, and $\Pi(\rho)$ the set of perturbed plants. We call the configuration $\xi = S(G)$ *robust* for $\Pi(\rho)$ if applying protocol S yields the same configuration almost everywhere in $\Pi(\rho)$, that is, if

$$S(\widetilde{G}) = \xi \quad \text{a.e. in } \Pi(\rho). \tag{9}$$

Define the following binary property over $\Delta_{\boldsymbol{w}}$

$$\mathcal{P}(\boldsymbol{\delta}) \doteq \begin{cases} 1 & \text{if } S(\pi(\boldsymbol{\delta})) = S(G) \\ 0 & \text{otherwise.} \end{cases} \tag{10}$$

and the sets

$$\Omega_i \doteq \{\boldsymbol{\delta} \in \Delta_{\boldsymbol{w}} : \mathcal{P}(\boldsymbol{\delta}) = i\}, \quad i = 0, 1 \tag{11}$$

$$\Omega(\rho) \doteq \rho\Delta_{\boldsymbol{w}}, \quad 0 < \rho \leq 1. \tag{12}$$

Here we are interested in finding the largest radius ρ for which the nominal configuration is robust (see Figure 1).

Problem 4. (Allowed perturbation radius). Let G, $\boldsymbol{w}$, π, and S be given. Find the largest radius $\rho^\star \in]0, 1]$ such that

$$|\Omega(\rho^\star)| - |\Omega(\rho^\star) \cap \Omega_1| = 0. \tag{13}$$

[1] For the sake of a simpler discussion, here we set $S(G) = \mathbf{0}_{q\times m}$ when problem (8) has multiple optimizers.

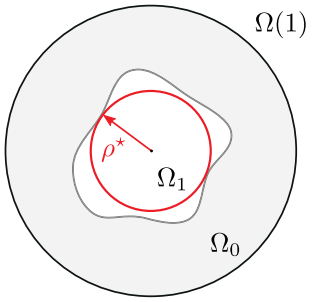

Figure 1. Graphical depiction of the problem statement in Section 3.

4. A RANDOM SAMPLING SEARCH

In this section, we sketch a randomized strategy that iteratively refines an estimate $\widehat{\rho}$ of $\rho^\star$ to approximate Problem 4.

We start by pairing the sets $\{\Omega(\rho)\}$ with a family of Probability Density Functions (PDFs) $\{\mathcal{F}_\rho\}$ such that $\mathrm{supp}\,(\mathcal{F}_\rho) = \Omega(\rho)$. Consider then the simplest scenario in which ρ is fixed and let $\boldsymbol{x}_1, \ldots, \boldsymbol{x}_n \in \Omega(\rho)$, with $n > 0$ generic, be a sequence of i.i.d. samples from $\mathcal{F}_\rho$. Let moreover a corresponding vector of observations be defined as

$$\boldsymbol{y} \doteq \begin{bmatrix} y_1 & y_2 & \ldots & y_n \end{bmatrix}^\dagger, \tag{14}$$

where $y_i = \mathcal{P}(\boldsymbol{x}_i)$. Clearly, any realization of $(\boldsymbol{x}_1, \ldots, \boldsymbol{x}_n, \boldsymbol{y})$ immediately provides an upper bound $\widehat{\rho}$ on $\rho^\star$ (that is, $\mathbb{P}[\rho^\star \leq \widehat{\rho}] = 1$). Furthermore, $\boldsymbol{y}$ informs on the *accuracy* of using $\widehat{\rho}$ to approximate $\rho^\star$. Indeed, each y_i is by construction a Bernoulli random variable, $y_i \sim \mathcal{B}(1 - \vartheta_\rho)$, with success probability dependent on $\mathcal{P}$,

$$1 - \vartheta_\rho \doteq \mathbb{E}_\rho[\mathcal{P}], \tag{15}$$

where $\mathbb{E}_\rho[\cdot]$ denotes expectation with respect to $\mathcal{F}_\rho$. Moreover, the statistic

$$\widehat{\vartheta}_\rho \doteq \frac{1}{n}\sum_{i=1}^{n}(1 - y_i), \tag{16}$$

is a consistent estimator of the failure probability ϑ_ρ, and thus an accuracy-like indicator.

At each sample point there are two possible outcomes. If the preferred configuration at the current perturbed plant equals the nominal configuration, the sample gives no new indication on the value of the allowable perturbation radius. Otherwise, the sample upper-bounds ρ^* with probability one. In both cases, new information is accumulated in (16) providing an indication of the current accuracy of the radius estimate.

For details on the statistical characterization of the algorithm we refer the reader to Lucchese and Birk (2019).

5. EXAMPLE

Consider the following plant model for a heavy oil fractioner

$$\begin{bmatrix} y_1 \\ y_2 \end{bmatrix} = \begin{bmatrix} \dfrac{4.05\,e^{-27s}}{50s+1} & \dfrac{1.77\,e^{-28s}}{60s+1} \\ \dfrac{5.39\,e^{-18s}}{50s+1} & \dfrac{5.72\,e^{-14s}}{60s+1} \end{bmatrix} \begin{bmatrix} u_1 \\ u_2 \end{bmatrix} + \begin{bmatrix} \dfrac{5.88\,e^{-27s}}{50s+1} \\ \dfrac{6.90\,e^{-15s}}{40s+1} \end{bmatrix} d, \tag{17}$$

where $[u_1\ u_2]^\dagger$ is the input vector and d is a white gaussian process. In (Chen and Seborg, 2002, Example 3) a robust CCS analysis is conducted by simulating an experimental campaign. Estimates of the plant TF are drawn under two noise measurement scenarios characterized by Signal-to-noise Ratios (SNRs) 3 and 10 (see the reference for details).

Case SNR $= 3$. For this case, Chen and Seborg (2002) derive the following empirical characterization of the perturbed steady state gains

$$\widetilde{G}_{ij} \sim \mathcal{N}\left(\overline{G}_{ij}, \sigma_{ij}^2\right), \tag{18}$$

with

$$\overline{G} = \begin{bmatrix} 4.35 & 1.94 \\ 5.86 & 5.93 \end{bmatrix}, \quad \sigma^2 = \begin{bmatrix} 0.09331 & 0.105 \\ 0.129 & 0.145 \end{bmatrix}. \tag{19}$$

From knowledge of the entry-wise variances σ^2, using a statistical argument, the authors estimate the nominal RGA

$$\mu = \begin{bmatrix} \mu_{11} & 1-\mu_{11} \\ 1-\mu_{11} & \mu_{11} \end{bmatrix}, \quad \mu_{11} = 1.76 \tag{20}$$

and correspondingly the uncertain RGA bound $\mu_{11} \in [-0.27, 3.79]$. By inspection of this inclusion, it is concluded that no robust CCS decision can be inferred using the (noisier) data set.

We transport the uncertainty scenario (18) to our framework by observing that three standard deviations from the mean value are representative for the maximum extents of the entry-wise perturbations (2),(4). Specifically, we consider the set (2) with perturbation weights

$$\boldsymbol{w} = \frac{1}{3}\left[\sigma_{11}^{-1}\ \sigma_{21}^{-1}\ \sigma_{12}^{-1}\ \sigma_{22}^{-1}\right]^\dagger. \tag{21}$$

Applying the randomized search strategy to this setup yields the allowable perturbation radius estimate $\widehat{\rho}_3 = 0.8447$, corresponding to the entry-wise perturbations

$$\begin{bmatrix} 3.6842 & 1.1276 \\ 4.9595 & 4.9753 \end{bmatrix} \preceq \widetilde{G} \preceq \begin{bmatrix} 5.2158 & 2.7524 \\ 6.7605 & 6.8847 \end{bmatrix}. \tag{22}$$

Differently from the conclusion above, our algorithmic strategy can inform the allowable uncertainty despite the noise measurements.

Case SNR $= 10$. Repeating the in silico campaign with a higher SNR yields the empirical distribution (18) with

$$\overline{G} = \begin{bmatrix} 4.035 & 1.64 \\ 5.37 & 5.57 \end{bmatrix}, \quad \sigma^2 \begin{bmatrix} 0.0253 & 0.0272 \\ 0.0348 & 0.0375 \end{bmatrix}. \tag{23}$$

To capture this scenario we define (cf. (21))

$$\boldsymbol{w} = \left[1.0478\ 0.8934\ 1.0106\ 0.8607\right]^\dagger, \tag{24}$$

With this setup, Chen and Seborg (2002) conclude that the allowable perturbation ratio is lower bounded as $\rho^\star \geq 0.5$. The randomized search strategy yields instead the allowable perturbation radius $\widehat{\rho}_{10} = 0.8073$, corresponding to allowable entry-wise perturbations

$$\begin{bmatrix} 3.2795 & 0.9711 \\ 4.4864 & 4.7820 \end{bmatrix} \preceq \widetilde{G} \preceq \begin{bmatrix} 4.8205 & 2.5689 \\ 6.2936 & 6.6580 \end{bmatrix}. \tag{25}$$

The proposed strategy provides a more accurate and overall less conservative estimate (about 40 percent larger) then in Chen and Seborg (2002). Moreover, the allowable uncertainty indications overlap significantly with those of the previous case (cf. (23) and (25)). The proposed strategy provides more accurate estimates using noisier measuremnets.

6. CONCLUSIONS

We consider robust CCS problems and devise an algorithmic strategy to evaluated the allowable plant uncertainty. The proposed strategy can be applied to different IMs while taking into account heterogeneous decision metrics in the selection protocol. The main requirement is to be able to sample the protocol at a finite number of perturbed plants (not known a priori).

Future directions include lifting this methodology to automatic CCS frameworks for plant control reconfiguration. We moreover foresee addressing applications in economic cooling of data centers. In these context, multiple coolant flow rates (corresponding to inputs) are used to regulated multiple temperatures (the outputs) at different levels of the infrastructural hierarchy, from servers to the computer room Lucchese and Johansson (2019a,b); Lazic et al. (2018). While the adoption of formal methods could aid in the development of principled and more efficient controllers, the existing literature lacks to recognize the CCS aspect of these problems.

REFERENCES

Bristol, E. (1966). On a new measure of interaction for multivariable process control. *IEEE Transactions on Automatic Control*.

Castaño Arranz, M. and Birk, W. (2016). On the selection of control configurations for uncertain systems using gramian-based Interaction Measures. *Journal of Process Control*.

Chen, D. and Seborg, D. (2002). Relative Gain Array Analysis for Uncertain Process Models. *AIChE Journal*.

Grosdidier, P., Morari, M., and Holt, B. (1985). Closed-Loop Properties from Steady-State Gain Information. *Ind. Eng. Chem. Fundam.*

Kadhim, A., Castano, M., Birk, W., and Gustafsson, T. (2015). Relative Gain Array of Weakly Nonlinear Systems using a Nonparametric Identification Approach. In *IEEE Conference on Control Applications*.

Kariwala, V., Skogestad, S., and Forbes, F. (2006). Relative Gain Array for Norm-Bounded Uncertain Systems. *Ind. Eng. Chem. Res.*

Lazic, N., Lu, T., Boutilier, C., Ryu, M., Wong, E., Roy, B., and Imwalle, G. (2018). Data center cooling using model-predictive control. In *Neural Information processing Systems*.

Lucchese, R. and Birk, W. (2019). Computing the allowable uncertainty of sparse control configurations. *Journal of Process Control (submitted)*.

Lucchese, R. and Johansson, A. (2019a). ColdSpot: A thermal supervisor aimed at server rooms implementing a raised plenum cooling setup. In *IEEE American Control Conference*.

Lucchese, R. and Johansson, A. (2019b). On Energy Efficient Flow Provisioning in Air-Cooled Data Servers. *Control Engineering Practice*.

Moaveni, B. and Sedigh, A.K. (2008). Input–output pairing analysis for uncertain multivariable processes. *Journal of Process Control*.

Skogestad, S. and Postlethwaite, I. (2007). *Multivariable Feedback Control*.
van de Wal, M. and de Jager, B. (2001). A review of methods for input / output selection. *Automatica*.

Optimization of parametric uncertain designs using a novel stochastic optimization methodology.

Atli Freyr Magnússon, Resul Al, and Gürkan Sin

PROSYS, Technical University of Denmark (DTU), Lyngby, Denmark

ABSTRACT

Stochastic optimization methods are optimization methods that allow for the formulation of stochastic objective functions using random variables, which makes them more attractive for the optimization of engineering systems under various uncertainties. Bayesian optimization uses an iterative design strategy to solve global optimization problems of black-box functions without requiring derivatives. While it has traditionally been used to solve complex deterministic simulations, Bayesian optimization has recently shown promise for optimization of stochastic simulations with heteroscedastic noise variances. In this work we present a new methodology for stochastic optimization and explore its applicability to realistic chemical engineering problems that are subject to parametric uncertainties.

The methodology is an iterative process, where an algorithm suggests new sample points using a explore-exploit strategy on a Blackbox Stochastic Surrogate model. The optimization problem is treated as a stochastic simulation by calculating the propagation of uncertainty of the model parameters using Monte Carlo Sampling techniques with a defined error distribution. While there is a wide array of surrogate models available, the most commonly used and researched one is a Kriging model. Kriging models are popular surrogates for complex simulations with sparse data due to the inclusion of external uncertainty based on distance correlation which makes it an ideal candidate for explore-exploit strategies. The main issue with Kriging is that the parameters are estimated via inversion of a covariance matrix which becomes more computationally intensive as more data is fed into the algorithm. To overcome this, we adapt artificial neural network (ANN) to stochastic optimization using a Bootstrap method. The explore-exploit strategy applied is a new novel feasibility-enhanced expected improvement (FEI) infill strategy. For this study, both methods are applied to solving realistic case studies whose simulations are performed using Aspen Plus process simulator with an interface to MATLAB environment. Uncertainties in the thermodynamic models of Aspen Plus are calculated via regression of NIST TDE data and propagated to the results of the simulations. The results obtained show the advantages of the new methodology, which holds significant promise for the stochastic optimization of engineering systems under uncertainties.

Online model maintenance – combining Output Modifier Adaptation with simultaneous model structure identification and parameter estimation

Jose Matias and Johannes Jäschke.

Since 1980s, real-time optimization (RTO) has been implemented in refineries and chemical processes [1]. A successful implementation depends on a number of factors, among which the process model plays a critical role. It must be flexible in order to adjust the plant behavior in a large range of process conditions, and it should be able to guarantee convergence of the RTO scheme to the plant optimal operating conditions [2].

The latter requirement can be met by applying Output Modifier Adaptation (MAy) instead of the classical RTO approach [3]. In MAy, input-affine terms (also known as modifier terms or, simply, modifiers) correct the predictions of the model outputs such that the model-based optimization problem converges to the plant optimum given that the model follows some adequacy criteria (i.e. it is locally convex near the plant optimal inputs) [3]. On the other hand, the former requirement is harder to fulfill since the mathematical model is determined in the very beginning of the RTO implementation and the plant behavior often varies with time and/or the plant is operated differently (e.g. distinct campaigns of a batch reactor). Moreover, a number of mathematical models can be used for describing the same phenomenon and, frequently, there is not enough information to make proper choices during the model design phase [4].

Therefore, in some cases, using the modifiers or estimating the parameters may not suffice for readapting the model to the plant behavior [5]. The mathematical model needs maintenance; its structure should be allowed to change and evolve with time and not be fixed at the model deployment [4]. In Matias and Jäschke (2019)[6], we proposed a novel method where we optimize the process using MAy, but also use the modifier terms as a criterion for simultaneous model structure selection. Therefore, the modeler does not need to determine a model structure *a priori*. This method allows him/her to propose several model structures, which are combined and updated automatically based on the available operational data (modifiers). In this work, we extend the previous method in order to not only choose the model structure but also estimate its parameters. We are also working on a second paper in order to explore further issues regarding the parameter estimation, like identifiability problems related to non-unique parameters in addition to possibly non-unique models.

The basic idea of the method is to propose several model structure candidates that can describe the plant behavior. In order to determine this set of models, we divide the process model into blocks. The individual blocks represent a part of the process to be modeled, e.g. pressure drop of flowing liquids in a pipe. Next, we propose several candidate sub-models to describe a given block, where different set of equations constitute each sub-model. For example, different sub-model candidates for the pressure drop in a pipe may include (or exclude) effects of friction, hydrostatic pressure, turbulence, etc.. Depending on the sub-models that are chosen for each block, the process model has a different shape (gradients) and prediction capacity, which can be quantified by the modifiers.

Our problem set-up leads to a two-level optimization problem structure, where, in the first level, we use the modifiers as a criterion to choose the best model structure in the model set while simultaneously performing parameter estimation (which is the main difference between this work and Matias and Jäschke (2019)[6]). In the second level, we use the updated model to optimize the process in a classical MAy framework. As an additional feature, we keep the MAy property that guarantees convergence to the plant optimum even when the model at hand is structurally and parametrically wrong. Therefore, we can combine both tasks and still achieve the plant optimal operating conditions. A case study, a continuous stirred tank reactor, illustrates our approach. The results indicate that our

method chooses the best model structure with readapted parameters among several candidates and drives the process to its optimum without constraint violations.

[1] Darby, M. L.; Nikolaou, M.; Jones, J.; Nicholson, D. (2011). “RTO: An overview and assessment of current practice”. Journal of Process Control, 21(6), 874-884.

[2] Mendoza, D. F.; Palacio, L. M.; Graciano, J. E.; Riascos, C. A.: Vianna Jr, A. S.; Le Roux, G. A. C. (2013). “Real-time optimization of an industrial-scale vapor recompression distillation process. Model validation and analysis”. Industrial & Engineering Chemistry Research, 52, 5735-5746.

[3] Marchetti, A.; Chachuat, B.; Bonvin, D. (2009). “Modifier-adaptation methodology for real-time optimization”. Industrial & Engineering Chemistry Research, 48, 6022–6033.

[4] Bonvin, D.; Georgakis, C.; Pantelides, C.; Barolo, M.; Grover, M.; Rodrigues, D.; Schneider, R.; Dochain, D. (2016). “Linking models and experiments”. Industrial & Engineering Chemistry Research, 55, 6891–6903.

[5] Graciano, J. E.; Mendoza, D. F.; Le Roux, G. A. C. (2014). “Performance comparison of parameter estimation techniques for unidentifiable models”. Computers and Chemical Engineering, 64, 24-40.

[6] Matias, J.; Jäschke, J. (2019). “Online Model Maintenance via Output Modifier Adaptation”. Industrial & Engineering Chemistry Research, (IN PRESS – DOI: https://doi.org/10.1021/acs.iecr.9b00267).

Computing the Relative Gain Array for Uncertain Multivariable Processes

Bijan Moaveni[1,2], **Rojin Tahzibi**[1], **Wolfgang Birk**[2]

[1]*Faculty of Electrical Engineering, K. N. Toosi University of Technology (KNTU), Tehran, Iran*

[2]*Control Engineering Group, Luleå University of Technology, Luleå, Sweden*

Abstract: Control configuration selection or Input-output (I-O) pairing for uncertain multivariable plants is a challenge in decentralized control systems. Although there are different types of I-O pairing strategies for nominal linear multivariable processes, only a few of these can deal with model uncertainty and its effect on the control configuration selection. I-O pairing for uncertain multivariable processes using RGA has two main issues: (i) computation of the variation bounds of the relative gains and (ii) the subsequent selection of the appropriate I-O pairing. In this paper, a method to compute the variation bounds of relative gains in the RGA using the idea of Kharitonov's theorem together with optimization methods is introduced. The mathematical foundations of the method are presented for 2×2 and 3×3 multivariable plants. Simulation cases are used to show the feasibility and effectiveness of the method. To conclude the paper, the results are discussed and future research tracks are given.

Uncertainty-based causal analysis of process systems for causal inference

Emil K. Nielsen*. Gürkan Sin**
Xinxin Zhang*, Akio Gofuku*, Ole Ravn***

**Department of Electrical Engineering, Technical University of Denmark, Elektrovej 326, Kgs. Lyngby, 2800, Denmark*
***Department of Chemical Engineering, Technical University of Denmark, S\o ltofts Plads 227, Kgs. Lyngby, 2800, Denmark*
**** Graduate School of Interdisciplinary Science and Engineering in Health Systems, Okayama University, 3-1-1, Tsushima-Naka, Kita-ku, Okayama, 700-8530 Japan*

Abstract: Many approaches to handling anomalies and alarm management of process systems withcausal graphs have been proposed. These methods generally rely on the ability to analysehistorical and surrogate plant data with bi- or multivariate methods to derive causal relationsbetween process variables, and the direction of influence. General for such methods is thelack of tools to evaluate the validity of the causal analysis.

A univariate approach based on controlled and simulated experiments is proposed withthe ability to analyse the probability for a causal relationship to exist, and it's direction ofinfluence. A step change is applied to manipulable components of the system, and changedetection is used for detection of step responses to establish causal relations. A stochasticapproach to address process uncertainty as part of the causal relationship is proposed, bysampling a set of process conditions. Thus, a distribution of causal influence is obtainedbetween the manipulable components such as actuators regarded as causes, and the process variables. The distributions are converted to a deterministic and qualitative causalrelationship similar to alarms.

Approaches from uncertainty and sensitivity analysis are applied to evaluate the reliability of the results. Linearised regression models are used to identify the most influentialvariables. Scatterplots are used to identify regions of the process conditions that influencethe reliability of the qualitative causal relationship. Lastly, the variance of the causal resultsis analysed by introducing uncertainty to the parameters of the method used for establishinga causal relationship.

Keywords: Causal analysis, Uncertainty and Sensitivity analysis, Simulation

Sequential Monte Carlo to Model Lactic Acid Bacteria Fermentation

Ergys Pahija, Robert Spann, and Gürkan Sin

PROSYS Research Center, Department of Chemical and Biochemical Engineering, Technical University of Denmark, Kgs. Lyngby, Denmark

Lactic acid bacteria (LAB) are commonly used in the food industry, and in the dairy industry in particular (LAB are typically used as starter cultures) [1]. Like any other microorganisms, the LAB production is affected by the environmental conditions. The main conditions affecting the production of LAB are temperature, pH, substrate and lactic acid concentration. The production is carried on in batch or-fed – batch conditions and monitoring the environmental condition becomes a critical aspect of the production process [2]. However, the lack of some on-line measurements and rely on limited sensor placed in the fermenter (e.g., pH) makes the monitoring of the process difficult hence the usage of mechanistic models can give additional relevant information about the system.

In this study, monitoring of *Streptococcus thermophilus* production is investigated. The fermentation model has been proposed by Spann et al. [3]. The pH is also calculated by include the kinetics of mixed weak acid base [4]. Spann et al. [3] have applied traditional Monte Carlo method to perform parameter estimation off-line which provided estimation of parameters of the model and its covariance matrix of the estimated parameters. Using Monte Carlo simulations the uncertainty of estimated parameters were propagated to model outputs (states) thereby providing a model-based method to monitor LAB fermentation. In this contribution, our aim to is to update information (its quality) on estimating parameters and state of the model simultenously in a online application context. To this end, other approaches can be followed for the on-line monitoring of LAB production. For this purpose the possibility to use sequential Monte Carlo methods can be considered [5], [6]. In this case, a particle filter is applied to the state space representation of the system (hence focusing on the state estimation) recursively as each data is collected online during batch production. In this way, measurement errors and process disturbances are filtered which provides better estimation of the states and its uncertainty (probability density distribution) as new data is collected.

While many particle filters (SMC) methods focused on state estimation, the key challenge is to address both parameter and state estimation uncertainty. Several approaches can be followed when applying sequential Monte Carlo for on-line monitoring, such as defining an extended state that includes state and parameters, and then apply standard particle methods [5]. Further investigation can include artificial dynamics [7] and Markov Chain Monte Carlo within Sequential Monte Carlo algorithms [5], [8].

The aim of this study is develop a reliable process monitoring by using sequential monte carlo sampling techniques . The results will then be used to analyze and compare different SMC sampling methods and their ability to use few measured online data and predict unmeasured key process variables/states for monitoring production yield and impurities in a fermentation process. While the methods will be compared for LAB fermentation that contains typically few online data, future outlook and perspectives for extending the methods to reconcile noisy data from online aerobic fermentation systems (that features rich online data including offgas CO_2 and oxygen measurements, online pH, DO and weight among others) will be presented and discussed.

References

[1] F. Leroy and L. De Vuyst, “Lactic acid bacteria as functional starter cultures for the food fermentation industry,” *Trends Food Sci. Technol.*, vol. 15, no. 2, pp. 67–78, Feb. 2004.

[2] S. Ding and T. Tan, “l-lactic acid production by Lactobacillus casei fermentation using different fed-batch feeding strategies,” *Process Biochem.*, vol. 41, no. 6, pp. 1451–1454, Jun. 2006.

[3] R. Spann, C. Roca, D. Kold, A. Eliasson Lantz, K. V. Gernaey, and G. Sin, “A probabilistic model-based soft sensor to monitor lactic acid bacteria fermentations,” *Biochem. Eng. J.*, vol. 135, pp. 49–60, Jul. 2018.

[4] E. V. Musvoto, M. C. Wentzel, R. E. Loewenthal, and G. A. Ekama, “Integrated chemical–physical processes modelling—I. Development of a kinetic-based model for mixed weak acid/base systems,” *Water Res.*, vol. 34, no. 6, pp. 1857–1867, Apr. 2000.

[5] N. Kantas, A. Doucet, S. S. Singh, J. Maciejowski, and N. Chopin, “On Particle Methods for Parameter Estimation in State-Space Models,” *Stat. Sci.*, vol. 30, no. 3, pp. 328–351, Aug. 2015.

[6] N. Kantas, A. Doucet, S. S. Singh, and J. M. Maciejowski, “An Overview of Sequential Monte Carlo Methods for Parameter Estimation in General State-Space Models,” *IFAC Proc. Vol.*, vol. 42, no. 10, pp. 774–785, Jan. 2009.

[7] T. Higuchi, “Self-Organizing Time Series Model,” in *Sequential Monte Carlo Methods in Practice*, New York, NY: Springer New York, 2001, pp. 429–444.

[8] W. R. Gilks and C. Berzuini, “Following a moving target-Monte Carlo inference for dynamic Bayesian models,” *J. R. Stat. Soc. Ser. B (Statistical Methodol.*, vol. 63, no. 1, pp. 127–146, Feb. 2001.

Comparative analysis of plantwide control methodologies based on established benchmark models

M.L. Pedersen[1], F.D. Bähner[1], X. Zhang[2], and J.K. Huusom[1]

[1] *Process and Systems Engineering Center (PROSYS), Department of Chemical and Biochemical Engineering, Technical University of Denmark, 2800 Lyngby, Denmark.*
[2] *Institute of Process Engineering, Chinese Academy of Sciences (CAS), 100190 Beijing, China*

June 2019

Abstract

The increase of complexity in the chemical process makes the development of a control structure for full process plants an inherently complex task. The complexities are related to material recycling, energy integration, sharpened product quality control, and safety as well as environmental constraints. Therefore, formal methodologies for the derivation of plantwide control structures have gained significant interest over the last fifty years. The established plantwide control methodologies have been classified based on their main approach: Heuristic, Mathematical, Optimization oriented, and Mixed approach. Three of the methodologies have been selected due to their important impact on the field:

- Plantwide control design procedure, by Luyben et al. (Heuristic approach)
- Control structure design for complete chemical plants, by Skogestad (Mixed approach)
- Plantwide control of industrial processes: An integrated framework of simulation and heuristics, by Konda et al. (Heuristic approach)

These methodologies have been applied to established benchmarks models to compare their applicability and performance. The models utilized for the comparison are the Evaporator process by Newell and Lee, the Tennessee Eastman process by Downs and Vogel, and then an industrial case on two heat integrated distillation columns for solvent recovery. The methodology by Luyben et al. has the least requirements of information about the process but is heavily dependent on experience. The method by Konda et al. tries to combine the heuristics steps with simulations to lower the dependency of experience, creates the requirement for a suitable simulation model of the process. The methodology by Skogestad aims to find a cost-optimized control structure, using both process knowledge and mathematical models. For the Evaporator process, the methodologies came to different control structures. Through the method by Luyben et al. several alternative control structures were developed, without an indication of the best one, here further experience with the process is needed. The additional simulations suggested by Konda et al. made it possible to narrow it down to two control structures. The application of Skogestad's methodology, gave three alternative control structure, where a refined economical and engineering analysis should indicate the optimum implementable candidate.

Mechanistic modelling of heat and mass transfer coupled with pore-mechanics during the baking process

Felix Rabeler*, Aberham Hailu Feyissa*

**Technical University of Denmark, Kgs. Lyngby, Denmark*
(e-mail: felra@food.dtu.dk).

Abstract: The baking of bread rolls is a complex and energy intensive process which is still relying on the expertise of the baker or process operator. This, however, limits the possibilities for process control and automation. Thus, a deeper understanding of the impact of the oven conditions on the baking and especially on the quality of bread rolls is required to obtain a final product with the highest quality for the consumer. In this study we have, therefore, developed a mechanistic model (based on physical laws) for the baking of bread rolls that is coupled with the kinetics of the temperature and moisture induced color changes. The model is based on the transport of heat and mass (liquid water, water vapor and CO_2) through the porous media coupled with the expansion of the bread roll due to an internal pressure increase. Here, we used COMSOL Multiphysics® (finite element method) to solve the partial differential equations for the heat and mass transfer as well as the ordinary differential equations for the color changes. The validation of the developed model shows that the predicted temperature, moisture, volume and color changes agree with the experimental observations. The model was then used to show the clear effect of changing process settings (temperature, fan speed and humidity) on the expansion and surface color of the bread rolls during baking. Overall, the developed model allows the prediction of the local and spatial temperature, moisture, volume and color development, which provides deep insights into the complex mechanisms during the bread roll baking process that cannot be obtained by experimentation alone. By applying the developed model it is possible to obtain a better control over the baking process as well as to optimize the process settings to achieve the highest product quality for the consumer.

Keywords: Heat and mass transfer, Comsol Multiphysics, Quality prediction, Thermal treatment, Porous media, Baking process, Deformation.

Modelling of a Cyclic Distillation Process

**Jess B. Rasmussen, Seyed S. Mansouri,
Jens Abildskov, Jakob K. Huusom***

*PROSYS, Department of Chemical and Biochemical Engineering,
Technical University of Denmark, Søltofts Plads, Building 229,
2800 Kgs. Lyngby, Denmark.
Corresponding author (e-mail: jkh@kt.dtu.dk)

Abstract: A more detailed model has been developed for cyclic distillation. The developed stage model includes mass and energy balances, comparable to the MESH equations model for a conventional distillation stage. The developed model is capable of including multiple feed and side draw locations as well as taking temperature deviations from the boiling point into account. With the energy balances included it is possible to introduce disturbances in the feed temperature, which would not be possible with the simple mass balance model previously presented in literature. In order to identify potential disturbance and manipulated variables, which can be used for control of the column, a degree of freedom analysis have been performed.

Keywords: Periodic distillation, distillation control, feed disturbances

1. INTRODUCTION

Cyclic distillation is a promising method of optimizing a distillation process. By separating the vapour and the liquid flow in two periods: vapour flow period (VFP) and liquid flow period (LFP) the tray efficiency can be significantly improved compared to conventional distillation (Bîldea, 2016).

So far, the industrial application of cyclic distillation is very limited, despite the technology first being proposed in the early 1960's (Cannon, 1961). Until recently, a problem with cyclic distillation was back-mixing of the liquids during LFP, which defeats the purpose of separating the phase flows. However, Maleta et al. (2011) proposed a new tray design, which solved the draining issues. With this type of tray it is possible to operate a distillation column in periodic mode with simultaneous draining of the trays without back-mixing of liquids.

One issue that remains is the need for better models to describe the cyclic distillation. Since the 1960's the developed models have been mass balance based, with assumption of a single saturated liquid feed (Bîldea, 2016). These models are suitable for understanding the overall process. But, they lack the necessary complexity to predict realistic operation, for example to be used in designing of a control structure.

When the energy balances are not included, the vapour flow rate inside the column and the temperature of each holdup are constant. This gives poor results when disturbances in temperature is considered. Furthermore, proper energy balances are crucial to incorporate the effect of a feed that is not saturated liquid or endo-/exothermic reactions take place.

In this paper a new model for cyclic distillation is developed, which includes the energy balances. This is necessary in order to describe the temperature inside a distillation column. First the development of the model is described, including the modelling of separate phase flows. The developed model is tested in a case study and compared to the previous models that only includes mass balances. With the energy balances included disturbances in the feed temperature and composition is tested. Finally, a degree of freedom analysis is performed in order to identify possibly actuators that can be used in the control of the process.

2. MODEL DEVELOPMENT

In order to get a better overview of the operational and regulating challenges in a cyclic distillation, a new and more detailed model for cyclic distillation was developed. A stage model was developed that is comparable to the well-known MESH (Material balances, Equilibrium relations, Summation equations and Heat balances) stage model.

The novel features of the developed model for cyclic distillation are:

- Energy balances to account for time dependent vapour flow rate. Including energy added or removed from the stage.
- Feed that is not necessarily saturated liquid. I.e. pure vapour, cold liquid or a mixture of vapour and liquid.
- Taking tray temperature deviations from boiling point into account. I.e. heating of tray holdup if the temperature is too low or flash if it is too high.

- Multiple feed and side draw locations.

An illustration of a tray in a cyclic distillation column is shown (Fig. 1). This representation is similar to a MESH tray, but due to the separate phase flows, the inlets and outlets are different during VFP and LFP.

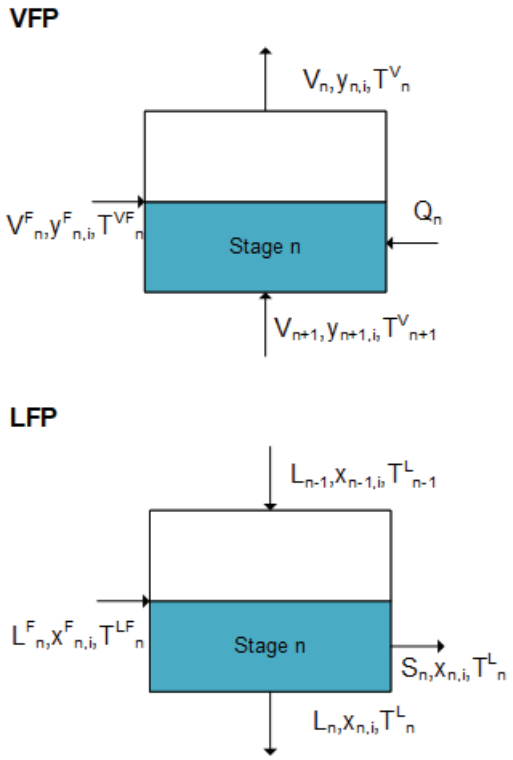

Fig. 1. Variables in a cyclic distillation stage during VFP (top) and LFP (bottom).

The general stage equations can be written similar to the MESH equations, however, a distinction between VFP and LFP is necessary.

During VFP, the model equations for stage *n*, counted from the top down, and components *i=1,2…NC* are:

$$\frac{dM_{n,i}}{dt} = V_{n+1}\, y_{n+1,i} - V_n\, y_{n,i} + V^F_{n+1}\, y^F_{n+1,i} \quad (1)$$

$$\frac{dh_n}{dt} = V_{n+1}\, H_{n+1} - V_n\, H_n + V^F_{n+1}\, H^F_{n+1} + Q_n \quad (2)$$

$$y_{n,i} = K_{n,i}\, x_{n,i} \quad (3)$$

$$\sum_{i=1}^{NC} x_{n,i} = 1 \quad (4)$$

$$\sum_{i=1}^{NC} y_{n,i} = 1 \quad (5)$$

$$x_{n,i}\, M_n = M_{n,i} \quad (6)$$

Using the expressions for the vapour and liquid enthalpies (H_n and h_n respectively) in the energy balance (2), it is possible to isolate and calculate the vapour flow.

For the liquid flow period, the mass and energy balance can be written:

$$M^{(LFP)}_{n,i} = M^{(VFP)}_{n-1,i} + M^F_{n-1,i} - S_n\, x^{(VFP)}_{n,i} \quad (7)$$

$$h^{(LFP)}_n = h^{(VFP)}_{n-1} + h^F_{n-1} - h^{SD}_n \quad (8)$$

$$x_{n,i}\, M_n = M_{n,i} \quad (9)$$

The superscript *(VFP)* denotes the end of the vapour flow period and *(LFP)* the end of the liquid flow period.

During the vapour flow period, the liquid is stationary on the trays, therefore, the accumulation term in the material and energy balances (1)-(2) are necessary. During the liquid flow period, the liquid holdup of each tray is dropped to the tray below. The condenser and reboiler always have a holdup, to avoid either from running dry.

This model is subject to assumptions of constant pressure, tray efficiencies equal to 1 and total condenser. It is assumed vapour feed is supplied during VFP and mixed with the feed tray vapour and liquid feed is added during LFP.

It is assumed the temperature in reboiler and condenser is equal to the boiling point after LFP.

3. RESULTS AND DISCUSSION

A simple case was chosen to investigate the effect of the complexity of the model. A ternary mixture of ethanol-methanol-water was implemented, assuming ideal gas and liquid described by Wilsons thermodynamic model. The Wilsons binary interaction parameters and molar volumes are shown in Table 1.

Table 1: Wilsons parameters (Holmes et al. 1970).

Binary pair (1)-(2)	a_{12} (K)	a_{21} (K)	$V_{m,1}$ (cm^3/mol)	$V_{m,2}$ (cm^3/mol)
EtOH – H_2O	192.38	480.80	58.7	18.1
MeOH – H_2O	103.31	242.63	40.6	18.1
EtOH - MeOH	-257.34	301.15	58.7	40.6

The models were simulated in pseudo-steady-state, i.e. periodic behaviour of the holdups in the column stages. The feed was set to be saturated liquid. The simulation parameters are shown in Table 2.

Table 2: Simulation parameters.

Parameter	Value
Pressure (P)	1 atm
Number of trays (NT)	15
Feed stage (NF)	12
Feed flow (M_{12}^F)	200 mol/cycle
EtOH in feed (x_{EtOH}^F)	15 mol%
MeOH in feed (x_{MeOH}^F)	5 mol%
Water in feed ($x_{H_2O}^F$)	80 mol%
VFP duration (t_{VFP})	25 s
LFP duration (t_{LFP})	5 s

To ensure pseudo-steady-state the bottom and reflux flow rates were set to keep holdups in the reboiler and condenser the same after each LFP. The distillate flow rate was set to 25 mol/cycle.

Comparisons of the simple mass balance model (red) and the simple mass and energy balance model (black) at $t = t_{VFP}$ are shown in Fig. 2.

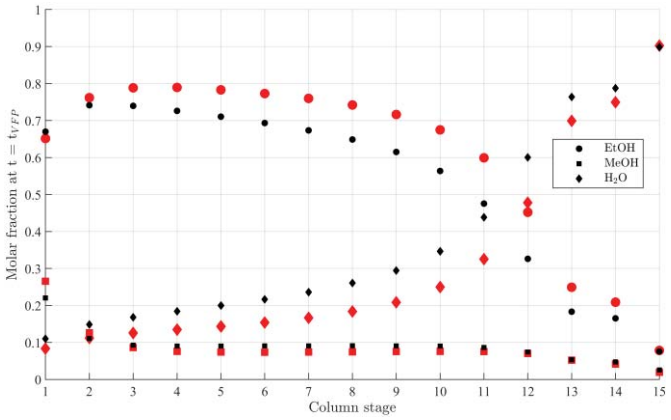

Fig. 2. Molar composition in column stages at $t = t_{VFP}$, in pseudo-steady-state. Simple mass balance model (red), mass and energy balance model (black).

As can be seen there is an effect of including the energy balances in the model. By including the energy balances it is possible to describe the stage temperatures over time, which for example can be used to better predict a proper control strategy.

A +5% change in the feed temperature has been investigated. Fig. 3 shows the ethanol composition at $t = t_{VFP}$ in the reboiler (bottom) and in the condenser (top) for no changes in the feed temperature (black) and a 5% increase in the feed temperature (red). The mass and energy balance model, is used for this simulation.

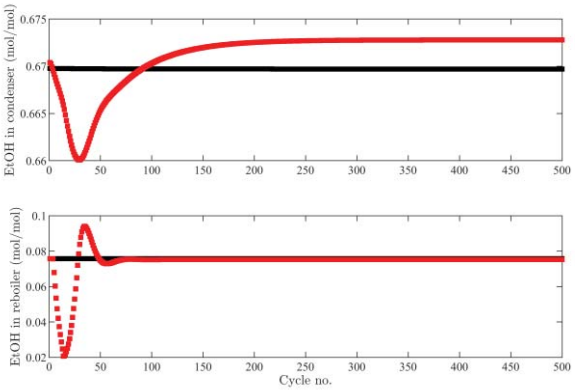

Fig. 3. Ethanol composition at $t = t_{VFP}$ in reboiler (top) and condenser (bottom) in pseudo-steady-state (black) and for a 5% increase in feed temperature (red).

An increase in the feed temperature does not seem to have a significant effect on the ethanol composition in the bottom product, but it does in the top product. When the feed temperature is above the boiling point, flash occurs and vapour feed is supplied to the column, which has an effect on the trays above the feed location. This would not be seen if energy balances and variations in the feed were not implemented.

The base case is then compared to an increase in the ethanol content of the feed, going from 15 mol% to 20 mol%, while the water content is decreased to 75 mol%. For this disturbance, it is assumed the feed is saturated liquid. The ethanol composition in condenser (top) and reboiler (bottom) can be seen in Fig. 4, for the base case (black) and the change in feed composition (red).

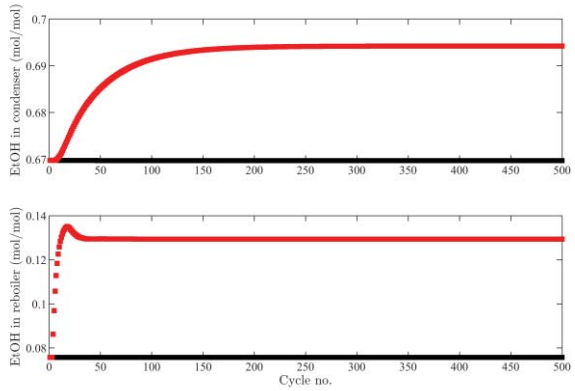

Fig. 4. Ethanol composition at $t = t_{VFP}$ in reboiler (top) and condenser (bottom) in pseudo-steady-state (black) and for a 33.33% increase in feed content of ethanol (red).

As expected, when the ethanol composition in the feed is increased, and the water is decreased, the ethanol in the top and bottom is also increased. As with the change in the feed

temperature, the new steady-state is found fast in the reboiler, but it takes many cycles to get to the new steady-state in the condenser.

As mentioned considerations of temperature deviating from boiling point and multiple feed and side draw locations have not been shown here. Implementation of multiple feed and side draws is relatively simple, since another feed or side draw is added by setting $M_{n,i}^{F}$ or S_n to greater than zero.

Implementation of temperature deviations, that is flash or heating of liquid if the temperature is above or below boiling point, is more difficult. It is time consuming to perform flash calculations, so it is assumed flash only occurs if the liquid temperature is above boiling point after LFP. Heating occurs during VFP and only if the temperature is below boiling point. During heating no mass transfer occurs for the heating stage. Therefore, if the entire VFP is spent on heating a liquid, then the overall separation will suffer.

With the developed mass and energy model, it is possible to perform a degree of freedom analysis in order to identify suitable manipulated variables.

4. CONTROL OF CYCLIC DISTILLATION

When designing a control structure for a distillation column, there are many important variables, and many options for choosing manipulated and controlled variables pairings. With cyclic distillation two important variables, which conventional distillation does not have, is the time for the LFP and the VFP period. Especially t_{VFP} is important, since a longer time for VFP increases the overall time for mass transfer, but can decrease the throughput. The time for LFP should be set to ensure a complete draining before the next VFP is initiated in order to avoid back-mixing. The time for LFP should be set to the minimum value that allows complete draining.

To get an overview of the variables in the cyclic distillation column a degrees of freedom analysis is made. For the degrees of freedom analysis the process is once again divided in VFP and LFP. For VFP the number of equations is $N_e^{VFP} = NT(3 + 3NC)$ and the number of variables is $N_v^{VFP} = 2 + NT(8 + 5NC)$, where *NT* is the number of trays and *NC* the number of components. This gives the degrees of freedom for a stage during VFP as:

$$N_{DoF}^{VFP} = 2 + NT(5 + 2NC) \tag{10}$$

The variables that are specified for a given tray are: P, t_{VFP}, $y_{n,i}^{F}$, V_n^F, T_n^F, Q_n, V_{n+1}, $y_{n+1,i}$, T_{n+1}. The variables V_{n+1}, $y_{n+1,i}$ and T_{n+1} are known from the stage below. For LFP the number of equations is $N_e^{LFP} = NT(2 + NC)$ and the number of variables is $N_v^{LFP} = 2 + NT(5 + 4NC)$, which gives the degrees of freedom:

$$N_{DoF}^{LFP} = 2 + NT(3 + 3NC) \tag{11}$$

The specified variables are: P, t_{LFP}, S_n, T_n^F, $M_{n,i}^{F}$, $M_{n,i}^{(VFP)}$, $x_{n,i}^{(VFP)}$, T_n. Where the variables $M_{n,i}^{(VFP)}$, $x_{n,i}^{(VFP)}$ and T_n are known from the end of VFP.

The control degrees of freedom are not the same as the process degrees of freedom, but is related to this with the number of disturbance variables (Seborg et al. 2011).

$$N_{CDoF} = N_{DoF} - N_{DV} \tag{12}$$

Disturbance variables are the input variables that are not manipulated. Assuming the temperature, composition as well as the vapour flow from the stage below and the stage pressure are disturbance variables then: $N_{DV}^{VFP} = 1 + NT(2 + NC)$, this gives the control degrees of freedom as:

$$N_{CDoF}^{VFP} = 1 + NT(3 + NC) \tag{13}$$

Similar for LFP, the number of disturbance variables is $N_{DV}^{LFP} = 1 + NT(1 + 2NC)$, if the disturbance variables are assumed to be the holdups and temperatures after VFP as well as the feed flow and temperature.

$$N_{CDoF}^{LFP} = 1 + NT(2 + NC) \tag{14}$$

The control degrees of freedom gives the total number of possible manipulated variables. However, often simpler control configurations can be made with just a couple of manipulated variables. For cyclic distillation, it is important to consider the duration of VFP as a manipulated variable. Other possible variables that can be used for control can also be found in conventional distillation. Actuators for cyclic distillation control with one saturated liquid feed and no side draws is shown in Table 3 and compared to conventional distillation.

Table 3: Actuators in cyclic and conventional distillation.

Actuators	**Cyclic**	**Conventional**
Feed flow rate	X	X
Product flows rates	X	X
Condenser and reboiler duty	X	X
Reflux flow rate	X	X
Vapour flow periods duration	X	

As mentioned, when operating a distillation in cyclic mode, the duration of vapour and liquid flow periods become important actuators that can be used in the control strategy. The other actuators in the cyclic distillation that are available for control are similar to the actuators for conventional distillation.

5. CONCLUSIONS

A model have been developed for cyclic distillation, which includes the energy balances. Furthermore, the developed model is capable of account for feed that is not necessarily saturated liquid. A model capable of accounting for tray temperatures above and below boiling point as well as having multiple feed and side draw location was discussed.

It was shown that the developed model is capable of describing a disturbance of +5% in the feed temperature and account for flashed feed. Furthermore, a disturbance in the feed composition was investigated. Both cases showed the developed model being capable of describing changes in the feed, and that new pseudo-steady-states could be found.

For a general overview of a cyclic distillation process it would be fine to use a simple model, but if disturbances that have effect on the temperatures or vapour flow are imposed, then a more detailed model is required.

A degree of freedom analysis is made for a cyclic distillation column and, based on this simple analysis, manipulated variables are identified for the control. The control of a cyclic distillation process is different from conventional distillation, since the time for vapour and liquid flow periods are also available as actuators and must be specified, which will have an effect on the process.

REFERENCES

Bîldea, C.S., Pătruţ, C., Jørgensen, S.B., Abildskov, J., Kiss, A.A. (2016). Cyclic distillation technology – a mini review. *Journal of Chemical Technology and Biotechnology*, 91 (5), 1215-1223.

Cannon, M. (1961). Controlled Cycling Improves Various Processes. *Industrial & Engineering Chemistry*, 53 (8), 629.

Holmes, M.J, Van Winkle, M. (1970). Prediction of Ternary Vapor-Liquid Equilibria from Binary Data. *Industrial & Engineering Chemistry*, 62 (1), 21-31.

Maleta, V.N, Kiss, A.A., Taran, V.M., Maleta, B.V. (2011). Understanding process intensification in cyclic distillation systems. *Chemical Engineering and Processing: Process Intensification*, 50 (7), 655-664.

Seborg, D.E, Edgar, T.F, Mellichamp, D.A, Doyle, F.J. (2011). *Process Dynamics and Control*. Wiley.

GRAY-BOX IDENTIFICATION USING POLYNOMIAL NARMAX MODELS

Allyne M. dos Santos*,[1], Argimiro R. Secchi[2], Maurício B. de Souza Jr[2], Sigurd Skogestad[1] and Dinesh Krishnamoorthy[1]
[1] Department of Chemical Engineering, Norwegian University of Science and Technology - Trondheim
7491 Trondheim, Norway
[2] PEQ/COPPE/UFRJ - Chemical Engineering Program - Rio de Janeiro
RJ 21.941-914, Brazil

Abstract Overview

It is common to approximate nonlinear models with a collection of linear models, but sometimes it can cause problems, such as lack of representativeness of the nonlinear behavior and generation of nonexistent peaks. Nonlinear identification has been improved to overcome these problems. The type of nonlinear model used in this work is the polynomial Nonlinear AutoRegressive Moving Average models with eXogenous inputs (NARMAX). In the present work, a gray-box identification is compared with the black-box one for optimization and control purposes. The identification was performed using an orthogonal least square algorithm and validation was made using k-step-ahead cross-validation method. Dynamic real-time optimization was set based on both first-principle models and identified models, and compared, to evaluate the performance of identified nonlinear models. The gray-box model was more representative in relation to the nonlinearity of the system and generated closer solutions in the dynamic real-time optimization, when comparing with the solutions based on first-principle model.

Keywords

NARMAX models, Gray-box, System Identification.

Introduction

Nonlinear models have received more attention during the past decades as the computational capacity of solving complex problems has increased. The Nonlinear AutoRegressive Moving Average models with eXogenous inputs (NARMAX) is a parametric model, which uses measured discrete data set from industrial or simulated plant, typically as a black-box model. However, it can also be used with some system information, such as static gain, number of stationary states on the output variables, mass balance, energy balance or qualitative characteristics with respect to the dynamic behavior of the system (as a gray-box model).

The improvement of using some type of system information motivated many researchers to apply system identification using NARMAX models with different types of estimation algorithm (Johansen, 1996). The parameter estimation algorithm used in this work is the Orthogonal Least Square algorithm developed by Chen et al. (1989).

In this work, qualitative characteristics of the case study are available. This type is not much explored because it depends on the quality of the available qualitative characteristics, which usually comes from system manipulation by the user. When high quality information is acquired, gray-box identification improves the capacity of

* To whom all correspondence should be addressed

mathematical models to represent the dynamic behavior of nonlinear systems.

The main objective of this work is to develop a methodology for identifying nonlinear systems with prior knowledge using polynomial NARMAX models. The proposed methodology is then compared with a typical black-box approach and applied on dynamic real-time optimization.

Proposed Methodology

In order to acquire nonlinear data, each input variable was perturbed in a way that each excitation lasts enough time to reach a stable response in the its end and with the range of the operating interval (as widely as possible). Measurement uncertainty was added in the form of white noise to all input and output data. Normalization was performed taking the minimum of each variable as reference.

The general structure of NARMAX models is given by,

$$y(k) = P^{\ell}[y(k-1), \dots, y(k-n_y), u_i(k-d), \dots, u_i(k-d-n_{u_i}), e(k-1), \dots, e(k-n_e)] + \varepsilon(k) \quad (1)$$

where P is a nonlinear function with nonlinearity degree ℓ in relation to all variables, with $k = 1, \dots, N$. $y(k)$, $u_i(k)$, $e(k)$ and $\varepsilon(k)$ are the output variable, input variables, noise and prediction error at instant k, respectively. n_y, n_{u_i} and n_e are the maximum lags of system output, inputs, noise, respectively, d is the time delay of the model. The polynomial type is given by,

$$y(k) = \sum_{m_1=1}^{n} \theta_{m_1}\psi_{km_1} + \sum_{m_1=1}^{n}\sum_{m_2=m_1}^{n} \theta_{m_1 m_2}\psi_{km_1}\psi_{km_2} + \sum_{m_1=1}^{n}\cdots\sum_{m_\ell=m_{\ell-1}}^{n} \theta_{m_1\dots m_\ell}\psi_{km_1}\cdots\psi_{km_\ell} + \varepsilon(k) \quad (2)$$

$$n = n_y + n_e + \sum_{j=1}^{i} n_{u_j} \quad (3)$$

where i is the number of input variables, ψ_{km_ℓ} is a regressor with nonlinearity degree ℓ at instant k.

The parameter estimation was performed using an orthogonal least square algorithm named Golub-Householder with Error Reduction Rate (ERR) (Aguirre, 2000). The problem was divided into two parts: NARX part; and MA part (where noise modeling is made). Each part used the OLS algorithm.

The identification algorithm used in this work can be summarized as shown in Figure 1, where J is the objective function of the OLS algorithm. n_{pNARX} and n_{pMA} are the number of terms of the NARX and MA part of the model, respectively.

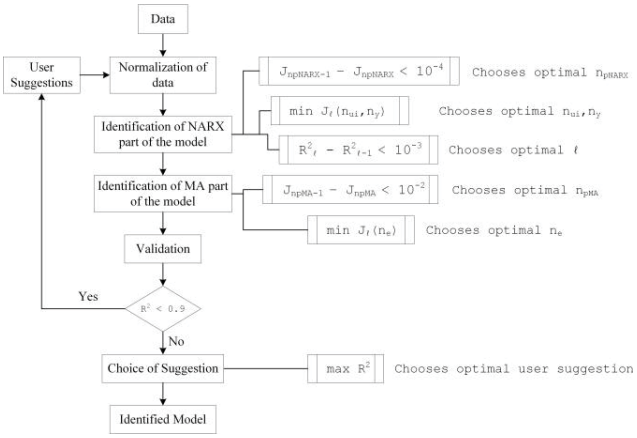

Figure 1. Block diagram of the gray-box identification algorithm

The gray-box identification can be divided into seven main steps:

1. The user starts by suggesting some change on the coordinates or not.
2. The user specifies a range of values for the model orders (n_y, n_{u_i}, n_e and d).
3. Synthetic data is acquired from first-principle models.
4. Normalization is done.
5. Off-line identification algorithm chooses regressors, estimates parameters and optimizes the number of features for each type of model (varying the nonlinearity degree, ℓ) and for each suggestion on coordinate change.
6. Validation step compares the R-squared value of all types of models and chooses the model that has the highest one.
7. The suggestion on coordinate change is also chosen comparing the R-squared values with the one of the black-box identification.

Application Example

The identification was performed on an oil production system with two gas-lift wells (Krishnamoorthy et al., 2018). First, a black-box model was developed according to Eq. (4) and (5).

$$\boldsymbol{y}_{p_{bh_2}} = \boldsymbol{\Psi}^{*}_{p_{bh_2}}\boldsymbol{\theta}_{p_{bh_2}} \quad (4)$$

$$\Psi_{p_{bh_2}}^{*T} = \begin{bmatrix} y_{p_{bh_2}}(k-1) \\ y_{p_{bh_2}}(k-2) \\ y_{p_{bh_2}}(k-1)u_2(k-1) \\ y_{p_{bh_2}}(k-1)^2 \\ y_{p_{bh_2}}(k-1)u_2(k-2) \\ y_{p_{bh_2}}(k-2)u_2(k-1) \\ u_2(k-4)^2 \\ y_{p_{bh_2}}(k-1)u_2(k-4) \\ y_{p_{bh_2}}(k-2)u_2(k-3) \\ y_{p_{bh_2}}(k-2)^2 \\ u_1(k-1)u_2(k-4) \\ y_{p_{bh_2}}(k-1)u_1(k-3) \\ y_{p_{bh_2}}(k-1)u_1(k-1) \\ y_{p_{bh_2}}(k-2)u_2(k-4) \\ e(k-1)u_2(k-2) \end{bmatrix} \quad \theta_{p_{bh_2}} = \begin{bmatrix} 1.8734 \\ -0.6051 \\ -0.0395 \\ -0.8908 \\ -0.2835 \\ 0.4207 \\ 0.0399 \\ -0.3133 \\ -0.1858 \\ 0.5294 \\ 0.0177 \\ -0.0498 \\ 0.0276 \\ 0.1388 \\ 0.026872 \end{bmatrix} \tag{5}$$

The validation of the black-box model gave a R-squared value of 0.5038.

The change in the coordinates that gave higher improvement was substituting u_1 for u_1/u_2 and u_2 for u_2/u_1. Using this information, a gray-box model was developed according to Eq. (4) and (6). The validation of the gray-box model gave an R-squared value of 0.8867, which is higher than the one from black-box model. This is because the algorithm chose a NARX model instead of a NARMAX one.

$$\Psi_{p_{bh_2}}^{*T} = \begin{bmatrix} y_{p_{bh_2}}(k-1) \\ y_{p_{bh_2}}(k-2) \\ u_1(k-1) \\ u_2(k-4) \\ u_2(k-2) \\ u_1(k-4) \\ u_1(k-2) \\ u_2(k-3) \\ y_{p_{bh_2}}(k-3) \\ u_1(k-3) \end{bmatrix} \quad \theta_{p_{bh_2}} = \begin{bmatrix} 1.4030 \\ -0.4210 \\ 0.0325 \\ 0.0063 \\ -0.0053 \\ -0.0422 \\ 0.0458 \\ 0.0104 \\ -0.0194 \\ -0.0014 \end{bmatrix} \tag{6}$$

Dynamic Real-time Optimization

The closed loop responses of the NARMAX models to the DRTO actions on the input variables were compared with the one using the first-principle model, the result is shown in Figure 2.

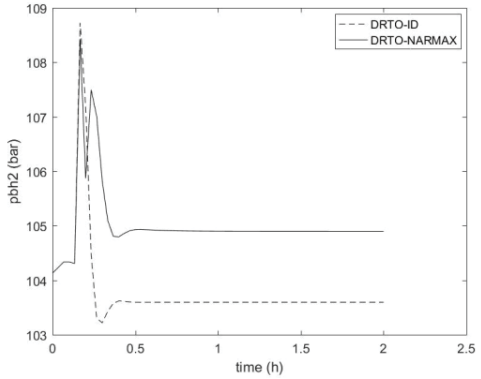

Figure 2. Comparison of DRTO performances (first-principle model and black-box model)

The difference between the solutions was expected because the NARMAX model accounts with noise, which is different (none in this case) than the noise in the original data set. When using gray-box models, the difference between the solutions reduced significantly, reassuring the improvement noted with the system identification results.

Conclusion

The gray-box identification algorithm used in this work has low complexity, although it can take a lot of time depending on the knowledge of the user about the process (if one makes a lot of suggestions to the change in coordinates). The gray-box method improved the modeling of the system, generating higher R-squared value, which was illustrated with an application in dynamic real-time optimization.

Acknowledgments

The main author gratefully acknowledge financial support from the Fundação de Amparo à Pesquisa do Estado do Rio de Janeiro (FAPERJ); the International Partnerships for Excellence Education, Research and Innovation (INTPART); and the Coordenação de Aperfeiçoamento de Pessoal de Nível Superior (CAPES).

References

Aguirre, L. A. (2000). *Introdução à identificação de sistemas: técnicas lineares e não-lineares aplicadas a sistemas reais*, Belo Horizonte, UFMG.

Chen, S., Billings, S. A., Luo, W. (1989). Orthogonal least squares methods and their application to non-linear system identification, *Int. J. Control*, 50, 5, 1873.

Krishnamoorthy, D., Foss, B., Skogestad, S. (2018). Steady-state real-time optimization using transient measurements. *Comput. Chem. Eng.*, 115, 34.

Johansen, T. A. (1996). Identification of non-linear systems using empirical data and prior knowledge – an optimization approach, *Automatica*, 32, 3, 337-356.

Heat load prediction for district heating using a latent variable approach

Johan Simonsson [*,**] **Khalid Atta** [*] **Dave Zachariah** [***]
Wolfgang Birk [*]

[*] *Control Engineering Group, Luleå University of Technology, Luleå, Sweden*
[**] *Optimation AB, Uppsala, Sweden*
[***] *Department of Information Technology, Uppsala University, Uppsala, Sweden*

Abstract: Due to the different characteristics of space heating load and heating for domestic hot tap water consumption, a common approach for heat load prediction for buildings is to use separate models for the two. Using a latent variable framework as described in the article, both models can be calculated recursively and simultaneously. A nominal model is used to model the outdoor temperature dependent behavior:

$$\hat{y}_{nom}(t) = \Theta\varphi(t) + \varepsilon(t), \tag{1}$$

mainly modeling space heating load. Using a sufficient number of lagged inputs and the concept of maximum likelihood results in an ARX model. The residual $\varepsilon(t)$ is assumed to be distributed as

$$\varepsilon(t) \sim \mathcal{N}(Z\gamma(t), \Sigma). \tag{2}$$

The residual prediction

$$\hat{y}_{res}(t) = Z\gamma(t) \tag{3}$$

is then modeled using a data driven latent variable approach, where $\gamma(t)$ is calculated from temporal data such as time of the day and work day / not workday. The prediction of the total heat load can then be written as

$$\hat{y}(t) = \Theta\varphi(t) + Z\gamma(t). \tag{4}$$

The described method results in a parsimonious model, allowing for a computationally efficient implementation and avoiding overfitting. Individual building model matrices can be summed when the same covariates are used, allowing for straight forward aggregation of predictions when applicable. The method is validated using measurement data from a multi-dwelling building located in the city of Luleå, in general showing a good fit given the irregular patterns of hot water consumption for single buildings. It is concluded that the method shows promising results, and that further research is needed to validate the method against a larger building stock, with a corresponding categorization of buildings.

Keywords: Heat load prediction, 4GDH, District heating, Consumer model

Systematic tuning of PI controllers in non-steady-state return sludge flow of wastewater treatment systems

A.K. Vangsgaard*, S. Bach Jepsen, J. Kjøbsted Huusom**, T. Munk-Nielsen***

**Krüger A/S, Veolia Water Technologies, 2860 Søborg, Denmark, (e-mail: akv@kruger.dk, thm@kruger.dk)*
***Department of Chemical and Biochemical Engineering, Technical University of Denmark (e-mail: s164063@student.dtu.dk, jkh@kt.dtu.dk)*

Abstract: Performance of the secondary settling tanks at a wastewater treatment plant determines the amount of nutrients released into the environment and consequently the impact on the receiving water bodies. In order to ensure sufficient biomass in the activated sludge biological treatment tanks, a stable sludge blanket (to avoid sludge escape), and a stable solids concentration in the waste sludge for good dewatering conditions, the return activated sludge flow is controlled using a feedback cascade control loop consisting of two proportional-integral (PI) controllers. In the outer loop, the sludge blanket level set point is compared to the measured sludge blanket level and the calculated error signal (ϵSlbl) is transmitted to the master PI controller. The output of the master PI controller is used as the set point for the solids concentration in the return sludge in the inner loop. Here, the set point is compared to the measured solids concentration of return sludge and the calculated error signal (ϵSS) is transmitted to the slave PI controller. The output of the slave PI controller is used as a set point for the flow rate of return activated sludge. The system is influenced by disturbances from the variation in inlet flow, originating from both daily water consumption dynamics and from wet weather events, as well as changes in the sludge properties affecting the settlability. The performance of the control system is thus influenced by the parameters of the PI controllers. Previously, these parameters have been chosen based on operational experience and not on systematic procedures. In this work an attempt to retune the inner PI controller in the cascaded control loop was conducted. From this, a second order transfer function with an inverse response was assumed to be the process model of the inner control loop. Data was used to estimate the dominant time constant of the inner loop model to a value of 60 minutes. Using the internal model control method, it was found that the previously used PI parameters were optimal for a dominant time constant of 30 minutes. This resulted in a doubling of the previously used integral time. Qualitative evaluation of the system performance after doubling the integral time, indicates a more stable performance than prior to the change.

Health-aware control – current status and future outlook

Adriaen Verheyleweghen

Equipment in chemical process industry is subject to wear-and-tear induced degradation when used during normal operation. To maximize the value of the asset, maintenance must be performed when the asset health is critical in order to keep the asset operational. This raises the question of how to schedule maintenance, and how to operate the asset optimally between scheduled maintenance interventions. Although considering the equipment health state in the decision process is not a new idea (controllers robust to plant-model-mismatch have been around since the very early days of process control), there has been increased interest in developing so-called “health-aware” controllers (HAC) in recent years. The term “health-aware” control was first coined by (Escobet, Puig, & Nejjari, 2012), but we adopted the term in this work to describe any control structure in which asset health is constraining or otherwise directly influencing the permissible set of controls. Furthermore, we choose to think of HAC as optimization-based control structures where asset degradation models are included in the optimization problem. In other words, HAC is a proactive approach to handle and influence asset degradation, rather than traditional, reactive approaches such as fault-tolerant control (FTC). By having a proactive approach to degradation, the control structure does not have to overly conservative in order to avoid unplanned and costly plant shutdowns, thus resulting in more operational flexibility, less conservative operation and larger profit margins.

In this work, we discuss the challenges and prerequisites that must be addressed in order to obtain a HAC structure. In particular, we discuss the issues pertaining to obtaining asset degradation models, which are necessary to give an accurate prognosis of how future operational strategies will influence the asset health. Furthermore, we discuss the issues related to real-time diagnostics of the asset health. Since measurements of the health state of the asset are rarely available, estimators and soft sensors are usually necessary for diagnostic purposes. However, due to the lack of detailed first principles degradation models, the diagnostic predictions are often highly uncertain. This uncertainty must be handled in a system manner. Lastly, the problems stemming from an HAC structure formulation may end up being quite complex and require special solution methods. In this work, we discuss the aforementioned problems, current industrial and academic status, as well as possible solutions and future outlooks. We also present a framework for formulating and solving HAC problems. Finally, an illustrative case study is presented.

Bibliography

Escobet, T., Puig, V., & Nejjari, F. (2012). Health aware control and model-based prognosis. *20th Mediterranean Conference on Control & Automation* (pp. 691 - 696). Barcelona: IEEE.

Langeron, Y., Grall, A., & Barros, A. (2015, August). A modeling framework for deteriorating control system and predictive maintenance of actuators. *Reliability Engineering& System Safety, 140*, 22-36.

Pereira, E. B., Galvão, R. K., & Yoneyama, T. (2010). Model Predictive Control using Prognosis and Health Monitoring of actuators. *International Symposium on Industrial Electronics* (pp. 237-243). Bari: IEEE.

Salazar, J. C., Weber, P., Nejjari, F., Theilliol, D., & Sarrate, R. (2016). MPC framework for system reliability optimization. In Z. (. Kowalczuk, *Advanced and Intelligent Computations in Diagnosis and Control* (pp. 161-177). Springer.

Verheyleweghen, A., & Jäschke, J. (2017). Framework for Combined Diagnostics, Prognostics and Optimal Operation of a Subsea Gas Compression System. *IFAC-PapersOnLine*, 15916-15921.

Verheyleweghen, A., Srivastav, H., Barros, A., & Jäschke, J. (2019). Combined Maintenance Scheduling and Production Optimization. *29th European Safety and Reliability Conference.* Research Publishing.

Vieira, J. P., Galvão, R. K., & Yoneyama, T. (2015, December). Predictive Control for Systems with Loss of Actuator Effectiveness Resulting from Degradation Effects. *Journal of Control, Automation and Electrical Systems, 26*(6), 589-598.

Zagorowska, M., Thornhill, N., Haugen, T., & and Skourup, C. (2018). Load-sharing strategy taking account of compressor degradation. *2nd IEEE Conference on Control Technology and Applications.* Copenhagen.

Sustainable Value Chain Design for Biorefineries

Nikolaus I. Vollmer[1*], Krist V. Gernaey[1], Solange I. Mussatto[2], Gürkan Sin[1]

[1] PROSYS Research Centre, Department of Chemical Engineering, Technical University of Denmark

[2] Novo Nordisk Foundation Center for Biosustainability, Technical University of Denmark

*nikov@kt.dtu.dk

Sustainable value chains are an important element to achieve the UN 2030 Sustainable Development Agenda (SDA) [1]. For this purpose, an integrated biorefinery is an essential concept for the sustainable production of food, chemicals and power generation, utilizing e.g. lignocellulosic waste from agricultural waste as feedstock [2]. The crux of this concept is a poor economic potential due to the multitude of costly process steps. [3]. Therefore, the process design of a new biorefinery has to be performed systematically [4]. Besides, designing the process and the utilized feedstocks, special focus lies on the selection of products, since they will determine the overall profitability. Only by optimizing the integration of feedstock, biorefinery processes and co-products, the whole value chain will be both economically viable and sustainable [5].

In detail, the systematic approach to design a sustainable value chain with a biorefinery in its core avails methodologies from Process Systems Engineering and comprises three main steps: (1) Process Design, (2) Process Optimization and (3) Value Chain Optimization. (1) In the first step, first-order models for possible unit operations in a biorefinery are developed, calibrated and validated with own experimental and literature data. Together with a combined Uncertainty and Sensitivity Analysis quantifying the model robustness, surrogate models are developed. These models are integrated into a superstructure, which is then optimized to yield an optimal process design. (2) With the optimal design, the process is optimized both unit-wise and plant-wide. Primarily, this serves to find optimal operation conditions for the process units and to develop scheduling and control strategies for the process. Furthermore, it iteratively gives feedback for the extension of the process design, by increasing the overall utilization of the feedstock by co-production strategies and performing process integration and intensification. (3) Finally, by including feedstock and product markets in the optimization, the whole value chain is displayed. Besides a risk-based economic evaluation, different assessments, e.g. on the life-cycle are performed. This results in several target indicators for the value chain.

Apart from design heuristics and instigations for development of microorganisms and processes for the optimized biorefinery, the result is an overall proof of the economic viability of the value chain with a biorefinery as part of a sustainable production pattern, perfectly matching the goals of the UN-SDA.

[1] United Nations, Transforming our world: The 2030 agenda for sustainable development, 2015.
[2] F. Cherubini, Energy Conversion and Management, Vol. 51, 2010, pp. 1412-1421.
[3] A. Chandel et al., Bioresource Technology, Vol. 264, 2018, pp. 370-381.
[4] C. Gargalo et al. in: J. Klemens (Ed.), Assessing and Measuring Environmental Impact and Sustainability, Elsevier, Oxford, 2015, pp. 277-321.
[5] C. Gargalo et al., Industrial & Engineering Chemistry Research, Vol. 56, 2017, pp. 6711-6727

Technical University of Denmark

DTU Chemical Engineering

DK-2800 Kgs. Lyngby

Denmark